

Durham E-Theses

Systematic routes to improved approximations in Kohn–Sham theory

CALLOW, TIMOTHY,JAMES

How to cite:

CALLOW, TIMOTHY,JAMES (2020). *Systematic routes to improved approximations in Kohn–Sham theory*, Durham e-Theses. <http://etheses.dur.ac.uk/13817/>

Use policy

The full-text may be used and/or reproduced, and given to third parties in any format or medium, without prior permission or charge, for personal research or study, educational, or not-for-profit purposes provided that:

- a full bibliographic reference is made to the original source
- a [link](#) is made to the metadata record in Durham E-Theses
- the full-text is not changed in any way

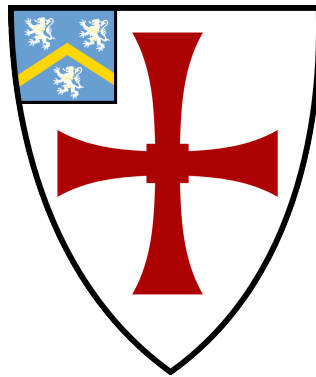
The full-text must not be sold in any format or medium without the formal permission of the copyright holders.

Please consult the [full Durham E-Theses policy](#) for further details.

Systematic routes to improved approximations in Kohn–Sham theory

Timothy James Callow

A thesis presented for the degree of
Doctor of Philosophy



Department of Physics
Durham University
United Kingdom
December 2020

Systematic routes to improved approximations in Kohn–Sham theory

Timothy James Callow

Abstract

The Kohn–Sham (KS) formulation of density-functional theory (DFT) has become the pre-eminent method for modelling electrons in matter. In many calculations, KS theory offers an unrivalled balance between accuracy and speed. However, the most widely-used approximations are known to be inadequate in certain applications, such as strongly-correlated systems. Furthermore, it is not straightforward to systematically converge to the correct result in these cases; this is in contrast to wave-function methods, which lend themselves more naturally to systematic improvements. In this thesis, we develop methods to help understand and improve systematic failings of common approximations for the exchange and correlation functional in KS theory.

One major theme of this thesis is the use of wave-function theories to develop accurate reference KS potentials in DFT. We consider an alternative derivation of the KS potential based on the minimization of a wave-function expression, which establishes a link between DFT and wave-function theories. We use this tool to develop perturbative expansions of the KS potential: one such expansion yields a novel KS potential which is expected to have exact exchange and accurate correlation character. Continuing this theme, we explore a method to obtain the KS potential corresponding to a given density. We focus on the role of the screening density in this method, a concept which also helps our understanding of the pervasive self-interaction error in DFT.

The other major theme of this thesis is the development and application of implicit density functionals. We explore how this class of functionals can be used to develop a new formalism for open-shell systems in KS theory. Implicit density functionals in KS theory require the optimized effective potential framework, whose implementation in finite basis set codes has proven problematic in the past. We develop an implementation which is both simple to apply and formally avoids these mathematical difficulties.

Declaration

The work in this thesis is based on research carried out in the Department of Physics, University of Durham, England. No part of this thesis has been submitted elsewhere for any other degree or qualification, and it is the sole work of the author unless referenced to the contrary in the text.

Much of the work in this thesis is based on collaborative work that has been published, or is due to be submitted, in journals. These publications are listed below.

- **T.J. Callow** and N.I. Gidopoulos. “Optimal power series expansions of the Kohn–Sham potential.” *Eur. Phys. J. B*, **91**, 209 (2018).
- **T.J. Callow**, N.N. Lathiotakis, and N.I. Gidopoulos. “Density-inversion method for the Kohn–Sham potential: Role of the screening density.” *J. Chem. Phys.*, **152**, 164114 (2020).
- **T.J. Callow**, B.J. Pearce, T. Pitts, N.N. Lathiotakis, M.J.P. Hodgson and N.I. Gidopoulos. “Improving the exchange and correlation potential in density functional approximations through constraints”. *Faraday Discuss.* (2020).
- **T.J. Callow**, B.J. Pearce, N.N. Lathiotakis, and N.I. Gidopoulos. “Exchange-correlation density functionals with spin-density accuracy for open shells”. *To be submitted*.

Copyright © 2020 by Timothy James Callow.

“The copyright of this thesis rests with the author. No quotation from it should be published without the author’s prior written consent and information derived from it should be acknowledged”.

Acknowledgements

Throughout my PhD, I have been lucky to count on the support of a great number of people. First and foremost, I thank my supervisor, Nikitas Gidopoulos, whose enthusiasm for all matters DFT rubbed off onto me. I am very grateful for his guidance. Plus, he had a great coffee machine which not only served its intended purpose with distinction, but even proved to be something of a social hub.

Nikitas also introduced me to Nektarios Lathiotakis, whose code HIPPO formed the basis for much of the work in this thesis. I thank Nektarios for all his help running and developing the code, and for hosting me in Athens. I was lucky to have Stewart Clark as my co-supervisor, who was ready to assist with any kind of computational issue, as well as being a keen supporter of the group's social events. I also thank Hardy Gross and Rod Bartlett for interesting and lively discussions; moreover, I thank Hardy for arranging my financial support from the Max Planck Institute.

The office environment has consistently been a highlight of my PhD studies: thanks to Rob, Matt (x2), Ben, Tom, Faten, Zac, Matjaz and the 'Coding Gremlin' for the discussions, distractions and infamous Newcastle expeditions. I would like to give a special shout-out to the Coding Gremlin for introducing Wine Fridays to the office, which were something of a revelation.

My friends have been an important diversion from the world of DFT. I was lucky to share a house with Ben and Stu — our discussions on the best kind of potato never grew old. Additionally, I thank those from St Chad's and the tennis club (especially Emily, who was in both groups); and my friends from my undergraduate and even school days, who frequently (sometimes too frequently) made the trip from London to Durham.

I am grateful to my family for supporting me throughout my PhD and the many

years that preceded it. In particular, I thank my parents, who have always enthusiastically supported my education; and my grandma, for her advice and documentary suggestions, who would likely have read this thesis in full had she been able to.

Last but certainly not least, I thank Sophie for her great companionship and being my biggest cheerleader. I hope that the next few years will be as good as the past ones!

Finally, I thank Durham University and the Max Planck Institute of Microstructure Physics for co-funding my PhD studies.

Contents

Abstract	i
Declaration	ii
Acknowledgements	iii
1 Introduction	1
1.1 Outline of thesis	2
1.2 Hartree atomic units	3
2 The many-electron problem	5
2.1 The Born–Oppenheimer approximation	6
2.2 Hartree–Fock theory	7
2.2.1 The Hartree–Fock equations	9
2.2.2 Solving the Hartree–Fock equations	10
2.2.3 Restricted and unrestricted Hartree–Fock	11
2.3 Electron correlation	12
2.4 Correlated methods	13
2.4.1 Configuration interaction	15
2.4.2 Many-body perturbation theory	16
2.4.3 Coupled cluster	17

3	Density-functional theory	20
3.1	Hohenberg–Kohn theorems	21
3.1.1	Hohenberg Kohn first theorem: one-to-one mapping	21
3.1.2	Hohenberg–Kohn second theorem: variational principle	23
3.2	The constrained search formulation	24
3.3	Thomas–Fermi and orbital-free DFT	25
3.4	Kohn–Sham theory	26
3.5	Spin density-functional theory and open-shell systems	28
3.6	Exchange-correlation functionals	29
3.6.1	Local spin density approximation	30
3.6.2	Generalized gradient approximations	30
3.6.3	Hybrid functionals and generalized Kohn–Sham	31
3.6.4	The path to the ‘exact’ functional	33
3.7	Limitations of common functionals	36
3.7.1	Self-interaction	36
3.7.2	The derivative discontinuity and fundamental gap	39
3.7.3	Static and dynamic correlation	43
3.8	The optimized effective potential method	44
3.8.1	KLI and CEDA approximations	46
3.9	Implementation	47
3.9.1	Gaussian basis sets	48
3.9.2	SCF convergence	50
3.9.3	OEP implementation	52
4	Optimal power series expansions of the Kohn–Sham potential	58
4.1	Review of integration of density and wave-function theories	59
4.1.1	Adiabatic connection and DFT perturbation theory	60
4.1.2	Gidopoulos variational principle	62
4.2	Reference determinants with minimum correlation energy	66
4.3	Comparison of DFT perturbation theory and present method	69

4.3.1	Traditional DFT PT method	69
4.3.2	Present WFT-DFT method	70
4.4	Local exchange potentials	71
4.4.1	Exact exchange potential	72
4.4.2	Local Fock exchange potential	74
4.5	First order exchange and correlation potential	75
4.6	Analysis of variational collapse in DFT PT	86
4.7	Summary and discussion	88
5	Density-to-potential inversion: role of the screening density	90
5.1	Motivation and review of existing methods	90
5.2	Method	93
5.2.1	Algorithm	95
5.2.2	Choice of basis set representation for the screening density	97
5.2.3	Convergence criteria	99
5.3	Results	103
5.3.1	Inversion of LDA densities	103
5.3.2	Constrained inversion of LDA densities	106
5.3.3	Inversion of densities from wave-function theories	107
5.4	Comparison with the method by Zhao, Morrison and Parr	111
5.5	Summary and discussion	112
6	Open-shell systems in Kohn–Sham theory via implicit density functionals	114
6.1	Motivation and the ‘ghost’ exchange error	115
6.2	Theory	119
6.3	Implementation of the OEP equation	122
6.3.1	Implementation for (semi)-local density-functionals	123
6.3.2	Implementation of exact exchange energy functional	126
6.4	Results	128

6.4.1	(Semi)-local density-functionals	128
6.4.2	Exact exchange	134
6.5	Summary and discussion	137
6.5.1	Unrestricted KS equations from generalized KS theory	139
7	Conclusions and further work	143
7.1	Modelling the derivative discontinuity	146
Appendix A Quadratic line search method		151
Appendix B Alternative construction of b_k in OEP equation		153
Bibliography		157

Introduction

The role of simulations in science is growing ever more important, due to the consistent advancements in computing power over the last several decades [1], coupled with the increasing capability of scientists and engineers to exploit these advancements. Indeed, computational modelling has become the fundamental instrument in guiding public policy in response to major global challenges such as the COVID-19 pandemic [2] and climate change [3]. This underlines the critical importance of developing scientific models that are accurate, reliable, and understandable [4].

This thesis is concerned with the development and understanding of models in electronic structure theory. Electronic structure theory is the study of electrons in matter: a vast field that encompasses many different methods and applications, from drug discovery [5] to astrophysical processes [6]. Electronic structure methods are so widely used that they take up a significant fraction ($\sim 30\%$) of all high-performance computing hours in the UK and USA [7].

The main focus of this thesis is density-functional theory (DFT) [8, 9], which can justifiably be considered the most widely-used electronic structure method. In 2014, two of the ten most-cited scientific papers of all time (and twelve of the top hundred) were DFT papers [10]; meanwhile in 2013, almost 30,000 papers used DFT [11], a number which appears to be doubling every 5-10 years. DFT's popularity is due in part to its enviable balance between accuracy and speed, together with

the development of several large DFT codes [12] which has enabled it to become a ‘black-box’ method for many users. It is most commonly used in chemistry and materials science, to help understand or complement experimental results; however, it also enjoys success as a predictive tool of its own accord [13–16].

Regardless of DFT’s many successes, it is vulnerable to various criticisms. One of the main limitations of DFT is the difficulty in systematically improving the approximations; by contrast, it is usually possible to systematically converge to the correct result using wave-function methods [17]. This weakness is reflected in the fact that the two most popular approximations today were both developed in the 1990s [18, 19]; no general-purpose approximation has since challenged their popularity. Moreover, there is now such a range of approximations that one can pick an approximation that best agrees with the experimental data or hypothesis, raising questions about scientific integrity.

Motivated by the above problems, the common theme of this thesis is the development of systematic routes to improved approximations in DFT. We tackle this theme in several ways, for example through the integration of techniques and results from wave-function theories in DFT, and through the development of improved algorithms for a certain class of approximations.

1.1 Outline of thesis

This thesis is structured as follows:

- Chapter 2: We introduce fundamental concepts in electronic structure theory such as the Born–Oppenheimer approximation and Hartree–Fock theory. We also briefly review a few popular wave-function methods.
- Chapter 3: We review the formal theories underpinning DFT, namely the Hohenberg–Kohn theorems and Kohn–Sham (KS) theory. We introduce the established approximations and discuss common failings. We also introduce

the optimized effective potential (OEP) method which is fundamental to much of the work in this thesis. Finally, we discuss some implementation details.

- Chapter 4: We introduce a theory connecting wave-function theory (WFT) with DFT, and explore the development of perturbative expansions for the KS potential using this theory. One such expansion leads to a new KS potential with exchange and correlation character. We also compare our work with other approaches linking DFT and WFT.
- Chapter 5: We present a method to obtain the KS potential from a given density, and discuss the importance of the screening density in this method. We analyse the technical details of our approach, which can be implemented easily in DFT codes, and apply it to a variety of systems and input densities.
- Chapter 6: We introduce a method to treat open-shell systems within restricted KS theory, by treating standard exchange-correlation functionals as implicit density functionals. This leads to an OEP equation which we solve using a recently developed method; we demonstrate the reliability of this technique for a variety of systems. Finally, we discuss our findings in the context of a well-known paradox in DFT, the spin-symmetry dilemma.
- Chapter 7: We draw conclusions and consider avenues for future work, with a particular focus on modelling the derivative discontinuity.

1.2 Hartree atomic units

Throughout this thesis, we adopt Hartree atomic units unless otherwise specified. This is a convenient practice because the following fundamental physical constants are all equal to one:

- \hbar , reduced Planck's constant;

- e , elementary charge;
- a_0 . Bohr radius;
- m_e , atomic mass unit.

This simplifies the notation of various expressions in quantum mechanics. The unit of energy in this system is the Hartree (H), with $1 \text{ H} \approx 27.211 \text{ eV}$. Some results are quoted in eV (electron-Volts) to improve readability.

The many-electron problem

The behaviour and properties of a quantum-mechanical system are described by the Schrödinger equation, which in its most general form is given by

$$i \frac{d}{dt} |\Psi(t)\rangle = \hat{H}(t) |\Psi(t)\rangle, \quad (2.1)$$

where $\hat{H}(t)$ is the time-dependent Hamiltonian, and $|\Psi(t)\rangle$ the time-dependent wave-function. Observable quantities of interest can be calculated from the wave-function,

$$O(t) = \langle \Psi(t) | \hat{O}(t) | \Psi(t) \rangle, \quad (2.2)$$

where $\hat{O}(t)$ is the corresponding operator for the desired observable.

For the work in this thesis, we focus on the specific situation in which the Hamiltonian is time-independent and relativistic effects are ignored. This leads to the following form of the Schrödinger equation,

$$\hat{H} |\Psi_i\rangle = E_i |\Psi_i\rangle, \quad (2.3)$$

where E_i is the energy level corresponding to the i th eigenvector Ψ_i . From now on, we assume we're only interested in finding the ground-state solution $\{\Psi_0, E_0\}$.

For a finite system with N electrons and M nuclei, the Schrödinger equation (2.3)

can be written as

$$\hat{H}\Psi_0(\mathbf{x}_1, \dots, \mathbf{x}_N; \mathbf{R}_1, \dots, \mathbf{R}_M) = E_0\Psi_0(\mathbf{x}_1, \dots, \mathbf{x}_N; \mathbf{R}_1, \dots, \mathbf{R}_M), \text{ with} \quad (2.4)$$

$$\hat{H} = \hat{T}_n + \hat{T}_e + \hat{V}_{nn} + \hat{V}_{ee} + \hat{V}_{en} + \hat{V}_{\text{ext}} \quad (2.5)$$

$$\begin{aligned} &= -\frac{1}{2} \sum_{\alpha}^M \nabla_{\mathbf{R}_{\alpha}}^2 - \frac{1}{2} \sum_i^N \nabla_{\mathbf{x}_i}^2 + \sum_{\alpha < \beta} \frac{Z_{\alpha}Z_{\beta}}{|\mathbf{R}_{\alpha} - \mathbf{R}_{\beta}|} + \sum_{i < j} \frac{1}{|\mathbf{x}_i - \mathbf{x}_j|} \\ &\quad + \sum_{i, \alpha} \frac{Z_{\alpha}}{|\mathbf{x}_i - \mathbf{R}_{\alpha}|} + \hat{V}_{\text{ext}}, \end{aligned} \quad (2.6)$$

where \hat{T}_n and \hat{T}_e are respectively the nuclear and electron kinetic energy terms, \hat{V}_{nn} and \hat{V}_{ee} the nuclear-nuclear and electron-electron repulsions, and \hat{V}_{en} the electron-nuclear attraction. \hat{V}_{ext} represents all terms due to any external (such as magnetic) fields; for the remainder of this thesis we restrict ourselves to cases where any external fields are negligible, $\hat{V}_{\text{ext}} = 0$. We use \mathbf{x}_i to denote the spatial and spin co-ordinates (\mathbf{r}_i, σ_i) of the i th electron, and likewise \mathbf{R}_{α} for spatial and spin co-ordinates of the α th nucleus.

2.1 The Born–Oppenheimer approximation

Solving the full Schrödinger equation (2.4,2.5) can be simplified using the Born–Oppenheimer (BO) approximation [20], in which the motion of the electrons is decoupled from that of the nuclei. This approximation is motivated by the much higher masses of the nuclei relative to the electrons, meaning the nuclei can be approximately treated as classical particles with fixed positions relative to the electrons.

Within the BO approximation, the total wave-function is written as a simple product of the electronic and nuclear states,

$$\Psi^{\text{tot}}(\mathbf{x}_1, \dots, \mathbf{x}_N; \mathbf{R}_1, \dots, \mathbf{R}_M) = \chi(\mathbf{R}_1, \dots, \mathbf{R}_M)\Psi_{\mathbf{R}_1, \dots, \mathbf{R}_M}^{\text{elec}}(\mathbf{x}_1, \dots, \mathbf{x}_N), \quad (2.7)$$

where χ is the nuclear wave-function, and the electronic wave-function Ψ^{elec} depends parametrically on the nuclear co-ordinates. Substituting the product (2.7)

into the Schrödinger equation (2.4), and neglecting terms that couple electronic and nuclear motion, yields the decoupled equations for the electrons and nuclei,

$$\left(\hat{T}_e + \hat{V}_{en} + \hat{V}_{ee}\right) \Psi_{\mathbf{R}}^{\text{elec}}(\mathbf{x}) = E_{\text{elec}}(\mathbf{R}) \Psi_{\mathbf{R}}^{\text{elec}}(\mathbf{x}) \quad (2.8)$$

$$\left(\hat{T}_n + \hat{V}_{nn} + E_{\text{elec}}(\mathbf{R})\right) \chi(\mathbf{R}) = E_{\text{tot}} \chi(\mathbf{R}), \quad (2.9)$$

where the simpler notation \mathbf{R} denotes all the nuclear coordinates and \mathbf{x} the electronic coordinates.

In the BO approximation, the electrons move adiabatically on a potential energy surface $E_{\text{elec}}(\mathbf{R})$ defined by the nuclear positions $\mathbf{R}_1 \dots \mathbf{R}_M$. The BO approximation is usually accurate, but breaks down when different solutions to the electronic Schrödinger equation (2.8) are energetically close. In such situations, it is necessary to go beyond the BO approximation [21]. However, in the remainder of this thesis, it is assumed we do not encounter such situations and hence the BO approximation is used throughout.

2.2 Hartree–Fock theory

We now focus on solving the electronic Schrödinger equation (2.8), which we now denote simply as

$$\left(\hat{T}_e + \hat{V}_{en} + \hat{V}_{ee}\right) \Psi = E \Psi. \quad (2.10)$$

Computationally, this equation is impossible to solve exactly for any system containing more than a few electrons for both memory and speed reasons, and therefore some level of approximation is necessary [17, 22].

In this section, we introduce the Hartree–Fock (HF) method [23]. Although it is not typically still used in calculations, HF is a historically significant method, and the starting point for more advanced wave-function methods; it also features in an important class of approximations in density-functional theory, as we shall see in § 3.6.3. Furthermore, it is insightful tool for understanding the effects of exchange and correlation in electronic structure theory.

We first consider some basic physical properties that the wave-function should satisfy. Firstly, it must be normalized, ie

$$\int d\mathbf{x}_1 \cdots \int d\mathbf{x}_N |\Psi(\mathbf{x}_1, \dots, \mathbf{x}_N)|^2 = 1. \quad (2.11)$$

This condition ensures the probability of finding the N electrons over all space is equal to one. Secondly, because electrons are fermions, it must be antisymmetric with respect to the exchange of two electrons, ie

$$\Psi(\mathbf{x}_1, \dots, \mathbf{x}_i, \dots, \mathbf{x}_j, \dots, \mathbf{x}_N) = -\Psi(\mathbf{x}_1, \dots, \mathbf{x}_j, \dots, \mathbf{x}_i, \dots, \mathbf{x}_N). \quad (2.12)$$

The simplest expression that satisfies the requirements (2.11,2.12) is a single Slater determinant,

$$\Phi_{\text{SD}} = \frac{1}{\sqrt{N!}} = \begin{vmatrix} \psi_1(\mathbf{x}_1) & \psi_2(\mathbf{x}_1) & \dots & \psi_N(\mathbf{x}_1) \\ \psi_1(\mathbf{x}_2) & \psi_2(\mathbf{x}_2) & \dots & \psi_N(\mathbf{x}_2) \\ \vdots & \vdots & \ddots & \vdots \\ \psi_1(\mathbf{x}_N) & \psi_2(\mathbf{x}_N) & \dots & \psi_N(\mathbf{x}_N) \end{vmatrix},$$

where the single-particle orbitals $\psi_i(\mathbf{r})$ are products of spatial and spin functions,

$$\psi_i(\mathbf{r}) = \phi_i(\mathbf{r})\sigma_i(s). \quad (2.13)$$

In Hartree–Fock (HF) theory, we represent the wave-function in the above manner using a single Slater determinant, with the optimal determinant calculated from the Rayleigh-Ritz variational principle. The variational principle states that for a normalized and anti-symmetric trial wave-function $\tilde{\Psi}$,

$$\langle \tilde{\Psi} | \hat{H} | \tilde{\Psi} \rangle \geq E_0, \quad (2.14)$$

with E_0 the ground-state energy of the exact wave-function. Searching the N -electron Hilbert space to find the wave-function which minimizes $\langle \tilde{\Psi} | \hat{H} | \tilde{\Psi} \rangle$ would yield the exact wave-function, the only $\tilde{\Psi}$ for which equality holds in inequality (2.14) (assuming no degeneracies). In HF theory, this search is restricted to

single Slater determinants of N -electrons, and thus the HF wave-function is defined as

$$\Phi_{\text{HF}} = \min_{\Phi_{\text{SD}} \rightarrow N} \langle \tilde{\Psi} | \hat{H} | \tilde{\Psi} \rangle, \quad (2.15)$$

under the additional constraint that the single-particle orbitals in the Slater determinant are orthonormal.

2.2.1 The Hartree–Fock equations

We perform the minimization over all Slater determinants (2.15) by making the energy stationary with respect to variations in the single-particle orbitals, under the constraint that the spatial orbitals are orthonormal (the spin orbitals are orthonormal by definition). Imposing the orthonormality constraint through Lagrange multipliers, the minimization leads to the following HF equations,

$$\hat{F}_i \phi_i = \sum_j^N \lambda_{ij} \phi_j \quad (2.16)$$

where λ_{ij} are the Lagrange multipliers. \hat{F}_i is known as the Fock operator and it is equal to

$$\hat{F}_i = \hat{h}_i + \hat{J}_i - \hat{K}_i, \quad (2.17)$$

where \hat{h}_0 defines the local part of the Hamiltonian consisting of kinetic and electron-nuclear potential terms,

$$\hat{h}_i = -\frac{\nabla_i^2}{2} + v_{\text{en}}(\mathbf{r}_i). \quad (2.18)$$

\hat{J}_i and \hat{K}_i are respectively the Coulomb and non-local exchange operators,

$$\hat{J}_i \phi_i(\mathbf{r}_i) = \sum_j^N \phi_i(\mathbf{r}_i) \int d\mathbf{r}_j \frac{|\phi_j(\mathbf{r}_j)|^2}{|\mathbf{r}_i - \mathbf{r}_j|}, \quad (2.19)$$

$$\hat{K}_i \phi_i(\mathbf{r}_i) = \sum_{j \in \sigma}^N \phi_j(\mathbf{r}_i) \int d\mathbf{r}_j \frac{\phi_j^*(\mathbf{r}_j) \phi_i(\mathbf{r}_j)}{|\mathbf{r}_i - \mathbf{r}_j|}, \quad (2.20)$$

where the summation in the exchange term (2.20) only includes orbitals ϕ_j with the same spin as ϕ_i . This is because the exchange term arises from the indistinguishability of two electrons with the same spin; if two such electrons are exchanged, the energy is unchanged and the wave-function changes only by a sign.

By making a unitary transformation the HF equations (2.16) are transformed into the following eigenvalue form,

$$\hat{F}\phi_i = \epsilon_i\phi_i. \quad (2.21)$$

This defines a set of simultaneous equations for each of the orbitals in the HF Slater determinant Φ_{HF} .

The HF energy is equal to

$$E_{\text{HF}} = \langle \Phi_{\text{HF}} | \hat{H} | \Phi_{\text{HF}} \rangle \quad (2.22)$$

$$= \sum_{i=1}^N \left[\langle \phi_i | \hat{h}_i | \phi_i \rangle + \frac{1}{2} \langle \phi_i | \hat{J}_i - \hat{K}_i | \phi_i \rangle \right]. \quad (2.23)$$

The HF orbitals do not have a strict physical interpretation; however, they are often associated with the molecular orbitals (MOs), and the corresponding quantities $\epsilon_{i\sigma}$ as the energy eigenvalues of these MOs. In fact, these eigenvalues do have physical meaning. In Koopman’s theorem [24], it is shown that the k th ionization energy I_k is equal to the negative of the k th eigenvalue ϵ_k ,

$$I_k = E[N - 1, k] - E[N] = -\epsilon_k, \quad (2.24)$$

where $E[N - 1, k]$ is the energy with the k th electron removed. The above relation assumes the “frozen MO” approximation, in which the MOs of the systems with N and $N - 1$ electrons are taken to be identical.

2.2.2 Solving the Hartree–Fock equations

To solve the HF equation (2.21), one typically expands the orbitals in a basis set,

$$\phi_i(\mathbf{r}) = \sum_k c_{ik} \xi_k(\mathbf{r}). \quad (2.25)$$

There are various choices for the basis set which will be discussed in § 3.9.1. For now, we assume the chosen basis represents the orbitals sufficiently well.

Expanding the orbitals in the above manner, and taking the inner product with a basis element $\xi_l(\mathbf{r})$, defines the matrix equation

$$FC = SC\epsilon, \quad (2.26)$$

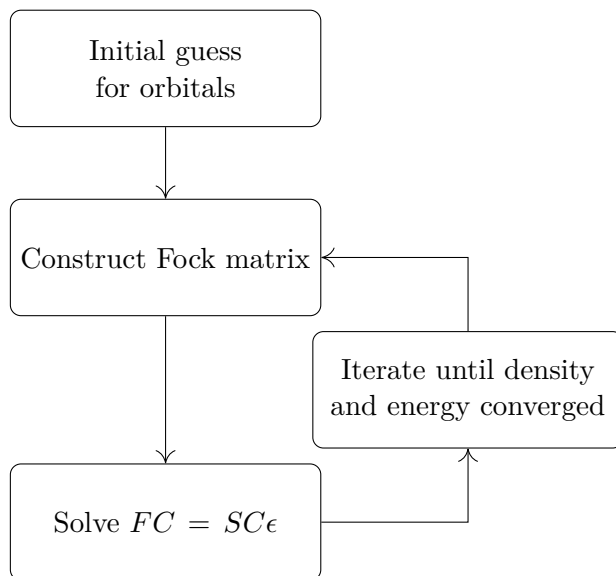


Figure 2.1: Illustration of the SCF procedure

where F and S are the Fock and overlap matrices respectively,

$$F_{kl} = \langle \xi_k | \hat{F} | \xi_l \rangle, \quad (2.27)$$

$$S_{kl} = \langle \xi_k | \xi_l \rangle; \quad (2.28)$$

and C and ϵ are the matrices containing the coefficients c_{ik} and ϵ_i . The matrix equation (2.26), which is known as the Roothaan-Hall equation [25, 26], can be solved with standard linear algebra techniques. However, because the HF orbitals, and thus the coefficients c_{ik} , are present in the Fock matrix F_{kl} , this equation has to be solved in a self-consistent manner. This self-consistent field procedure (SCF) is outlined in Fig. 2.1.

2.2.3 Restricted and unrestricted Hartree–Fock

The only restriction we’ve so far imposed on the spatial orbitals that form the HF determinant is that they must be orthonormal. However, in closed-shell calculations, there is usually an additional restriction imposed, namely that each spatial orbital can accommodate two electrons of opposite spins, or in other words $\phi_i^\uparrow = \phi_i^\downarrow$. This is known as the restricted Hartree–Fock (RHF) method.

We can impose this kind of restriction for an open-shell calculation, by forcing all the spatial orbitals except that of the unpaired electron to be doubly occupied. This is known as restricted open-shell Hartree–Fock (ROHF) [27]. However, this restriction is typically not imposed for an open-shell system, so $\phi_i^\uparrow \neq \phi_i^\downarrow$ in general: this is known as unrestricted Hartree–Fock (UHF), and it can also be used in closed-shell calculations.

It is important to note that the UHF wave-function is not an eigenfunction of the operator \hat{S}^2 , or in other words it is said to be spin-contaminated. This means it can contain contributions from different spin states which can be advantageous in accounting for certain types of electron correlation, as we shall see in the next section. However, this spin-contamination is also the source of various problems [28], for example erroneous potential energy surfaces [29], inaccurate reaction barrier predictions [30], and difficulties computing spectroscopic properties [28]; furthermore, these errors often propagate to the ‘post-HF’ correlated methods which we discuss shortly in § 2.4 [31].

2.3 Electron correlation

In the broadest possible sense, electron correlation simply refers to the interacting nature of electrons, in that the electron density in one region is not independent of the electron density elsewhere. However, in quantum chemistry, the term electron correlation describes all the effects that are not captured by the (restricted) HF approximation. The correlation energy is usually defined as

$$E_c = E_0 - E_{\text{RHF}}, \quad (2.29)$$

where E_0 is the total (exact) energy. Although the correlation energy usually only contributes around 1% of the total energy [32], it is important in many applications (as we are rarely interested in simply finding the total energy).

HF theory is often described as a ‘mean-field’ theory, because each electron experiences a potential which depends only on the average positions of the other electrons, and not on their individual positions. In reality, the potential experienced by an electron does depend on the instantaneous positions of all the other electrons. This effect, which is not captured in any HF implementation, is commonly referred to as ‘dynamic’ correlation. The absence of dynamic correlation in the HF approximation means the probability of an electron being in the vicinity of another is slightly higher in HF than it should be (in other words, the electron charge has a tendency to over-localize).

Another correlation effect arises when degenerate Slater determinants emerge, which is commonly called ‘static’ correlation. A typical example of when this kind of correlation is important is when an H_2 molecule is stretched: in the RHF approximation, there is just a single determinant which assigns equal probability to the molecule dissociating into two ions as into two neutral atoms, when the correct behaviour is to dissociate into two atoms. This kind of correlation is, to an extent, captured by UHF, because it can break symmetry and form a mixed singlet and triplet state. A comparison of energy dissociation curves for H_2 between the RHF, UHF and CCSD(T) (a correlated method introduced in the next section) methods is shown in Fig. 2.2. However, this is only an example of static correlation, and other static correlation effects cannot be captured so well with an unrestricted description [33]. Furthermore, although we have drawn a distinction between static and dynamic correlation, the two are intrinsically linked and thus it is notoriously difficult to formally define them as separate effects [34].

2.4 Correlated methods

In this section, we briefly introduce three of the most popular methods which go beyond HF by including correlation effects: configuration interaction, many-body

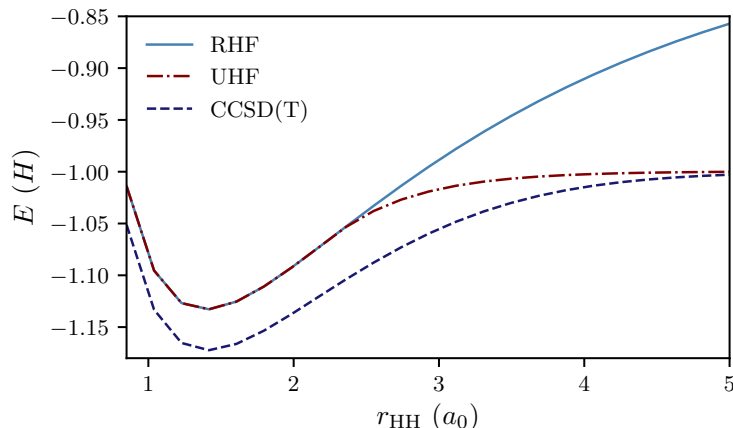


Figure 2.2: Energy dissociation curves for the H_2 molecule, for RHF, UHF and CCSD(T) methods.

perturbation theory (Møller–Plesset)*, and coupled cluster. An understanding of these methods is relevant to the objectives of this thesis, since we shall use them in Chapters 4 and 5 to guide the development of new approximations in DFT. All the methods are based on expanding the wave-function using multiple determinants,

$$\Psi = a_0\Psi_{\text{HF}} + \sum_{i=1} a_i\Phi_i, \quad (2.30)$$

with the coefficients a_i being determined by the method being used. These methods are often described as ‘post Hartree–Fock’ because the first term in the expansion is the HF determinant.

In all the methods to be described, the determinants Φ_i are formed by removing occupied orbitals in the HF determinant, and replacing them with virtual (unoccupied) ones in the basis set. These are akin to excitations from the HF determinant and are labelled according to the number of excitations: so one swap is a single excitation, two is a double, and so on.

*We focus here on the flavour of many-body perturbation theory which is popular in quantum chemistry. We do not discuss the Green’s function approach to many-body perturbation theory [35], which is widely-used in the solid-state community, because it is less relevant to this thesis.

2.4.1 Configuration interaction

Configuration interaction (CI) methods [36], like HF, are based on the variational principle. The wave-function is expanded as follows

$$\Psi_{\text{CI}} = (\hat{1} + \hat{C}_1 + \hat{C}_2 + \dots)\Phi_0, \quad (2.31)$$

with \hat{C}_k denoting the set of excitations with k orbitals excited from the ground-state determinant Φ_0 to the virtual space. The expression $\langle \Psi_{\text{CI}} | \hat{H} | \Psi_{\text{CI}} \rangle$ is minimized, under the constraint that the wave-function is normalized.

If all excitations in the given basis set are included (up to $\hat{C}_{n_{\text{bas}}}$), the method is known as full CI. In this case, all possible correlation in that basis is accounted for, and the results can only be improved by using a larger basis set.

It is impossible to do a full CI calculation for any system which contains more than a handful of electrons. This is because the number of determinants scales factorially with the size of the basis set, making it rapidly inaccessible (although a novel stochastic approach enables far larger systems to be studied with almost full CI accuracy [37, 38]). Instead, it is normal to only consider excitations up to a certain order, which is known as truncated CI. The most common approach is to include singlet and doublet terms (CISD). Higher-order terms can be included, but it is necessary to include at least doublet excitations as singlets alone have no effect due to Brillouin's Theorem [39].

Before continuing, we introduce the following two concepts:

- i *Size consistency*: This means the energy of a dissociated molecule should equal the energy of the separate atomic fragments, or in other words

$$E(A + B)_{r_{AB} \rightarrow \infty} = E(A) + E(B); \quad (2.32)$$

- ii *Size extensivity*: This means the energy of a system which consists of n_A identical components A , where A is (for example) an atom or molecule, should

correctly scale with n_A , or in other words

$$E(n_AA) = n_A E(A), \quad (2.33)$$

Full CI satisfies both of the above criteria, however truncated CI satisfies neither. In particular, the absence of size extensivity in truncated CI means that it performs worse with increasing system size.

2.4.2 Many-body perturbation theory

A different route, many-body perturbation theory (MPBT), begins with a perturbative expansion for the Hamiltonian

$$\hat{H} = \hat{H}_0 + \lambda V'. \quad (2.34)$$

If the zeroth-order term \hat{H}_0 is chosen to be non-interacting, then the zeroth-order wave-function is known exactly and is a single determinant. The idea is then to use an interacting perturbation V' to introduce correlation. The first-order energy and wave-function are given in the standard perturbative manner by

$$E^{(1)} = \langle \Phi_0 | V' | \Phi_0 \rangle, \text{ and} \quad (2.35)$$

$$|\Phi^{(1)}\rangle = \sum_{n \text{ sgl}} \frac{\langle \Phi_n | V' | \Phi_0 \rangle}{E_0 - E_1} |\Phi_n\rangle, \quad (2.36)$$

where the summation (2.36) runs over all singlet excitations from Φ_0 .

Thus far, we have not specified what the unperturbed term H_0 and perturbation V' are given by. The most common choice is the following,

$$\hat{H}_0 = \sum_i^N \hat{F}_i = \sum_i^N \hat{h}_i + (\hat{J}_i - \hat{K}_i) \quad (2.37)$$

$$\hat{V}' = \hat{V}_{ee} - \sum_i^N (\hat{J}_i - \hat{K}_i), \quad (2.38)$$

where the single-particle terms h_i , \hat{J}_i and \hat{K}_i are defined by equations (2.18,2.20). With this choice, the method is often called Møller–Plesset (MP) perturbation

theory [40, 41], or just MBPT [42]. The energy up to first order E_{MP1} is given by

$$E_{\text{MP0}} = \langle \Phi_{\text{HF}} | \sum_i \hat{F}_i | \Phi_{\text{HF}} \rangle = \sum_i^N \langle \phi_i | \hat{h}_i | \phi_i \rangle + \langle \phi_i | \hat{J}_i - \hat{K}_i | \phi_i \rangle \quad (2.39)$$

$$E_{\text{MP1}} = \langle \Phi_{\text{HF}} | \hat{V}_{\text{ee}} - \sum_i (\hat{J}_i - \hat{K}_i) | \Phi_{\text{HF}} \rangle = -\frac{1}{2} \sum_i^N \langle \phi_i | \hat{J}_i - \hat{K}_i | \phi_i \rangle. \quad (2.40)$$

Hence we see that, up to first order, the energy is identical to HF as $E_{\text{MP0}} + E_{\text{MP1}} = E_{\text{HF}}$. The first contribution which includes correlation effects is therefore the second-order term in the perturbation. Due to Brillouin's theorem [39], all contributions to the second-order energy from singlet excitations vanish, and thus the second order energy is given by the sum over doublet excitations only,

$$E_{\text{MP2}} = \sum_{i < j}^{\text{occ}} \sum_{a < b}^{\text{unocc}} \frac{\langle \Phi_0 | V' | \Phi_{ij}^{ab} \rangle \langle \Phi_{ij}^{ab} | V' | \Phi_0 \rangle}{E_0 - E_{ij}^{ab}}, \quad (2.41)$$

where occ and unocc denote the occupied and unoccupied (virtual) orbitals in the HF determinant. The MP2 energy tends to account for 80%-95% [32, 43] of the total correlation energy. Its accuracy combined with its moderate scaling of n_{bas}^5 , and the fact that it satisfies size extensivity, makes MP2 a popular post-HF method, even though it is not variational.

It is of course possible to add higher-order perturbative terms. However, this highlights one of the problems with MBPT methods, in that the perturbative corrections are not guaranteed to converge monotonically to the correct answer. This is related to the fact that the zeroth-order wave-function is not necessarily close to the fully-interacting one. Indeed, it is observed that going to third-order usually gives a worse answer than MP2; however, once fourth-order terms are introduced (MP4), we do see improvement compared to MP2, albeit at a worse cost of n_{bas}^7 .

2.4.3 Coupled cluster

In MBPT, all types of *excitation* (singles, doubles, and so on) are included up to a given order. As discussed, this perturbative approach does not guarantee

convergence to the exact answer. The idea behind coupled cluster (CC) theory [44] is to include all *orders* of perturbation for a given group of excitations. Thus, CC can be thought of as an infinite-order perturbation theory.

In CC, we use the following exponential ansatz for the wave-function,

$$\Psi_{CC} = e^{\hat{T}} \Phi_0; \quad (2.42)$$

where \hat{T} is a sum over excitation operators,

$$\hat{T} = \hat{T}_1 + \hat{T}_2 + \dots + \hat{T}_N, \text{ with} \quad (2.43)$$

$$\hat{T}_1 \Phi_0 = \sum_i^{\text{occ}} \sum_a^{\text{unocc}} t_i^a \Phi_i^a, \quad \hat{T}_2 \Phi_0 = \sum_{i < j}^{\text{occ}} \sum_{a < b}^{\text{unocc}} t_{ij}^{ab} \Phi_{ij}^{ab}, \quad (2.44)$$

and so on. The amplitudes t_i^a, t_{ij}^{ab} are determined by solving the Schrödinger equation using the CC ansatz for the wave-function (2.42). Writing the exponential operator $e^{\hat{T}}$ as a Taylor expansion, we see how to generate expansions for a given level of excitations:

$$e^{\hat{T}} = \hat{1} + \hat{T}_1 + \left(\hat{T}_2 + \frac{\hat{T}_1^2}{2} \right) + \left(\hat{T}_3 + \hat{T}_1 \hat{T}_2 + \frac{\hat{T}_1^3}{6} \right) + \dots \quad (2.45)$$

Let us analyse the terms that contribute to double excitations from Φ_0 . There are two terms, \hat{T}_2 and $\frac{\hat{T}_1^2}{2}$. The \hat{T}_2 term is called ‘disconnected’ and it is the same as the configuration interaction doubles (CID) expression. We see therefore that an additional term, $\frac{\hat{T}_1^2}{2}$, emerges in CC doubles (CCD) which is not present in CID. We call this a ‘connected’ term and we can see similar excitations are present at all orders of the expansion. Thanks to the presence of these terms, CC methods are size extensive regardless of when they are truncated, unlike truncated CI.

The CC energy is calculated as follows

$$\hat{H} \Psi_{CC} = E_{CC} \Psi_{CC} \Rightarrow \hat{H} e^{\hat{T}} \Phi_0 = E_{CC} e^{\hat{T}} \Phi_0 \Rightarrow E_{CC} = \langle \Phi_0 | \hat{H} e^{\hat{T}} | \Phi_0 \rangle, \quad (2.46)$$

where the final equation drops out because there is no overlap between Φ_0 and its excited states.

Including higher order excitations in CC methods will give convergence to the full CI solution. CC with singles and doubles, CCSD, has comparable accuracy to

MP4 with better scaling of n_{bas}^6 . Including triples, CCSDT, scales as n_{bas}^8 and is thus usually considered too computationally demanding. However, a very popular approach involves combining CC and MBPT to include triple order excitations in a perturbative manner, by choosing those from MBPT which give the largest contributions to the energy: this is known as CCSD(T) [45].

Density-functional theory

As discussed in the previous chapter, the electronic Schrödinger equation (2.10) is impossible to solve exactly for any system larger than a few electrons, making approximate methods essential. The methods in the last chapter were all focussed on approximating the *wave-function*; in this chapter, we introduce density-functional theory (DFT), which takes a very different approach by instead using the electronic *density* to calculate observables.

Before considering the question of whether it is actually possible to bypass the wave-function and compute observables with the density, we comment on the considerable advantages of this approach. The electronic density, given by

$$\rho(\mathbf{r}) = N \int d\sigma \int d\mathbf{x}_1 \cdots \int d\mathbf{x}_N |\Psi(\mathbf{r}, \sigma; \mathbf{x}_1; \dots; \mathbf{x}_N)|^2, \quad (3.1)$$

is just a function of three spatial variables. The density therefore has vastly superior scaling compared to the wave-function-based methods described in the last chapter. This scalability, alongside many other desirable properties, has made DFT the most popular electronic structure method in materials, Chemistry and beyond [11].

In this chapter, we first review the theoretical foundations of DFT, and the Kohn–Sham scheme which is the most widely-used formulation of DFT. Later, we discuss some of the most popular approximations used and their limitations. We finish with a discussion of computational implementation, with a particular focus on the type of implementation used for calculations in this thesis.

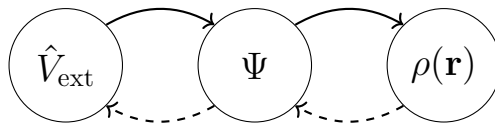


Figure 3.1: Schematic of the 1:1 mapping in the first HK theorem

3.1 Hohenberg–Kohn theorems

The question of whether we are justified in using the electronic density as a fundamental variable for calculations is answered by the Hohenberg–Kohn (HK) theorems [8]. The first theorem proves there exists a one-to-one mapping between the ground-state density and the external potential; since the external potential defines the Hamiltonian, this means the wave-function is a unique *functional* of the density and thus all ground-state observables are (in principle) determined by the density alone. The second theorem, using the variational principle, establishes a path to determine this ground-state density.

3.1.1 Hohenberg Kohn first theorem: one-to-one mapping

The first HK theorem proves that the ground-state density uniquely determines the external potential, up to an additive constant. The proof is in two parts:

1. **Two potentials differing by more than a constant yield different wave-functions.**

Proof. The proof is by contradiction. Consider two potentials, \hat{V}_1 and \hat{V}_2 , which share the same wave-function Ψ and differ by more than a constant.

The Schrödinger equations for these two systems are

$$(\hat{T} + \hat{V}_{\text{ee}} + \hat{V}_1)\Psi = E_1\Psi; \quad (3.2)$$

$$(\hat{T} + \hat{V}_{\text{ee}} + \hat{V}_2)\Psi = E_2\Psi. \quad (3.3)$$

Taking the difference of the above equalities gives

$$(\hat{V}_1 - \hat{V}_2)\Psi = (E_1 - E_2)\Psi = c\Psi; \quad (3.4)$$

because \hat{V} is a multiplicative potential we can divide both sides of the above equation by Ψ (assuming $\Psi \neq 0$) which gives

$$\hat{V}_1 - \hat{V}_2 = \sum_i v_1(\mathbf{r}_i) - v_2(\mathbf{r}_i) = c. \quad (3.5)$$

Hence we see that two potentials giving the same wave-function can differ only by a constant, which contradicts the initial premise and completes the proof.*

2. Two ground-state wave-functions, arising from different potentials, yield two different ground-state densities.

Proof. This also proceeds by contradiction. Consider two different wave-functions, Ψ_1 and Ψ_2 , which by the first step of the proof must emerge from different potentials \hat{V}_1 and \hat{V}_2 . By the variational principle, the following conditions must hold:

$$\langle \Psi_1 | \hat{H}_1 | \Psi_1 \rangle < \langle \Psi_2 | \hat{H}_1 | \Psi_2 \rangle, \text{ and} \quad (3.6)$$

$$\langle \Psi_2 | \hat{H}_2 | \Psi_2 \rangle < \langle \Psi_1 | \hat{H}_2 | \Psi_1 \rangle. \quad (3.7)$$

Taking the difference of the above inequalities yields

$$\int d\mathbf{r} [v_1(\mathbf{r}) - v_2(\mathbf{r})][\rho_1(\mathbf{r}) - \rho_2(\mathbf{r})] < 0. \quad (3.8)$$

Clearly, if $\rho_1 = \rho_2$, the above expression is absurd and therefore $\rho_1 \neq \rho_2$, which completes the proof.

Inequalities (3.6) and (3.7), and by extension the HK proofs, hold only for non-degenerate ground-states. However, the requirement of non-degeneracy is lifted in the Levy constrained search formulation which we come to in § 3.2.

With the unique mapping between the density and external potential established, we can write the energy as a functional of the density. In DFT, this energy func-

*Strictly speaking, equation (3.5) does not guarantee that $v_1(\mathbf{r}) - v_2(\mathbf{r}) = c$ everywhere; however, under the reasonable assumption that the external potentials $v_1(\mathbf{r})$ and $v_2(\mathbf{r})$ are everywhere continuous, it holds that $v_1(\mathbf{r}) - v_2(\mathbf{r}) = c$.

tional is usually written as

$$E_{v_{\text{en}}}[\rho] = \int d\mathbf{r} \rho(\mathbf{r})v_{\text{en}}(\mathbf{r}) + F_{\text{HK}}[\rho], \text{ with} \quad (3.9)$$

$$F_{\text{HK}}[\rho] = T[\rho] + E_{\text{ee}}[\rho] = \langle \Psi_\rho | \hat{T} + \hat{V}_{\text{ee}} | \Psi_\rho \rangle. \quad (3.10)$$

This is a powerful equation: it states that, were the density and the HK functional F_{HK} known, then the energy would be known exactly without any knowledge of the wave-function. Of course, the exact form of the functional is unknown (and deriving it would be equally difficult as solving the full many-electron problem [46, 47]); however, a number of good approximations exist, which we shall visit later in this chapter.

3.1.2 Hohenberg–Kohn second theorem: variational principle

The first HK theorem establishes the density is sufficient as a basic variable in electronic structure theory, but does not indicate how to compute the density without knowledge of the wave-function. In other words, it raises the question: how do we know a given density is (or is close to) the ground-state density?

The second HK theorem addresses this question using the variational principle. Suppose we have a trial density, $\tilde{\rho}$, which has ground-state wave-function $\tilde{\Psi}$. By the variational principle,

$$\langle \tilde{\Psi} | \hat{H} | \tilde{\Psi} \rangle = E_{v_{\text{en}}}[\tilde{\rho}] \geq E_{v_{\text{en}}}[\rho_0] = \langle \Psi_0 | \hat{H} | \Psi_0 \rangle, \quad (3.11)$$

where ρ_0 and Ψ_0 are the ground-state density and wave-function of the fully-interacting system with Hamiltonian \hat{H} . This proves that we can find the ground-state energy (and wave-function) by finding the minimum of the energy functional over all densities. Thus, we have established not only that the density contains all the information we need, but also that this density can be uniquely determined in a variational manner. Varying the energy functional (3.9) with respect to the density yields the Euler equation in DFT,

$$\frac{\delta F_{\text{HK}}[\rho]}{\delta \rho(\mathbf{r})} + v_{\text{en}}(\mathbf{r}) = \mu. \quad (3.12)$$

In the original HK formulation, only variations which conserve the total electron number are permitted, and μ is a Lagrange multiplier which enforces this constraint. However, if this requirement is relaxed and the energy is allowed to vary with electron number, it can be shown that μ is equal to the partial derivative of the ground-state energy with respect to electron number N [48],

$$\mu = \frac{\partial E_{v_{\text{en}}}[\rho_0]}{\partial N}, \quad (3.13)$$

and thus μ is commonly known as the chemical potential. The identification of μ with the chemical potential can also be shown using the extension of DFT to thermal ensembles [49], and taking the limit of zero temperature to derive the ground-state relation (3.13).

3.2 The constrained search formulation

The HK functional $F_{\text{HK}}[\rho]$ (3.10) is only defined for densities which correspond to ground-state anti-symmetric wave-functions defined by an external field $v_{\text{en}}(\mathbf{r})$; we call these densities v -representable. This is a limitation of the second HK theorem because it is possible to construct trial densities which obey sensible physical restrictions, but are not v -representable.

This problem was addressed by Levy and Lieb in the so-called constrained search approach [50–52]. This formulation removes the condition on the density to be v -representable and instead imposes the much less severe restriction of N -representability. A N -representable density must only be normalized and everywhere non-negative.

This procedure connects with the variational search in wave-function theory seen in the previous chapter, in which we search over all possible anti-symmetric wave-functions Ψ (with correct normalization) to find that wave-function which minimizes the energy. The search proceeds in two steps as follows:

1. For a given density ρ_α , search over all normalized anti-symmetric wave-functions yielding that density, to find that which yields the minimum energy

for that density,

$$E_0[\rho_\alpha; v_{\text{en}}] = \min_{\Psi \rightarrow \rho_\alpha} \langle \Psi | \hat{H} | \Psi \rangle. \quad (3.14)$$

2. Now search over all the space of all densities considered in the prior step, $\rho_\alpha, \rho_\beta, \dots$, to find that density which minimizes the energy,

$$E_0[v_{\text{en}}] = \min_{\rho_\alpha} E_0[\rho_\alpha; v_{\text{en}}]. \quad (3.15)$$

This procedure ensures that only v -representable densities, ie those which come from a valid wave-function, are considered in the variational procedure in DFT. It can be succinctly expressed as

$$E_0[v_{\text{en}}] = \min_{\rho \rightarrow N} \left\{ F[\rho] + \int d\mathbf{r} \rho(\mathbf{r}) v_{\text{en}}(\mathbf{r}) \right\}, \quad (3.16)$$

with the so-called universal functional $F[\rho]$ given by

$$F[\rho] = \min_{\Psi \rightarrow \rho} \langle \Psi | \hat{T} + \hat{V}_{\text{ee}} | \Psi \rangle. \quad (3.17)$$

We note that, besides N -representability, the search is restricted to densities whose von Weizsaecker kinetic energy is finite, $\int d\mathbf{r} |\nabla \rho^{1/2}(\mathbf{r})|^2 < \infty$.

Additionally, we note that the above formulation lifts the non-degeneracy requirement of the original HK theorems, because during the initial search (3.14), only a single wave-function of the possible wave-functions that yield a certain ground-state energy is chosen.

3.3 Thomas–Fermi and orbital-free DFT

Having established that the electronic density can provide a complete description of electrons in matter, the question becomes: how do we express the energy as a functional of the density? The first attempt at this was made by Thomas and Fermi [53, 54], some time before the HK theorems themselves were introduced. In the Thomas–Fermi (TF) method, the kinetic energy functional is constructed by splitting the electron density into a series of small volume elements in momentum

space (with radius equal to the Fermi momentum), and approximating the density in these sub-regions to be uniform. This approximation is based on the homogeneous electron gas (HEG), which is an important concept in DFT, forming the basis for several important approximations. The electron-electron interactions are taken to be classical, leading to the following energy functional,

$$E_{\text{TF}}[\rho] = \frac{3}{10}(3\pi^2)^{\frac{2}{3}} \int d\mathbf{r} \rho^{\frac{5}{3}}(\mathbf{r}) + \int d\mathbf{r} \rho(\mathbf{r})v_{\text{en}}(\mathbf{r}) + \frac{1}{2} \int d\mathbf{r} \int d\mathbf{r}' \frac{\rho(\mathbf{r})\rho(\mathbf{r}')}{|\mathbf{r} - \mathbf{r}'|}. \quad (3.18)$$

This is a historically important result, being the first attempt to express the energy in terms of the density. Unfortunately, it is of no use in a practical sense as it fails to predict even the most basic material properties, due largely to the inadequacy of the TF kinetic energy functional, but also due to the neglect of exchange and correlation effects in the electron-electron interaction term.

As we shall soon see, the most popular approach in DFT is to begin with an auxiliary system of non-interacting electrons. Methods which construct the energy as a direct functional of the density in the style of Thomas–Fermi are known as ‘orbital-free’ DFT [55, 56]. These methods do not currently offer the level of accuracy required to be of practical use due to the challenge of constructing a kinetic energy density-functional [57]; but they continue to be of interest because they have significant computational advantages compared to using an auxiliary system. In particular, there has been a recent surge of interest in applying machine-learning techniques to develop orbital-free functionals [58–61].

3.4 Kohn–Sham theory

The Kohn–Sham (KS) formulation of DFT cunningly avoids the difficult problem of constructing a kinetic energy density functional, and is by far the most widely-used approach in DFT. The theory, developed by Kohn and Sham [9], imagines an auxiliary system of *non-interacting* electrons with the *same* density as the interacting system (see Fig. 3.2 for a visual representation of this concept). The advantage

of this is immediate, in that the kinetic energy for a non-interacting system (whose wave-function is a Slater determinant) is known exactly in terms of the orbitals,

$$T_s[\rho] = \langle \Phi_{\text{KS}} | \hat{T} | \Phi_{\text{KS}} \rangle = -\frac{1}{2} \sum_{i=1}^N \int d\mathbf{r} \phi_i^*(\mathbf{r}) \nabla^2 \phi_i(\mathbf{r}), \quad (3.19)$$

with the density defined in the usual way for a Slater-determinant,

$$\rho(\mathbf{r}) = \sum_{i=1}^N |\phi_i(\mathbf{r})|^2. \quad (3.20)$$

The kinetic energy functional is an *implicit* density-functional through its dependence on the KS orbitals, which depend implicitly on the density.

The electron-nuclear energy is defined exactly in terms of the density in the normal manner, and the electron-electron interaction energy is approximated using the classical (Hartree) expression,

$$E_{\text{en}}[\rho] = \int d\mathbf{r} \rho(\mathbf{r}) v_{\text{en}}(\mathbf{r}); \quad (3.21)$$

$$E_{\text{H}}[\rho] = \frac{1}{2} \int d\mathbf{r} \int d\mathbf{r}' \frac{\rho(\mathbf{r})\rho(\mathbf{r}')}{|\mathbf{r} - \mathbf{r}'|}. \quad (3.22)$$

The non-interacting kinetic energy and Hartree energy do not account for the quantum-mechanical nature of electron interactions. An extra term, the *exchange-correlation* (xc) energy, is therefore introduced in the total energy functional to include these effects. It is defined formally as

$$E_{\text{xc}}[\rho] = T[\rho] - T_s[\rho] + E_{\text{ee}}[\rho] - E_{\text{H}}[\rho], \quad (3.23)$$

with $E_{\text{ee}}[\rho]$ and $T[\rho]$ defined by the universal functional (3.17),

$$T[\rho] + E_{\text{ee}}[\rho] = \min_{\Psi \rightarrow \rho} \langle \Psi | \hat{T} + \hat{V}_{\text{ee}} | \Psi \rangle. \quad (3.24)$$

In principle, KS theory is formally exact (unlike HF); if the xc-energy were known exactly then we would have the exact energy functional. As we are about to see, this is not the case, although a number of good approximations exist.

With the KS energy functional given by

$$E_{\text{KS}}[\rho] = -\frac{1}{2} \sum_{i=1}^N \int d\mathbf{r} \phi_i^*(\mathbf{r}) \nabla^2 \phi_i(\mathbf{r}) + \int d\mathbf{r} \rho(\mathbf{r}) v_{\text{en}}(\mathbf{r}) + \frac{1}{2} \int d\mathbf{r} \int d\mathbf{r}' \frac{\rho(\mathbf{r})\rho(\mathbf{r}')}{|\mathbf{r} - \mathbf{r}'|} + E_{\text{xc}}[\rho], \quad (3.25)$$

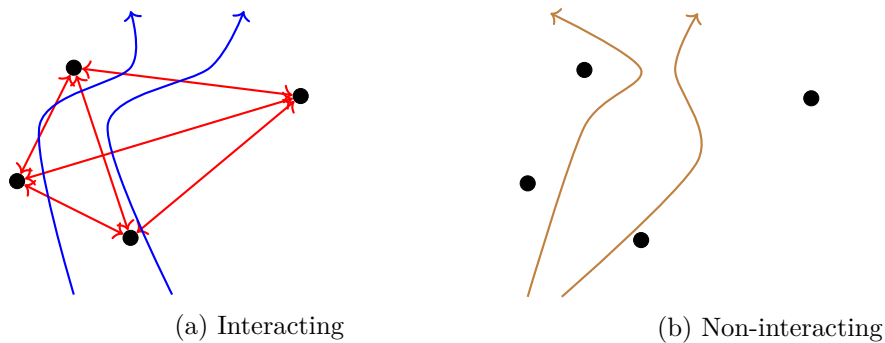


Figure 3.2: Illustration of the Kohn–Sham concept. An interacting system is transformed into a non-interacting one with the same density.

this is minimized with respect to the density which yields the KS equation for the orbitals,

$$\left(-\frac{\nabla^2}{2} + v_s[\rho](\mathbf{r})\right) \phi_i(\mathbf{r}) = \epsilon_i \phi_i(\mathbf{r}), \text{ with} \quad (3.26)$$

$$v_s[\rho](\mathbf{r}) = v_{\text{en}}(\mathbf{r}) + \int d\mathbf{r}' \frac{\rho(\mathbf{r}')}{|\mathbf{r} - \mathbf{r}'|} + \frac{\delta E_{\text{xc}}[\rho]}{\delta \rho(\mathbf{r})}. \quad (3.27)$$

Much like the HF equation (2.21), the KS equations must be solved in a self-consistent manner, as the orbitals define the KS potential $v_s[\rho]$. More details on the numerical implementation of KS DFT can be found at the end of this chapter.

3.5 Spin density-functional theory and open-shell systems

The unique mapping between the external potential and density in the original HK theorems is valid only for spin-unpolarized external potentials. The extension to spin-polarized systems, in which a unique map is established between a spin-polarized external potential and a spin-density, was first proposed by von Barth and Hedin [62]. The proof is similar to the HK theorem (see Fig. 3.1): two invertible maps are established, firstly between the spin-potential and ground-state wave-function, and then between the wave-function and spin-density. The uniqueness of the first mapping does not hold in general [63, 64]; however, it has been shown both

practically [65] and theoretically [66] that this mapping is indeed unique, except for fully spin-polarized systems (including one-electron systems).

In the KS formulation of spin-DFT, the KS energy functional (3.25) is minimized with respect to the spin-densities $\rho^\sigma(\mathbf{r})$, rather than the total density. This leads to the following spin-KS equations (sometimes referred to as the spin-unrestricted or just unrestricted KS equations),

$$\left\{ -\frac{\nabla^2}{2} + v_{\text{ext}}^\sigma(\mathbf{r}) + v_{\text{H}}(\mathbf{r}) + v_{\text{xc}}^\sigma(\mathbf{r}) \right\} \phi_i^\sigma(\mathbf{r}) = \epsilon_i^\sigma \phi_i^\sigma(\mathbf{r}), \text{ with} \quad (3.28)$$

$$v_{\text{xc}}(\mathbf{r}) = \frac{\delta E_{\text{xc}}[\rho^\uparrow, \rho^\downarrow]}{\delta \rho^\sigma(\mathbf{r})}, \text{ and} \quad (3.29)$$

$$\rho^\sigma(\mathbf{r}) = \sum_{i=1}^{N_\sigma} |\phi_i^\sigma(\mathbf{r})|^2. \quad (3.30)$$

From the above, it is clear that the spin-up and spin-down ($\sigma = \uparrow, \downarrow$) KS orbitals are defined by separate KS equations.

Although the spin-DFT formalism is strictly only required in the presence of an external spin-polarized field, the unrestricted KS equations are routinely employed in the absence of a magnetic field to study open-shell systems (whose net spin-density is non-zero). The optimal treatment of open-shell systems within KS-DFT is in some ways an unresolved question in DFT [67]; we discuss this topic in depth in Chapter 6 of this thesis, in which we develop a new formalism for open-shell systems within the normal (restricted) KS framework.

3.6 Exchange-correlation functionals

In this section, we discuss some of the most popular (and historically important) approximations for the xc-energy functional. The effectiveness of these approximations has been integral to the success of DFT; we also comment on how these approximations can be improved in a quasi-systematic manner, giving rise to more accurate functionals in DFT.

3.6.1 Local spin density approximation

The first approximation for the xc-functional in KS theory is the local density approximation (LDA) [9], usually generalised to the local spin density approximation (LSDA). In the LSD approximation, the xc-energy is modelled using the HEG; note the difference with Thomas–Fermi in which the much larger kinetic energy is modelled with the HEG. The LSDA xc-energy is

$$E_{\text{xc}}^{\text{LSDA}}[\rho] = \int \text{d}\mathbf{r} e_{\text{xc}}^{\text{h}}(\bar{\rho}^{\uparrow}, \bar{\rho}^{\downarrow})|_{\rho^{\uparrow}, \rho^{\downarrow}}, \quad (3.31)$$

where $e_{\text{xc}}^{\text{h}}(\bar{\rho}^{\uparrow}, \bar{\rho}^{\downarrow})$ is the xc-energy density for the HEG. The exchange part of this is known analytically, but the correlation part is parameterized from Monte-Carlo calculations; there are a few well-known parameterizations [68–70] which give slightly different results.

Whilst it might seem to be a severe approximation, the LSDA often yields accurate results, especially for bulk systems whose densities are more uniform; it is also computationally very fast, having a purely local density dependence. Its success is in part because the HEG is a real physical system, meaning it obeys various exact properties [71]. However, it is of limited use of in atomic and molecular systems. Although it gives total energies to within 1% ~ 5% of experimental results, one is usually interested in computing energy differences to determine quantities of interest, not simply the total energy. Qualitatively, it tends to overbind and does not produce stable anions; quantitatively, it does not yield ‘chemical accuracy’ (1 kcal/mol) for properties of interest.

3.6.2 Generalized gradient approximations

A logical extension to the LSDA is to use the gradient of the density in xc-functionals, in order to account for variations in the density. This class of functionals, known as generalized gradient approximations (GGAs), take the general form

$$E_{\text{xc}}^{\text{GGA}}[\rho^\uparrow, \rho^\downarrow] = \int \text{d}\mathbf{r} e_{\text{xc}}^{\text{GGA}}(\rho^\uparrow, \rho^\downarrow, \nabla\rho^\uparrow, \nabla\rho^\downarrow). \quad (3.32)$$

Unlike the LSDA, the above form does not define a unique functional and as such a large number of GGAs have been developed. GGAs can be roughly grouped into one of two categories: (i) those which are parameterized to fit known empirical data, and (ii) those which are parameterized to satisfy known exact properties (such as scaling relations). There are many well-known examples of both [19, 70, 72–75], but perhaps the most famous example of the former is the BLYP functional [75] which has played an important role in the application of DFT in chemistry; meanwhile the PBE functional [19] is the most prominent of the latter group, and tends to be favoured by those in the physics community. GGA functionals tend to systematically improve upon LDA for most properties, at a slightly increased cost due to the semi-local dependence on the density.

3.6.3 Hybrid functionals and generalized Kohn–Sham

The local (LSDA) and semi-local (GGA) functionals described thus far all fall within the KS formalism of DFT. We now introduce a class of functionals known as *hybrid* functionals, so-called because they mix a common KS xc-energy functional with some portion of Hartree–Fock (or other) exchange energy. The first well-known hybrid was proposed by Becke [76] and uses a simple mix of half HF exchange and half LSDA exchange–correlation (and is thus known as “Becke half-half”),

$$E_{\text{xc}}^{\text{HF}}[\rho; \{\phi_i\}] = \frac{1}{2}E_{\text{x}}^{\text{HF}}[\{\phi_i\}] + \frac{1}{2}U_{\text{xc}}^{\text{LSDA}}[\rho], \quad (3.33)$$

where $U_{\text{xc}}^{\text{LSDA}}$ denotes the potential xc-energy [70], as opposed to full xc-energy.

Becke’s original formulation was proposed based on the adiabatic-connection theorem [77–79]. Strictly speaking, this approach is only formally justified if the optimized effective potential method is used to compute the x(c)-potential. However, formal justification for hybrid functionals in Becke’s implementation (and other early hybrids) followed shortly after with the Generalized Kohn–Sham (GKS)

formalism [80]. The GKS formalism uses the constrained search formalism to define a generalized universal functional $F^S[\rho]$,

$$F^S[\rho] = \min_{\Phi \rightarrow \rho(\mathbf{r})} S[\Phi] = \min_{\{\phi_i\} \rightarrow \rho(\mathbf{r})} S[\{\phi_i\}], \quad (3.34)$$

for some functional of an N-electron Slater determinant $S[\Phi]$. This is a formal representation of DFT provided three conditions are met:

1. $F^S[\rho]$ and its functional derivative exist
2. Minimizing the energy defined by

$$E^S[\{\phi_i\}; v_{\text{eff}}] = S[\{\phi_i\}] + \int d\mathbf{r} v_{\text{eff}}(\mathbf{r})\rho(\mathbf{r}) \quad (3.35)$$

yields the set of single particle equations

$$\hat{O}^S[\{\phi_i\}]\phi_j + \hat{v}_{\text{eff}}\phi_j = \epsilon_j\phi_j, \quad (3.36)$$

where \hat{O}^S does not explicitly depend on the local effective potential \hat{v}_{eff} .

3. The densities of the interacting and GKS systems are v -representable.

The above conditions are met by several choices for $S[\Phi]$. One such choice,

$$S[\Phi] = \langle \Phi | \hat{T} | \Phi \rangle, \quad (3.37)$$

in other words the kinetic energy functional, yields the standard KS equations for Eq. (3.36). Thus, KS theory emerges from GKS theory. Another possible choice of $S[\Phi]$ is

$$S[\Phi] = \langle \Phi | \hat{T} | \Phi \rangle + a \{U_{\text{H}}[\Phi] + E_{\text{x}}[\Phi]\}, \quad (3.38)$$

which leads to the single particle equations

$$\begin{aligned} -\frac{\nabla^2}{2}\phi_i(\mathbf{r}) + v_{\text{en}}\phi_i(\mathbf{r}) + v_{\text{H}}(\mathbf{r})\phi_i(\mathbf{r}) - a \int d\mathbf{x} v_{\text{x}}^{\text{HF}}(\mathbf{r}, \mathbf{x})\phi_i(\mathbf{x}) \\ + (1-a)v_{\text{xc}}(\mathbf{r})\phi_i(\mathbf{r}) = \epsilon_i\phi_i(\mathbf{r}). \end{aligned} \quad (3.39)$$

This defines a hybrid functional with some fraction a of the local or semi-local exchange replaced with exact (HF) exchange.

Although simple in appearance, Becke’s half-half hybrid yields significant improvements over LSDA (and HF) for total energies, atomization energies, ionization energies and proton affinities [76]. Its success spawned the development of many subsequent hybrid functionals [18, 81–85], which have evolved to contain various fractions of different xc-functionals, including so-called local [86] and range-separated hybrids [87–92]. The most famous hybrid is the B3LYP functional [18, 81]: this is often credited with popularizing the use of DFT within the Chemistry community due to its ability to attain chemical accuracy for a range of systems and properties.

The mixing parameters in hybrid functionals are often fitted (to various extents) to data; this has led to criticism of over-parameterization (which also applies to empirically derived GGAs), and contributed to the belief that DFT cannot be considered an *ab initio* method. However, it should be noted that there is strong theoretical justification for the use of GKS and hybrid functionals. Burke, Ernzerhof and Perdew derived a non-empirical condition for the fraction of exact exchange to be combined with the PBE functional [93]; and it has also been demonstrated that a fraction of non-local exchange is crucial to improving band-gap calculations [94].

3.6.4 The path to the ‘exact’ functional

So far, we have discussed the three most historically important, and widely-used classes of functionals in KS calculations. Roughly speaking, GGAs offer more accuracy than LDAs at slightly increased cost; and hybrids improve on GGAs, at a more increased cost due to the non-local potential*. However, various other classes of functional exist, such as the meta-GGAs (mGGAs), which depend on the kinetic energy density τ [95],

$$E_{\text{xc}}^{\text{mGGA}}[\rho^\uparrow, \rho^\downarrow] = \int d\mathbf{r} e_{\text{xc}}^{\text{mGGA}}(\rho^\uparrow, \rho^\downarrow, \nabla\rho^\uparrow, \nabla\rho^\downarrow, \tau^\uparrow, \tau^\downarrow), \quad (3.40)$$

$$\tau^\sigma(\mathbf{r}) = \sum_i |\nabla\phi_{i\sigma}(\mathbf{r})|^2. \quad (3.41)$$

*It is unwise to make a general statement about hybrids being more accurate than GGAs due to the sheer number of both and the discussed problem of over-parameterization.

Like GGAs, mGGAs can be constructed non-empirically to satisfy exact known constraints; as they contain extra information, they can satisfy more of these properties than GGAs. However, despite early mGGAs showing promise [96], they do not consistently perform better than popular GGAs and so their use is less widespread. This may change in the future with the advent of more advanced mGGAs [97].

The final important class of functionals which we shall discuss are those which incorporate the exact exchange energy,

$$E_{\text{EXX}}[\{\phi_k[\rho]\}] = -\frac{1}{2} \sum_{\sigma} \sum_{i,j=1}^{N_{\sigma}} \int \int d\mathbf{r} d\mathbf{r}' \frac{\phi_{i\sigma}(\mathbf{r})\phi_{j\sigma}^*(\mathbf{r})\phi_{i\sigma}^*(\mathbf{r}')\phi_{j\sigma}(\mathbf{r}')}{|\mathbf{r} - \mathbf{r}'|}. \quad (3.42)$$

We differentiate this class of functionals from hybrid functionals because the functional derivative of the exact exchange energy (3.42) is taken with respect to the density, leading to the normal KS equations (3.26), in which the orbitals experience a strictly local potential. By contrast, the GKS scheme for hybrid functionals yields equations for the orbitals (3.39) containing a non-local potential.

Like the kinetic energy functional (3.19), the exact-exchange functional is an implicit density-functional through its dependence on the KS orbitals. We therefore cannot obtain the xc-potential directly from the functional derivative of the xc-energy, and instead it must be solved using the optimized effective potential (OEP) method, which is the subject of § 3.8. Strictly speaking, mGGAs are also orbital-dependent functionals and thus should be solved using the OEP method: although this is sometimes done [98], it is more common to use a trick that takes mGGAs within the GKS formalism [96, 99], which is computationally simpler than solving the OEP equation.

Unfortunately, pairing the exact exchange functional with (for example) a semi-local correlation energy functional does not tend to yield good results*, as the correlation functionals for semi-local functionals benefit from self-cancellation with

*This would be analogous to using full HF exchange, $a = 1$ in a hybrid functional (3.39); typically optimal value of a is found to be ~ 0.25 [93].

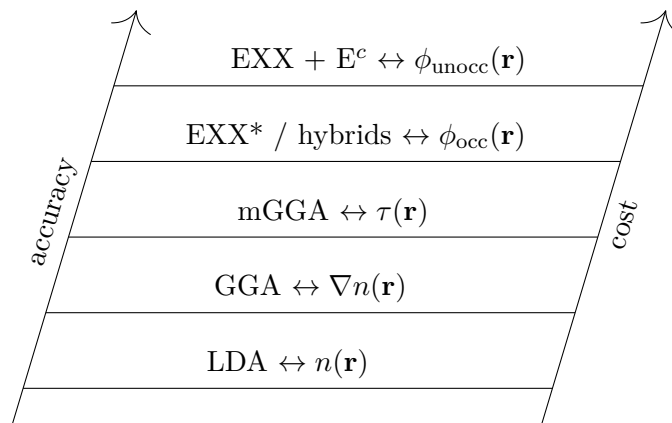


Figure 3.3: The so-called Jacob’s Ladder [101] of DFT functionals

their exchange counterparts and are thus typically very crude approximations to the actual correlation energy [100].

Therefore, the exact exchange energy is typically paired with a correlation energy derived using MBPT; in Chapter 4 of this thesis, we review some example functionals of this type in § 4.1 and derive a new xc-potential using MBPT techniques. For now, we remark that these functionals are used rarely in DFT calculations, due to both cost and difficulties in solving the OEP equation (which are discussed in § 3.9.3). However, development of these functionals is a very active area of research as they are capable of offering far greater accuracy than semi-local functionals.

This brings to a close our discussion on the various flavours of DFT functionals. The PBE and B3LYP functionals are by far the most widely-used, accounting for around 2/3 of all DFT calculations [11]. Nevertheless, there is a continuing drive to develop more accurate functionals, due to systematic failings of typical functionals which are discussed in the following section. The inclusion of more density-related variables to develop more accurate functionals is often referred to as climbing ‘Jacob’s Ladder’ [101], as illustrated in Fig. 3.3.

*EXX has a similar cost to hybrids, but unless paired with a suitable correlation functional, is less accurate than LDA.

3.7 Limitations of common functionals

In this section we discuss some general limitations of common functionals in KS DFT. By general limitations, we refer to features that the exact KS functional and potential should satisfy, but which are not captured by semi-local and hybrid functionals in general use. We note that this is by no means an exhaustive list of deficiencies in common functionals, nor are all of these limitations shared by all functionals; more comprehensive reviews can be found, for example, in Refs. [102] and [103]. However, there is not yet a functional in widespread use that captures any of these features properly; and their proper description is critical to improving many of the systematic failures prevalent in DFT.

3.7.1 Self-interaction

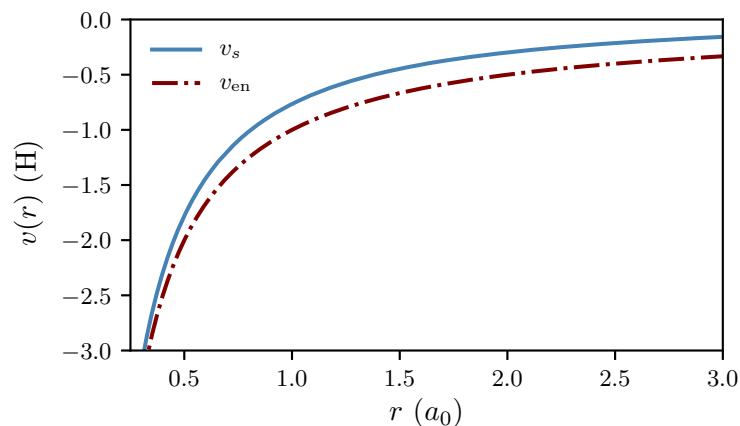
In the KS energy functional, the Coulomb repulsion energy of the electrons is modelled by the classical Hartree term (3.22). This energy is contaminated by an error because each electron experiences a repulsive force from its own charge density: this is known as the self-interaction (SI) error [69, 104]. This error is fully cancelled by the exact xc-functional (and hence there is no SI error in HF, as exchange is treated exactly and there is no correlation); however, it turns out to be only partially cancelled by the vast majority of semi-local approximations.

The SI error is easiest to conceptualize by considering the KS equation for a one-electron system, which is given by

$$\left(-\frac{\nabla^2}{2} + v_{\text{en}}(\mathbf{r}) + \int d\mathbf{r}' \frac{|\phi_1(\mathbf{r}')|^2}{|\mathbf{r} - \mathbf{r}'|} + v_{\text{xc}}(\mathbf{r}) \right) \phi_1(\mathbf{r}) = \epsilon \phi_1(\mathbf{r}). \quad (3.43)$$

Since there are no inter-electron interactions in a one-electron system, it is clear that the exact xc-potential (or more accurately the exchange potential as there is no correlation in a one-electron system) should exactly cancel the Hartree potential,

$$v_{\text{xc}}(\mathbf{r}) = - \int d\mathbf{r}' \frac{|\phi_1(\mathbf{r}')|^2}{|\mathbf{r} - \mathbf{r}'|}. \quad (3.44)$$



(a) Hydrogen atom

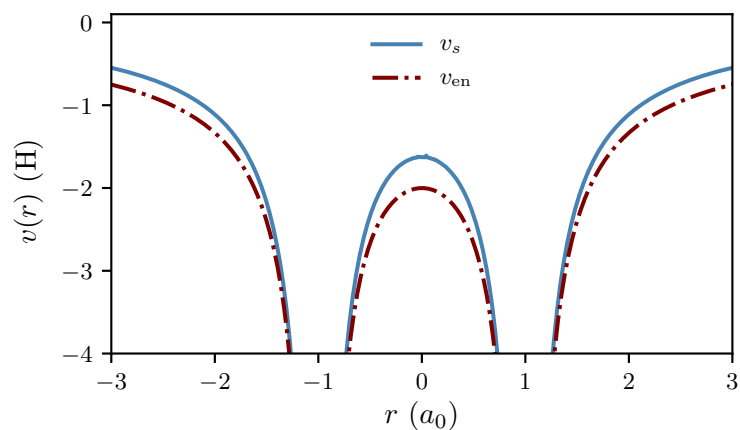
(b) H_2^+ ion

Figure 3.4: The electron-nuclear potential, v_{en} , and the KS potential, v_s , (with the PBE xc-functional), for one-electron systems.

However, this simple relation is not satisfied by LDA and most semi-local DFT functionals (it is broken less severely for hybrids as they contain a fraction of exact exchange). In Fig. 3.4, we have plotted the KS potential against the external potential for the Hydrogen atom and H_2^+ ion; in an exact KS formulation these would be identical, but they are clearly different with the PBE approximation used here.

Though easiest to understand and define for the one-electron case, the SI problem is prevalent in many-electron systems [105, 106]. One manifestation of the SI error

is in the asymptotic decay of the Hxc-potential: it should decay as $v_{\text{Hxc}}(\mathbf{r}) \sim (N - 1)/r$, but for LDA and most GGAs it instead decays as $v_{\text{Hxc}}(\mathbf{r}) \sim N/r$ [107]. This incorrect behaviour causes serious under-estimation by up to 50% of ionization potentials from KS eigenvalues [107–109].

One framework we can use to conceptualize SI in many-electron systems is by considering that the potential experienced by electrons arises from an effective screening density. This concept was first conceived by Görling [110] and Liu *et al* [111] in terms of an xc-screening density, but here we consider the slightly more general case of a screening density for the full Hartree and xc (Hxc) potential [108, 109]. The relationship between the Hxc-potential and screening density is

$$v_{\text{Hxc}}(\mathbf{r}) = \int d\mathbf{r}' \frac{\rho_{\text{scr}}(\mathbf{r}')}{|\mathbf{r} - \mathbf{r}'|}. \quad (3.45)$$

To consider how this aids our understanding of SI errors in many-electron systems, we note that each electron should be repelled by the other $N - 1$ electrons; the screening charge Q_{scr} (the screening density integrated over all space), for an approximation free from self-interaction should therefore integrate to $N - 1$,

$$Q_{\text{scr}} = \int d\mathbf{r} \rho_{\text{scr}}(\mathbf{r}) = N - 1. \quad (3.46)$$

However, the above equation does not hold for LDA and the vast-majority of GGAs such as PBE: in fact, $Q_{\text{scr}} = N$, meaning their xc-potentials are fully contaminated with SIs.

Many of the systematic errors present in semi-local DFT functionals can be (at least partly) traced back to the presence of SI errors. Various methods have been developed to remove (or at least reduce) the SI error. The most famous SI-correction (SIC) scheme is the Perdew-Zunger (PZ) method [69], in which an xc-functional (most commonly LSDA) is modified such that the following condition is satisfied

$$E_{\text{H}}[|\phi_{i\sigma}|^2] + E_{\text{xc}}[|\phi_{i\sigma}|^2] = 0. \quad (3.47)$$

The above condition ensures the self-Hartree energy of an electron is cancelled by a corresponding term in the xc-energy. The PZ scheme is advantageous in some

respects, for example correcting the long-range decay of the Hxc-potential [112], but yields worse results than the original functionals for some properties [113] as self-cancellation benefits between exchange and correlation are lost [114]; the PZ-SIC corrected energy is also not invariant with respect to unitary transformations of the orbitals. Separately, functionals which are naturally free from SIs for one-electron systems have been developed [115, 116]; but problems associated with SIs persist with these functionals for many-electron systems [105, 106].

3.7.2 The derivative discontinuity and fundamental gap

An important quantity in materials science is the band-gap (or fundamental gap), which is defined by

$$E_g(N) = I(N) - A(N), \quad (3.48)$$

where $I(N)$ and $A(N)$ are, respectively the ionization energy and electron affinity for the N -electron system. LSDA and typical semi-local functionals seriously underestimate E_g , often by up to 50% [117, 118], severely limiting the predictive power of DFT in this area.

To understand the origin of this error, we first note the relationships between (i) ionization energy $E(N)$ and the highest-occupied molecular orbital (HOMO) energy $\epsilon_N(N)$, and (ii) electron affinity $A(N)$ and the lowest-occupied molecular orbital (LUMO) energy $\epsilon_{N+1}(N+1)$ (of the $N+1$ electron system) [119],

$$I(N) = -\epsilon_N(N) = E(N-1) - E(N); \quad (3.49)$$

$$A(N) = -\epsilon_{N+1}(N+1) = E(N) - E(N+1). \quad (3.50)$$

For periodic systems one cannot easily vary the electron number and thus the definitions of $A(N)$ and $I(N)$ involving the orbital energies must be employed.

Defining the KS energy gap as the difference between the HOMO and LUMO energies of the same N -electron system,

$$E_{g,KS} = \epsilon_{N+1}(N) - \epsilon_N(N), \quad (3.51)$$

one can re-express the fundamental gap as the sum of the KS energy gap and a so-called many-body correction term Δ_{xc} ,

$$E_g = E_{\text{g,KS}} + \Delta_{\text{xc}} = \epsilon_{\text{L}} - \epsilon_{\text{H}} + \Delta_{\text{xc}}, \quad (3.52)$$

where ϵ_{H} and ϵ_{L} refer to the KS HOMO and LUMO eigenvalues. Given that these quantities are readily available, we turn our attention to the term Δ_{xc} .

Consider an ensemble with $N + \omega$ electrons, from two systems of N and $N + 1$ electrons. In this case, Perdew *et al* [119] showed the energy of the ensemble varies linearly with ω (piecewise linearity),

$$E(N + \omega) = (1 - \omega)E(N) + \omega E(N + 1), \quad 0 < \omega \leq 1. \quad (3.53)$$

As a consequence of the above relation, there is a derivative discontinuity (DD) in the energy as it crosses an integer number of electrons; see Fig. 3.5 for a visualization of this concept. This discontinuity defines the fundamental gap E_g , through the definitions of I and A :

$$-A(N) = E(N + 1) - E(N) = \left. \frac{\delta E}{\delta N} \right|_{N^+} = \left. \frac{\delta E}{\delta \rho(\mathbf{r})} \right|_{N^+} \quad (3.54)$$

$$-I(N) = E(N) - E(N - 1) = \left. \frac{\delta E}{\delta N} \right|_{N^-} = \left. \frac{\delta E}{\delta \rho(\mathbf{r})} \right|_{N^-} \quad (3.55)$$

$$\Rightarrow E_g(N) = \left. \frac{\delta E}{\delta \rho(\mathbf{r})} \right|_{N^+} - \left. \frac{\delta E}{\delta \rho(\mathbf{r})} \right|_{N^-}, \quad (3.56)$$

where the final equality in equations (3.54) and (3.55) follows from the Euler equation (3.12) and the definition of the chemical potential μ (3.13) [120]. From the definition of the energy functional for the interacting and non-interacting systems, and the relation (3.52), one can equate Δ_{xc} with the DD of the xc-energy,

$$\Delta_{\text{xc}} = \left. \frac{\delta E_{\text{xc}}}{\delta \rho(\mathbf{r})} \right|_{N^+} - \left. \frac{\delta E_{\text{xc}}}{\delta \rho(\mathbf{r})} \right|_{N^-} \quad (3.57)$$

$$= \lim_{\omega \rightarrow 0} \left\{ v_{\text{xc}}^{N+\omega}(\mathbf{r}) - v_{\text{xc}}^{N-\omega}(\mathbf{r}) \right\}, \quad (3.58)$$

where $v_{\text{xc}}^{N+\omega}(\mathbf{r})$ and $v_{\text{xc}}^{N-\omega}(\mathbf{r})$ are the xc-potentials of the $N + \omega$ and $N - \omega$ ensembles respectively.

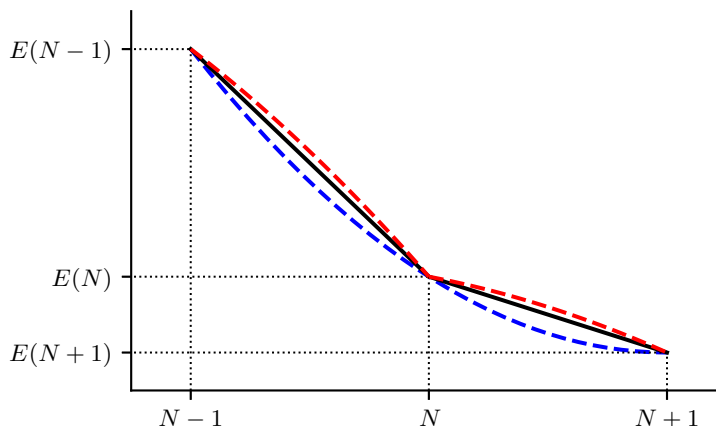


Figure 3.5: Ensemble energy curves: the behaviour for the fully interacting system is shown by the straight lines between energies. Semi-local DFT functionals tend to over-delocalize electron density, as shown in the blue convex curves; HF has the opposite tendency yielding the red concave curves.

Unfortunately, most semi-local functionals in DFT completely lack a DD ($\Delta_{xc} = 0$) in their standard implementation. As illustrated in Fig. 3.5, their energy curves are actually convex instead of being piecewise linear: this is a manifestation of SI errors but is more commonly deemed the delocalization error [121, 122], as this describes the tendency for electrons to over-delocalize their charge density in standard DFT approximations. In fact, it has been shown that (almost) piecewise linearity is restored for semi-local functionals using an ensemble DFT framework, which yields a non-zero DD for finite systems [123]; however, the DD still vanishes for periodic systems [124].

The delocalization error has been identified as a pervasive source of systematic errors in KS theory [121]. Firstly, band-gap predictions using standard functionals are severely underestimated since $\Delta_{xc} = 0$. The delocalization error also causes qualitatively incorrect energy dissociation curves for diatomic molecules, as it is energetically favourable for the species to dissociate into partially charged fragments instead of neutral atoms: see Fig. 3.6(a) for an example with the H_2^+ ion. It has been shown that the DD is also related to another kind of discontinuity in DFT [125], steps in the KS potential which form when molecules are stretched [126]; this

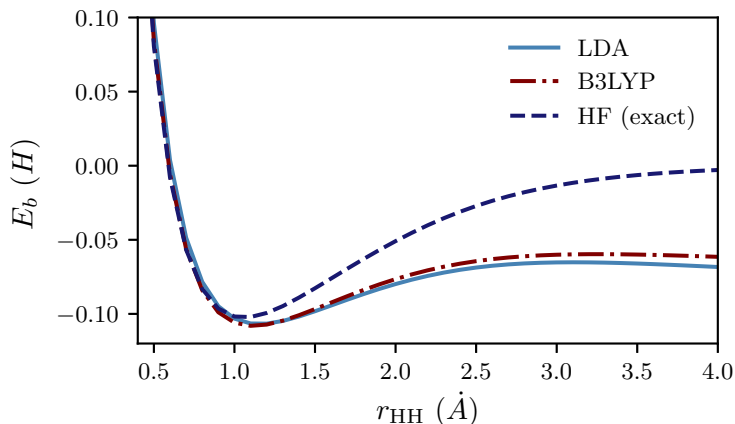
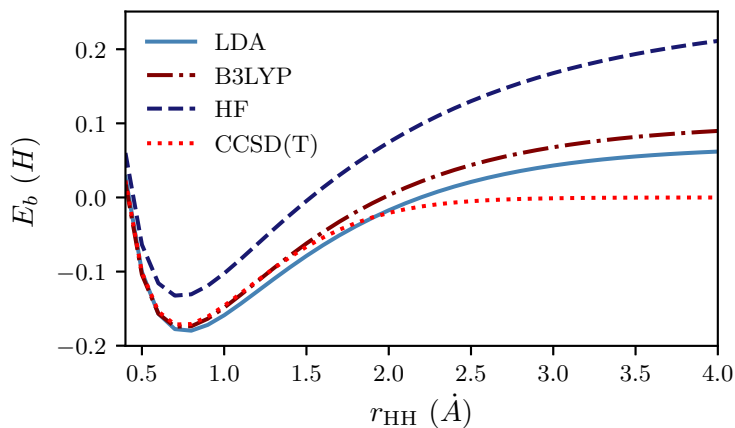
(a) H_2^+ ion(b) H_2 molecule

Figure 3.6: Dissociation energy curves for the H_2 molecule and H_2^+ ion. LDA predicts qualitatively incorrect binding energies for both these simple systems.

presents an additional challenge for DFT in charge-transfer applications [127].

In contrast to KS theory, HF has a tendency to over-localize electron density, producing a slightly concave ensemble energy as illustrated in Fig. 3.5. Hybrid functionals, in particular range-separated hybrids [87–92], therefore yield more accurate band-gap predictions [94] due to cancellation of errors between semi-local DFT functionals and non-local exchange. SI-free functionals also predict a DD [107]; however, the search for a non-empirical functional with semi-local cost that captures the DD is a very active area of research [128].

3.7.3 Static and dynamic correlation

Another challenge for DFT is the accurate description of systems where electron correlation plays a significant role. As discussed in § 2.3, it is helpful to distinguish between static (or more generally ‘strong’) and dynamic correlation. Both these kinds of effects are considered to require a multi-determinant state in quantum chemical methods; however, in KS theory they can be captured in principle through the xc-functional.

Semi-local functionals describe short-range dynamic correlation well [129]; however, they struggle with long-range dynamic correlation effects. For example, they fail to capture vdW interactions because their binding energy curves do not have the correct $-1/R^6$ behaviour [130]. However, there has been progress in this area: Langreth and Lundquist constructed a non-empirical functional [131, 132] which is fairly accurate and widely-applicable; meanwhile Grimme developed the DFT+D approach [133, 134] which loses generality due to empiricism but is often very accurate, and more recently a less-empirical alternative to the DFT+D method has been developed which is more widely applicable [135]. However, the goal of capturing dynamic correlation effects accurately with a general non-empirical functional remains.

Traditional DFT methods notoriously struggle to capture strong correlation, which is pervasive in electronic structure applications as it occurs whenever there are degeneracies such as in stretched molecules [136] and Mott insulators [137]. The exact KS functional should satisfy the so-called constancy condition [138], which requires that the energy of an ensemble consisting of fractional spin-densities must be a constant function of the ensemble mixing parameter. Semi-local functionals do not satisfy this condition, as they energetically favour the fractional-spin state; see Fig. 3.6 (b) for the manifestation of this error in H_2 . One can draw an analogy here with the delocalization error in which fractional-charge states are energetically favoured, and Yang and co-workers have unified the constancy condition and

the piecewise linearity into the so-called flat-plane condition [139]. An empirical correction scheme, known as DFT+U [140] is used widely in calculations involving Mott insulators, but developing a first-principles approach for strongly-correlated systems is still very much an ongoing effort in DFT.

3.8 The optimized effective potential method

As discussed in §3.6.4, when the xc-functional is not an explicit functional of the density, the optimized effective potential (OEP) method is required to find its functional derivative. In fact, the OEP method predates the HK theorems and KS theory: Sharp and Horton [141] first considered the OEP as a constrained minimization of the HF energy expression, in which the orbitals are described by an effective (local) potential. This is identical to using the exact exchange functional (with no correlation) in the KS framework, but the OEP method can be applied more generally to any xc-functional in DFT [142].

There are several ways to derive the general OEP equation. Below we present a derivation which uses the chain rule to directly find the functional derivative of the xc-energy with respect to the density; a detailed review by Engel [143] considers the alternative mechanisms from which the OEP equation arises. Starting with the usual expression for the xc-potential and then applying the chain rule yields

$$v_{\text{xc}}(\mathbf{r}) = \frac{\delta E_{\text{xc}}[\{\phi_k, \epsilon_k\}]}{\delta \rho(\mathbf{r})} = \int d\mathbf{r}' \frac{\delta E_{\text{xc}}[\{\phi_k, \epsilon_k\}]}{\delta v(\mathbf{r}')} \frac{\delta v(\mathbf{r}')}{\delta \rho(\mathbf{r})}, \quad (3.59)$$

where $\delta v(\mathbf{r})$ denotes a variation of the KS potential. The functional derivative of the xc-functional with respect to the potential can be determined directly using perturbation theory. The expression $\frac{\delta v(\mathbf{r}')}{\delta \rho(\mathbf{r})}$ we recognise as the inverse of the so-called density-density response function $\chi(\mathbf{r}, \mathbf{r}')$ which describes the response of the density to an infinitesimal change in the KS potential. The KS response function is

$$\chi(\mathbf{r}, \mathbf{r}') = \frac{\delta \rho(\mathbf{r})}{\delta v(\mathbf{r}')} = \frac{\delta}{\delta v(\mathbf{r}')} \sum_{\sigma} \sum_{i=1}^{N_{\sigma}} |\phi_i(\mathbf{r})|^2 = \sum_{\sigma} \sum_{i=1}^{N_{\sigma}} \phi_i^*(\mathbf{r}) \frac{\delta \phi_i(\mathbf{r})}{\delta v(\mathbf{r}')} + \text{c.c.}; \quad (3.60)$$

the expression $\frac{\delta\phi_i(\mathbf{r})}{\delta v(\mathbf{r}'')}$ can be determined with perturbation theory,

$$\frac{\delta\phi_i(\mathbf{r})}{\delta v(\mathbf{r}'')} = \sum_{k \neq i} \frac{\phi_i(\mathbf{r}'')\phi_k^*(\mathbf{r}'')\phi_k(\mathbf{r})}{\epsilon_i - \epsilon_a}. \quad (3.61)$$

Hence the response function is equal to

$$\chi(\mathbf{r}, \mathbf{r}'') = \sum_{\sigma} \sum_{i=1}^{N_{\sigma}} \sum_{a=N_{\sigma}+1}^{\infty} \frac{\phi_i^*(\mathbf{r})\phi_i(\mathbf{r}'')\phi_a(\mathbf{r})\phi_a^*(\mathbf{r}'')}{\epsilon_i - \epsilon_a} + \text{c.c.}, \quad (3.62)$$

where the summation over all orbitals $k \neq i$ has been reduced to a summation over just the unoccupied orbitals due to cancellation of some terms.

Hence the OEP equation for the xc-potential is given by

$$v_{\text{xc}}(\mathbf{r}) = \int d\mathbf{r}'' \frac{\delta E_{\text{xc}}[\{\phi_k, \epsilon_k\}]}{\delta v(\mathbf{r}'')} \chi^{-1}(\mathbf{r}, \mathbf{r}''); \quad (3.63)$$

but it is more commonly given in the following (equivalent) form, because the analytic form for the response function is known but the same is not true for its inverse,

$$\int d\mathbf{r}'' \chi(\mathbf{r}, \mathbf{r}'') v_{\text{xc}}(\mathbf{r}'') = \frac{\delta E_{\text{xc}}[\{\phi_k, \epsilon_k\}]}{\delta v(\mathbf{r})}. \quad (3.64)$$

The above equation, a Fredholm equation of the first kind, determines the xc-potential within the OEP method. We note that, if (for example) we were to treat the whole Hxc-potential within the OEP framework, this follows exactly the above procedure, but with the xc-potential and energy functional replaced by the Hxc equivalents.

As an example, we consider the OEP equation for the specific case of the exact exchange energy (3.42). The functional derivative of the EXX energy with respect to $v(\mathbf{r})$ (the right hand side of the OEP equation) is

$$\frac{\delta E_{\text{EXX}}[\{\phi_k\}]}{\delta v(\mathbf{r})} = \frac{\delta}{\delta v(\mathbf{r})} \frac{1}{2} \sum_{\sigma} \int \int d\mathbf{r}' d\mathbf{x} \frac{|\rho_{\sigma}(\mathbf{r}', \mathbf{x})|^2}{|\mathbf{r}' - \mathbf{x}|} \quad (3.65)$$

$$= \sum_{\sigma} \int d\mathbf{r}' \int d\mathbf{x} \frac{\delta \rho_{\sigma}(\mathbf{r}', \mathbf{x})}{\delta v(\mathbf{r})} \frac{\rho_{\sigma}(\mathbf{x}, \mathbf{r}')}{|\mathbf{r}' - \mathbf{x}|} \quad (3.66)$$

$$= \sum_{\sigma} \sum_{i=1}^{N_{\sigma}} \sum_{a=N_{\sigma}+1}^{\infty} \int \int d\mathbf{r}' d\mathbf{x} \frac{\phi_i^*(\mathbf{r})\phi_i(\mathbf{x})\phi_a(\mathbf{r})\phi_a^*(\mathbf{r}')}{\epsilon_i - \epsilon_a} \frac{\rho_{\sigma}(\mathbf{x}, \mathbf{r}')}{|\mathbf{r}' - \mathbf{x}|} + \text{c.c.} \quad (3.67)$$

3.8.1 KLI and CEDA approximations

The OEP equation involves a sum over the virtual KS orbitals which is computationally expensive, and thus an approximate scheme was developed by Krieger, Li and Iarfrate (KLI) [144, 145] and later slightly improved in the common energy denominator approximation (CEDA) [146, 147]. CEDA uses the Ünsold approximation [148], which approximates the energy differences between the occupied and unoccupied KS orbitals as an average value*,

$$\epsilon_a - \epsilon_i \approx \Delta, \quad (3.68)$$

together with the completeness relation,

$$\sum_{a=N_\sigma+1}^{\infty} \phi_a(\mathbf{r})\phi_a^*(\mathbf{r}') = \delta(\mathbf{r} - \mathbf{r}') - \sum_{i=1}^{N_\sigma} \phi_i(\mathbf{r})\phi_i^*(\mathbf{r}'). \quad (3.69)$$

This means that the left-hand-side of the OEP equation becomes

$$\int d\mathbf{r}' \chi(\mathbf{r}, \mathbf{r}') v_{xc}(\mathbf{r}') = -\frac{2}{\Delta} \left\{ \int \rho(\mathbf{r}) v_{xc}(\mathbf{r}) - \sum_{\sigma} \sum_{i,j=1}^{N_\sigma} \phi_i^*(\mathbf{r}) \phi_j(\mathbf{r}) \int d\mathbf{r}' v_{xc}(\mathbf{r}') \phi_i(\mathbf{r}') \phi_j^*(\mathbf{r}') \right\}, \quad (3.70)$$

with a similar transformation occurring for the right-hand side. From the above, the computational advantage of CEDA is clear, as the sum over the unoccupied orbitals (the number of which corresponds directly to the basis set size) is transformed to a sum over the occupied orbitals.

Moreover, CEDA preserves many of the desirable features of the full OEP solution such as the Hxc-screening charge (3.46); it has also been demonstrated to give close accuracy to the full OEP solutions in applications such as exact exchange [143] and the PZ-SIC scheme [149]. An example comparison between the full exact exchange potential and the CEDA result is given in Fig. 3.7. Finally, the full OEP solution frequently suffers from numerical instabilities which will be discussed in more detail in § 3.9.3; CEDA is free from these problems making it a more robust approach.

*The average in the KLI approximation is over all the orbitals regardless of their occupation, and is thus less accurate as $\epsilon_k - \epsilon_l$ is not of fixed sign in this case.

3.9 Implementation

There are several options to solving the KS equations (3.26)-(3.27) computationally; however, the most appropriate choice is typically dictated by the nature of the problem. It is possible to solve the KS equations (3.26)-(3.27) directly on a real-space grid, but only for very small or lower-dimensional systems. Therefore the KS orbitals are usually expanded in a basis set: the two most typical choices are plane wave basis sets, and linear combinations of atomic orbitals (LCAOs). Plane wave basis sets are the default choice in solid state applications involving bulk (periodic) systems; LCAOs are usually more appropriate for studying finite systems such as atoms and molecules.

In this thesis, all computations are based on the LCAO method. Code development was done in the Gaussian basis set code HIPPO*, with one- and two-electron integrals for the Cartesian Gaussian basis elements calculated using the GAMESS code [150, 151]. Some calculations, namely coupled cluster and unrestricted KS/HF calculations for which HIPPO does not have the capability, were done in the PSI4 code [152, 153]. In the LCAO approach, the KS orbitals are given by

$$\phi_i(\mathbf{r}) = \sum_k^{n_{\text{orb}}} c_{ik} \xi_k(\mathbf{r}), \quad (3.71)$$

where n_{orb} is the number of elements in the orbital basis set. We assume the normal convention that the KS orbitals are real-valued, although a complex representation is possible [154, 155]. The computational procedure to solve the KS equations is therefore the same as for HF as shown in Fig. 2.1, but with the Fock matrix now given by the KS Fock matrix,

$$F_{kl}^{\text{KS}} = \left\langle \xi_k \left| -\frac{\nabla^2}{2} + v_{\text{en}} + v_{\text{H}} + v_{\text{xc}} \right| \xi_l \right\rangle. \quad (3.72)$$

*Contact N. Lathiotakis at lathiot@eie.gr for information

3.9.1 Gaussian basis sets

The most common choice for the basis functions in the LCAO expansion. (3.71) are Gaussian-type orbitals (GTOs), which have the form (if expressed in Cartesian co-ordinates)

$$\xi_k^{\text{GTO}}(\mathbf{r}) = N_k x^{l_x} y^{l_y} z^{l_z} e^{-\alpha r^2}, \quad (3.73)$$

where $l_x + l_y + l_z = l$ represents the type of orbital according to its angular momentum ($l = 0$ is an s -function, $l = 1$ a p -function and so on), and N_k is a normalization factor such that $\langle \xi_k | \xi_k \rangle = 1$. The advantage of GTOs is that the integrals in the Fock matrix (3.72) can be determined analytically, which makes their computation efficient compared to other expansions such as Slater-type orbitals. The kinetic and electron-nuclear terms are usually grouped together as a ‘core’ integral,

$$F_{kl}^{\text{core}} = \left\langle \xi_k \left| -\frac{\nabla^2}{2} + v_{\text{en}} \right| \xi_l \right\rangle. \quad (3.74)$$

These are sometimes referred to as the one-body integrals as they involve only one integration variable. The Hartree term is a two-body integral, and is given by

$$\langle \xi_k | v_{\text{H}} | \xi_k \rangle = \sum_{\sigma} \sum_{m,n}^{n_{\text{orb}}} \sum_{i=1}^{N_{\sigma}} c_{im} c_{in} \int \int d\mathbf{r} d\mathbf{r}' \frac{\xi_k(\mathbf{r}) \xi_l(\mathbf{r}) \xi_m(\mathbf{r}') \xi_n(\mathbf{r}')}{|\mathbf{r} - \mathbf{r}'|}. \quad (3.75)$$

The term given by

$$\rho_{mn} = \sum_{i=1}^{N_{\sigma}} c_{im} c_{in} \quad (3.76)$$

is often referred to as the density matrix. The storage required for the integral (3.75) is often reduced by expanding the density in terms of an auxiliary basis set $\{\theta_k\}$ in a procedure known as density-fitting [156–158],

$$\rho(\mathbf{r}) = \sum_{m,n}^{n_{\text{orb}}} \rho_{mn} \xi_m(\mathbf{r}) \xi_n(\mathbf{r}) \quad (3.77)$$

$$\approx \tilde{\rho}(\mathbf{r}) = \sum_l \tilde{\rho}_l \theta_l(\mathbf{r}). \quad (3.78)$$

Most commonly, the auxiliary (density-fitted) basis is a few times larger than the orbital basis so that it can accurately approximate the density, and the coefficients

of the auxiliary basis are chosen to minimize the Coulomb energy,

$$U[\rho, \tilde{\rho}] = \int \int d\mathbf{r} d\mathbf{r}' \frac{[\rho(\mathbf{r}) - \tilde{\rho}(\mathbf{r})][\rho(\mathbf{r}') - \tilde{\rho}(\mathbf{r}')]}{|\mathbf{r} - \mathbf{r}'|}. \quad (3.79)$$

Due to the numerous and often complicated functional forms for the xc-term, the integral over the xc-potential is usually done numerically on a grid. As such, this integral is given by

$$\langle \xi_k | v_{\text{xc}} | \xi_l \rangle = \sum_{i=1}^{n_{\text{grid}}} W_i \xi_k(r_i) v_{\text{xc}}(r_i) \xi_l(r_i), \quad (3.80)$$

where W_i is the grid weighting at co-ordinate r_i . The grid construction is usually designed to take advantage of the relatively high electron density around atomic centres and low density elsewhere, as was proposed by Becke [159], which balances the requirements for accuracy and efficiency. The integrals over the atomic centres are computed using spherical grids, for which there are several choices: in HIPPO, the angular integral uses a Lebedev grid, meanwhile the radial part uses an Euler-McLaurin scheme [160]. In HIPPO, the computation of the xc-potential and energy density is done by passing the grid-density and its gradient (if required) to the external programme LIBXC [161], which returns the desired quantities.

The GTO representation (3.73) must be chosen to represent the density sufficiently well to yield accurate results, whilst also balancing the need for computational efficiency. The smallest possible basis set for a given atom is known as the *minimal* basis set, and contains exactly one angular momentum function for each orbital (for example two $1s$ and two $2s$ functions for Beryllium).

Minimal basis sets are not large enough to generate sufficiently accurate results and therefore larger basis sets are always used for calculations. A *double-zeta* basis set contains two angular momentum functions per orbital, a triple zeta set three, and so on. An historically popular class of basis sets was developed by Pople and co-workers [162], which use two angular momentum functions for the valence orbitals but just one for the core orbitals; however, most modern calculations use at least a double-zeta basis set. It is also common to add polarization functions,

that is higher angular momentum functions than the maximally occupied orbitals, for increased flexibility; basis sets can also be augmented with diffuse functions if longer-range interactions are to be studied.

Many kinds of basis sets exist which have been optimized for different purposes; see [43, pp.200-208] for a thorough review. An important feature of basis sets is that those belonging to the same family should converge to the complete basis set limit as the basis set size is increased. Perhaps the most well-known example of such a family are the correlation-consistent basis sets developed by Dunning and co-workers [163, 164]. These have the acronym cc-pVXZ, where X represents the number of angular momenta per orbital ($X = \text{D}$ for double-zeta, $X = \text{T}$ for triple-zeta, and so on).

In this thesis, we use the correlation-consistent basis sets for all calculations. Although they are not specifically optimized for DFT calculations - unlike for example Jensen's polarization-consistent basis sets [165] - this is an established practise as the ccPVXZ sets are well known to correctly converge to the complete basis set limit. Basis set data in this thesis has been obtained from the *Basis Set Exchange* database [166–168].

3.9.2 SCF convergence

With the KS orbitals expanded as LCAOs, the self-consistent procedure for solving the KS equations as shown in Fig. 2.1 is straightforward in principle. The diagonalization of the Fock matrix can be directly computed with standard routines and this process is iterated until convergence - usually measured by the density matrix (3.76) and the total energy - is reached. In practise, this does not lead to convergence as there are large oscillations between each SCF iteration. However, for many systems, a simple linear density mixing scheme for the Fock matrix,

$$F_{kl}^{(i)} = \alpha F_{kl}^{(i)} + (1 - \alpha) F_{kl}^{(i-1)}, \quad (3.81)$$

with α typically taking a value of around 0.2/0.3, is sufficient to converge many SCF calculations.

A more sophisticated mixing scheme which accelerates convergence is Pulay’s Direct Inversion in the Iterative Subspace (DIIS) algorithm [169], which is used by default in most SCF calculations. In the DIIS procedure, the new Fock matrix is formed using a linear combination of the n previous Fock matrices,

$$F_{kl}^{(i)} = \sum_{j=i-n}^{i-1} c_j F_{kl}^{(j)}. \quad (3.82)$$

The coefficients c are chosen to minimize the norm of the error of the interpolated error $e^{*(i)}$, where

$$e^{*(i)} = \sum_{j=i-n}^{i-1} c_j e_{kl}^{(j)}; \quad (3.83)$$

$$e_{kl}^{(j)} = \sum_{m,n}^{n_{\text{orb}}} \left(F_{km}^{(j)} \rho_{mn}^{(j)} S_{nl}^{(j)} - S_{km}^{(j)} \rho_{mn}^{(j)} F_{nl}^{(j)} \right), \quad (3.84)$$

under the normalization constraint $\sum_j c_j = 1$.

The DIIS procedure is sufficient to converge the majority of calculations, however it is prone to difficulties in certain situations, for example when the HOMO is (near) degenerate, which is often seen for open-shell systems and stretched molecules. This causes the orbital occupations to change between iterations and hence the density matrix never converges. There are various approaches to alleviate this problem, such as level-shifting [170] and the second-order SCF method [171].

In HIPPO, we have implemented the maximum overlap method (MOM) [172] for these situations. In the MOM method, after a certain number n_{MOM} iterations, the orbitals are no longer occupied according to the aufbau principle, but instead the occupied orbitals are chosen to have maximal overlap with the set of occupied orbitals that yielded the lowest total energy in the first n_{MOM} iterations. This done by occupying the N_σ orbitals with the highest projection p_j , where

$$p_j = \sum_{k,l}^{n_{\text{orb}}} \sum_{\mu=1}^{N_\sigma} \rho_{\mu k}^{(i)} S_{kl} \rho_{lj}^{(i-1)}. \quad (3.85)$$

3.9.3 OEP implementation

When part of the KS potential is given by the OEP equation (3.64), this part of the potential needs to be solved in a somewhat different manner before entering the Fock matrix (3.72). We represent the general OEP equation in the following form,

$$\int d\mathbf{r}' \chi(\mathbf{r}, \mathbf{r}') v_{\text{eff}}(\mathbf{r}') = b(\mathbf{r}). \quad (3.86)$$

The effective potential $v_{\text{eff}}(\mathbf{r})$ and right-hand side $b(\mathbf{r})$ depend on the specifics of the problem, such as whether we are finding the Hxc/xc/x-only potential, and the orbital-dependent energy functional.

We expand the effective potential in terms of a screening density (3.45), as is done in various implementations of the OEP in finite basis set codes [108–110, 173]. This means we can impose constraints on the screening charge as outlined in § 3.7.1, which is crucial as the solution to the OEP equation is only defined up to a constant [174]. It is then common practise to expand the screening density in terms of an auxiliary basis set $\{\theta_k\}$,

$$\rho_{\text{scr}}(\mathbf{r}) = \sum_k^{n_{\text{aux}}} \rho_k^s \theta_k(\mathbf{r}), \quad (3.87)$$

where n_{aux} denotes the number of elements in the auxiliary basis set.

The OEP equation now takes the form

$$\sum_k^{n_{\text{aux}}} \rho_k^s \int d\mathbf{r}' \chi(\mathbf{r}, \mathbf{r}') \tilde{\theta}_k(\mathbf{r}') = b(\mathbf{r}), \quad (3.88)$$

$$\tilde{\theta}_k(\mathbf{r}') = \int d\mathbf{x} \frac{\theta_k(\mathbf{x})}{|\mathbf{r}' - \mathbf{x}|}. \quad (3.89)$$

Multiplying both sides of the OEP equation (3.88) by $\tilde{\theta}_l(\mathbf{r})$ and integrating over all space means it is now expressed as a matrix equation,

$$\sum_k^{n_{\text{aux}}} \rho_k^s A_{kl} = b_l \Leftrightarrow \rho_k^s = \sum_l^{n_{\text{aux}}} (A^{-1})_{kl} b_l; \quad (3.90)$$

$$A_{kl} = \langle \tilde{\theta}_k | \chi | \tilde{\theta}_l \rangle, b_l = \langle b | \tilde{\theta}_l \rangle. \quad (3.91)$$

Given a finite orbital basis (and assuming real-valued orbitals), the matrix A_{kl} is equal to

$$A_{kl} = 2 \sum_{\sigma} \sum_{i=1}^{N_{\sigma}} \sum_{a=N_{\sigma}+1}^{n_{\text{orb}}} \frac{\langle \phi_i | \tilde{\theta}_k | \phi_a \rangle \langle \phi_i | \tilde{\theta}_l | \phi_a \rangle}{\epsilon_i - \epsilon_a}, \quad (3.92)$$

with the right-hand side b_l being dependent on the specific problem, but often taking a similar form to the above.

In principle, the solution to the OEP equation is given by the above matrix equation (3.90). However, as mentioned, this only determines the potential up to a constant, and therefore it is necessary to impose a constraint on the screening charge $Q_{\text{scr}} = \int d\mathbf{r} \rho_{\text{scr}}(\mathbf{r})$. This is done by reformulating the OEP matrix equation (3.90) as a minimization of the objective function $G[\{\rho_k^{\text{s}}\}]$ with respect to the coefficients ρ_k^{s} ,

$$G[\{\rho_k^{\text{s}}\}] = \frac{1}{2} \sum_{k,l}^{n_{\text{aux}}} \rho_k^{\text{s}} A_{kl} \rho_l^{\text{s}} - \sum_l^{n_{\text{aux}}} b_l \rho_l^{\text{s}} - \lambda \sum_l^{n_{\text{aux}}} X_l \rho_l^{\text{s}}, \quad (3.93)$$

$$X_l = \int d\mathbf{r} \theta_l(\mathbf{r}), \quad (3.94)$$

where λ is a Lagrange multiplier that constrains the screening charge. The coefficients $\{\rho_k^{\text{s}}\}$ are thus given by solving the equations

$$\rho_k^{\text{s}} = \sum_l^{n_{\text{aux}}} (A^{-1})_{kl} (b_l + \lambda X_l), \quad (3.95)$$

$$\lambda = \frac{Q_{\text{scr}} - \sum_{k,l}^{n_{\text{aux}}} X_k A_{kl} b_l}{\sum_k^{n_{\text{aux}}} X_k^2}. \quad (3.96)$$

In some implementations, either instead of, or in conjunction with, the screening charge constraint, the so-called ‘HOMO constraint’ is applied to enforce the correct asymptotic behaviour of the screening charge [175, 176]. However, because this constraint takes different forms depending on whether the potential is of Hxc/xc/x-only character [177], we only impose the more general screening charge constraint in HIPPO.

In principle, the above procedure determines the OEP in a straightforward manner; however, in practise, the solution to the OEP equation (in the above formulation) is riddled with mathematical and numerical problems which have hindered its use in the DFT community. These problems manifest themselves both in the effective

potential, which is often seen to exhibit spurious oscillations; and in the total energies, which have been shown to be unphysically low [178]. Below we discuss briefly the causes of this unphysical behaviour (which is still something of an unsolved problem), along with some of the remedies that have been proposed.

Hirata *et al* [174] proved that the solution to the OEP equation (3.86) is unique (up to a constant) in a complete (infinite) orbital basis set; however, with the orbitals represented in a finite basis set (3.71), the OEP is no longer determined uniquely [174, 178]. This is because, in a finite basis representation, the components ρ_k^s can be non-zero in the null-space of the matrix A_{kl} (3.92). However, as shown in Ref. [179], even when these components can be removed unambiguously through a singular value decomposition (SVD), the resulting potential is mathematically unique but still demonstrates unphysical characteristics. There are also further problems identified in Ref. [173] associated with choosing a suitable auxiliary basis set and the ability of the orbital basis set to accurately represent the virtual orbitals. However, the KLI and CEDA approximations in § 3.8.1 do not suffer from the majority of these problems because they only depend on the occupied orbitals.

A variety of approaches to avoid these difficulties in solving the OEP equation have been proposed. These include, for example, constructing the orbital and auxiliary basis sets ‘balanced’ manner to ensure the orbital basis is sufficiently converged with respect to the auxiliary basis [173, 180]; using regularization techniques to guarantee the OEP is smooth [181, 182]; expanding the screening density in products of the orbital basis to avoid problems with choosing an suitable auxiliary basis set [183]; and other approximate methods similar in style to CEDA [184, 185].

We now discuss in more detail the method proposed by Gidopoulos and Lathiotakis [179]. We use the main argument of this method to solve the OEP equation during this thesis, but with some important changes to the implementation which we discuss later. We restrict our analysis here to the response function $\chi(\mathbf{r}, \mathbf{r}')$, but the same procedure is applied to whatever form is taken by the right-hand side $b(\mathbf{r})$ of the OEP equation (3.86).

In this method, the response function is first split into two parts as follows,

$$\chi(\mathbf{r}, \mathbf{r}') = 2 \sum_{\sigma} \sum_{i=1}^{N_{\sigma}} \sum_{a=N_{\sigma}+1}^{\infty} \frac{\phi_i(\mathbf{r})\phi_i(\mathbf{r}')\phi_a(\mathbf{r})\phi_a(\mathbf{r}')}{\epsilon_i - \epsilon_a} \quad (3.97)$$

$$= 2 \sum_{\sigma} \sum_{i=1}^{N_{\sigma}} \left\{ \left(\sum_{a=N_{\sigma}+1}^{n_{\text{orb}}} + \sum_{n_{\text{orb}}+1}^{\infty} \right) \frac{\phi_i(\mathbf{r})\phi_i(\mathbf{r}')\phi_a(\mathbf{r})\phi_a(\mathbf{r}')}{\epsilon_i - \epsilon_a} \right\} \quad (3.98)$$

$$= \chi_0(\mathbf{r}, \mathbf{r}') + \tilde{\chi}(\mathbf{r}, \mathbf{r}'). \quad (3.99)$$

In the above, we have assumed for simplicity that the orbital basis consists of the occupied KS orbitals $\phi_i(\mathbf{r})$, and a subset of the (lower-lying) unoccupied orbitals $\phi_a(\mathbf{r})$. The first part χ_0 is expressed in terms of the orbitals up to n_{orb} and is thus known; the second part $\tilde{\chi}$, which we denote the ‘complement’ of the response function, is unknown as it contains unoccupied orbitals up to infinity outside the basis set.

The complement is usually ignored and larger than typical orbital basis sets are used to capture as much information about χ_0 as possible. However, in the method of Ref. [179] the complement is approximated using the Ünsold approximation [148] and the completeness relation (3.68),

$$\tilde{\chi}(\mathbf{r}, \mathbf{r}') = 2 \sum_{\sigma} \sum_{i=1}^{N_{\sigma}} \sum_{n_{\text{orb}}+1}^{\infty} \frac{\phi_i(\mathbf{r})\phi_i(\mathbf{r}')\phi_a(\mathbf{r})\phi_a(\mathbf{r}')}{\epsilon_i - \epsilon_a} \quad (3.100)$$

$$\approx -\frac{2}{\Delta} \sum_{\sigma} \sum_{i=1}^{N_{\sigma}} \sum_{n_{\text{orb}}+1}^{\infty} \phi_i(\mathbf{r})\phi_i(\mathbf{r}')\phi_a(\mathbf{r})\phi_a(\mathbf{r}') \quad (3.101)$$

$$= -\frac{2}{\Delta} \sum_{\sigma} \sum_{i=1}^{N_{\sigma}} \phi_i(\mathbf{r})\phi_i(\mathbf{r}') \left\{ \delta(\mathbf{r} - \mathbf{r}') - \sum_{j=1}^{N_{\sigma}} \phi_j(\mathbf{r})\phi_j(\mathbf{r}') - \sum_{j=N_{\sigma}+1}^{n_{\text{orb}}} \phi_j(\mathbf{r})\phi_j(\mathbf{r}') \right\}. \quad (3.102)$$

The crossed out term is neglected because when the method is applied in practise, the full response function is given by

$$\chi(\mathbf{r}, \mathbf{r}') = \chi_0(\mathbf{r}, \mathbf{r}') + \lambda \tilde{\chi}(\mathbf{r}, \mathbf{r}'), \quad (3.103)$$

where $\lambda/\Delta \ll 1$. Given that this term contains the same sum over orbitals as χ_0 , but it is multiplied a small constant, it is neglected.

The matrix A_{kl} is therefore also composed of two parts,

$$A_{kl} = A_{kl}^0 + \alpha \bar{A}_{kl}, \quad \alpha = \frac{\lambda}{\Delta}; \quad (3.104)$$

with A_{kl}^0 given by equation (3.92), and \bar{A}_{kl} equal to

$$\bar{A}_{kl} = - \sum_{\sigma} \sum_{i=1}^{N_{\sigma}} \left\{ \langle \phi_i | \tilde{\theta}_k \tilde{\theta}_l | \phi_i \rangle - \sum_{j=1}^{N_{\sigma}} \langle \phi_i | \tilde{\theta}_k | \phi_j \rangle \langle \phi_i | \tilde{\theta}_l | \phi_j \rangle \right\}. \quad (3.105)$$

As discussed, a similar process is carried out for the right-hand side vector b_k . As was proved in Ref. [179], the solution to the OEP equation has a discontinuity at $\lambda = 0$, so the inclusion of the complement terms with $\alpha \ll 1$ alleviates many of the OEP's associated problems. In Fig. 3.7, we solve the OEP equation for the EXX functional, with and without complement terms, in addition to the CEDA solution and an exact solution from a grid-based OEP method [142]. We see that with the complement, the exchange potential is much closer to the exact solution. As mentioned, the method we use to solve the OEP equation differs from what was used in Ref. [179]; in that paper, the exchange potential was expanded directly in a Gaussian basis set (which does not permit a screening charge constraint), as opposed to the expansion in terms of a screening density that we now employ. Furthermore, we have made modifications to the implementation of b_k to improve the efficiency. These developments are described in detail in § 6.3.2.

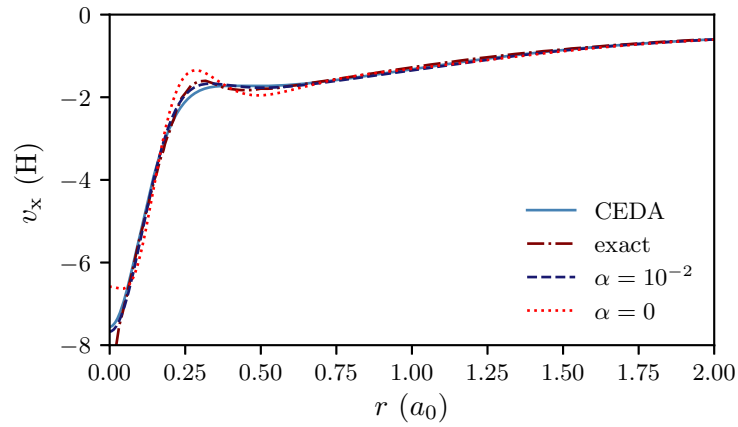


Figure 3.7: Exact exchange potentials for the Neon atom, with a cc-pVTZ orbital basis and uncontracted cc-pVDZ auxiliary basis (with the tightest three s -functions removed). The $\alpha = 0$ result displays unusual behaviour, especially in the core region; it can be much more pathological when $v_x(\mathbf{r})$ is expanded directly in the auxiliary basis set and thus without a screening charge constraint, as is seen for many examples in Ref. [179]. The exact (grid-based) result is taken from Ref. [173].

Optimal power series expansions of the Kohn–Sham potential

In this chapter, we consider the integration of density and wave-function (WFT) theories. A fundamental weakness of DFT is that it is difficult to systematically improve the approximation for the xc-functional. By contrast, approximations in WFT are generally derived from some form of perturbation theory, and thus lend themselves naturally to systematic improvement. Therefore, it would seem wise to use insights from WFT to help us climb to the highest rungs of Jacob’s ladder [101] in DFT. Furthermore, as noted in § 3.6.4, pairing semi-local DFT correlation functionals with exact exchange is not a viable strategy, and thus it is essential to develop new approximations for the correlation functional in order to improve on GGA and meta-GGA functionals.

We begin this chapter by reviewing the fusion of DFT and WFT: firstly, we consider the historically popular approaches based on Görling-Levy perturbation theory [186, 187], and then we introduce the variational principle by Gidopoulos [188] which forms the basis for our work. This variational principle requires an appropriate choice of reference determinant, which we discuss in § 4.2. We follow with a brief comparison of traditional DFT PT and our method in § 4.3. In § 4.4, we see how certain choices of determinant lead to two exchange-only potentials, the EXX

potential and the local Fock-exchange (LFX) potential [189, 190]. The main result of this chapter, in which we derive a new potential with exchange and correlation character to first order, appears in § 4.5.

4.1 Review of integration of density and wave-function theories

Historically, the Levy-Lieb constrained search formulation [50–52] and adiabatic connection approach [77–79] laid the foundation for the cross-fertilization of DFT and WFT. Görling and Levy utilized these concepts to create a perturbation theory scheme for DFT [186, 187], which in principle allows the exact xc-functional to be constructed using perturbation theory. This spawned the development of second-order correlation energy expressions [191, 192], including the development of *ab initio* DFT by Bartlett and co-workers [193–197]. More recently, the adiabatic connection has been combined with the random phase approximation (RPA) [78], with the adiabatic-connection and fluctuation dissipation theorem [198], which yields accurate correlation energy functionals [199–206]. MBPT approaches from the perspective of Green’s functions have also led to development of xc-functionals, using the Sham-Schlüter method [207–209].

An alternative approach, developed by Gidopoulos [188], does not require the adiabatic connection but instead the KS potential is found to be the minimizing potential of a wave-function expression. This variational principle was also considered in a different light by Davidson [210] and additionally has links with a variational principle by Lieb [52, 211]. It is this variational principle which we employ to derive xc-potentials later in this chapter.

4.1.1 Adiabatic connection and DFT perturbation theory

We start with a brief review of traditional DFT perturbation theory (DFT PT) [186, 187], which is the most well-known perturbative scheme in DFT for finite systems. The starting point for DFT PT is the adiabatic connection path [77, 78], in which a weakly-interacting system is defined by

$$\left[\hat{T} + \alpha \hat{V}_{ee} + \hat{v}_\alpha \right] \Psi_n(\alpha) = E_n(\alpha) \Psi_n(\alpha), \quad \lambda \in [0, 1]. \quad (4.1)$$

As the interaction strength λ is slowly varied, the multiplicative potential \hat{v}_α is also adjusted such that the weakly interacting density, $\rho_\alpha(\mathbf{r})$, is held fixed to the value of the ground-state fully-interacting density $\rho_0(\mathbf{r})$, ie

$$\rho_\alpha(\mathbf{r}) = \rho_{\alpha=1}(\mathbf{r}) = \rho_0(\mathbf{r}). \quad (4.2)$$

Using this scheme, the kinetic and electron-electron repulsion energies are expanded perturbatively in powers of the interaction strength α . The zeroth and first-order energy expansions are given by

$$E_0 = \langle \Phi_s | \hat{T} | \Phi_s \rangle = -\frac{1}{2} \sum_{\sigma} \sum_{i=1}^{N_{\sigma}} \int d\mathbf{r} \phi_{i\sigma}^*(\mathbf{r}) \nabla^2 \phi_{i\sigma}(\mathbf{r}) \quad (4.3)$$

$$E_1 = \langle \Phi_s | \hat{V}_{ee} | \Phi_s \rangle = \frac{1}{2} \int d\mathbf{r} \int d\mathbf{r}' \frac{\rho[\Phi_s](\mathbf{r}) \rho[\Phi_s](\mathbf{r}')}{|\mathbf{r} - \mathbf{r}'|} - \frac{1}{2} \sum_{\sigma} \sum_{i,j=1}^{N_{\sigma}} \int \int d\mathbf{r} d\mathbf{r}' \frac{\phi_{i\sigma}(\mathbf{r}) \phi_{j\sigma}^*(\mathbf{r}) \phi_{i\sigma}^*(\mathbf{r}') \phi_{j\sigma}(\mathbf{r}')}{|\mathbf{r} - \mathbf{r}'|} \quad (4.4)$$

In the above, Φ_s is the ground-state wave-function of the non-interacting ($\alpha = 0$) Hamiltonian (4.1), which is by definition the KS determinant. Therefore, from the above expressions, we observe that the zeroth-order energy E_0 is equal to the usual KS kinetic energy (3.19), and the first order energy E_1 is equal to the sum of the Hartree (3.22) and exact exchange (3.42) energies.

The correlation energy is thus given by all the higher-order terms in the perturbative expansion,

$$E_c[\rho] = \sum_{j=2}^{\infty} E_j[\rho]. \quad (4.5)$$

Of course, an infinite expansion is not computationally feasible, and thus only the second-order correlation energy has been included in DFT PT,

$$E_2[\rho] = \sum_{n \neq \text{g.s.}} \frac{|\langle \Phi_{s,0} | \hat{V}_{\text{ee}} - \hat{v}_{\text{Hx}} | \Phi_{s,n} \rangle|^2}{E_{s,0} - E_{s,n}}. \quad (4.6)$$

In KS theory, the KS potential is given by the functional derivative of the total energy with respect to the density; this is no different in DFT PT, in which the j^{th} -order energy defines the j^{th} -order term in the expansion of the KS potential,

$$v_j(\mathbf{r}) = \frac{\delta E_j[\rho]}{\delta \rho(\mathbf{r})}. \quad (4.7)$$

The functional derivative cannot be computed directly, as the exact exchange and correlation energies are only implicit functionals of the density. However, using the OEP method one can calculate these functional derivatives, with the xc-potential to infinite order in DFT PT being given by

$$v_{\text{xc}}(\mathbf{r}) = \int d\mathbf{x} \frac{\delta E_{\text{x}}[\{\phi_i\}]}{\delta v_s(\mathbf{x})} \chi^{-1}(\mathbf{x}, \mathbf{r}) + \sum_{j=2}^{\infty} \left\{ \int d\mathbf{x} \frac{\delta E_j[\{\phi_i\}, \{\epsilon_i\}]}{\delta v_s(\mathbf{x})} \chi^{-1}(\mathbf{x}, \mathbf{r}) \right\}, \quad (4.8)$$

where $\chi^{-1}(\mathbf{x}, \mathbf{r})$ is the inverse of the density-density response function (3.62).

DFT PT has formed the basis for a number of schemes which use perturbative expansions for the xc-energy and potential [191–197, 212]. However, these methods and the DFT PT scheme in general have not achieved widespread use in DFT. Besides mathematical and numerical issues in solving the OEP equation, and the high computational cost, there is a more serious error inherent in the method: when the energy expansion is truncated at second-order, the second-order correlation energy (4.6) is unbound from below.

Hence, when the total energy up to second-order is minimized, it is prone to variational collapse [213, 214]. This tendency to variational collapse is more prevalent than in the analogous MP2 expansion in WFT, and is analysed in more detail in § 4.6. For now, we note that this has prevented the proper self-consistent implementation of DFT PT; however, some practical applications have applied DFT PT

in a non self-consistent manner to avoid this problem, for example by using non-variational schemes [191], or by using the Fock exchange orbital energies in place of the true self-consistent KS orbital energies [194, 195].

4.1.2 **Gidopoulos variational principle**

In the variational principle by Gidopoulos [188], the energy difference

$$T_{\Psi}[v] = \langle \Psi | H_v | \Psi \rangle - E_v > 0 \quad (4.9)$$

is minimized. Here, Ψ is the ground-state of the physical (interacting) system, and H_v is an effective Hamiltonian,

$$H_v = \sum_{i=1}^N \left[-\frac{1}{2} \nabla_i^2 + v_{en}(\mathbf{r}_i) + v(\mathbf{r}_i) \right], \quad (4.10)$$

for some local potential $v(\mathbf{r})$, which simulates the electron-electron repulsion. The ground-state of H_v is Φ_v and the ground-state energy is E_v ,

$$H_v \Phi_v = E_v \Phi_v. \quad (4.11)$$

The energy difference $T_{\Psi}[v]$ is strictly positive due to the Rayleigh–Ritz inequality; this positivity is preserved even when it is expanded with perturbation theory and an approximation up to second order is kept. Hence when $T_{\Psi}[v]$ is minimized there is no possibility of incurring the variational collapse of DFT with a correlation energy functional from second order perturbation theory.

Inequality (4.9) holds because the interacting state Ψ cannot be the exact ground-state of a non-interacting Hamiltonian H_v ; however, we can view Ψ as an approximate ground-state of H_v . Then, choosing $v(\mathbf{r})$ to minimize $T_{\Psi}[v]$ amounts to selecting the Hamiltonian H_v in the class of Hamiltonians (4.10) which optimally adopts Ψ as its approximate ground-state.

We now draw the link between the energy difference (4.9), which is a wave-function expression, and DFT. Minimizing the energy difference (4.9) by taking the functional derivative of $T_{\Psi}[v]$ with respect to $v(\mathbf{r})$ and setting it to equal zero yields

$$\rho_{\Psi}(\mathbf{r}) - \rho_s(\mathbf{r}) = 0, \quad (4.12)$$

where ρ_{Ψ} is the density of Ψ and ρ_s is the density of v_s . The potential v_s is therefore defined as the KS potential, by the definition of the KS potential and the HK theorem (see Ref. [188] for a detailed proof).

There is no need to employ the adiabatic connection path formalism to keep the density fixed in this method, since it is naturally fixed by the minimization of the energy difference (4.9). This simplifies the problem of constructing a perturbative expansion for v_s , as we need only substitute a power series expansion of Ψ in $T_{\Psi}[v]$, truncating the energy difference $T_{\Psi}[v]$ at a finite order. Optimization over v for a given expansion of $T_{\Psi}[v]$ then yields a corresponding expansion for the KS potential. This procedure can be formally carried out for a whole class of Taylor series expansions of Ψ , characterized by the choice of zeroth-order Hamiltonian. It is then possible to consider the corresponding class of Taylor series expansions of the KS potential and search in that class for those expansions that converge faster than others, to find those expansions which are expected to be the most accurate when truncated at some finite order.

In the following, we review how to approximate the wave-function Ψ in a perturbative manner, and find the leading non-zero term in the energy difference (4.9). We expand the interacting state as $\Psi_u(\alpha)$, which is the ground-state of the perturbative Hamiltonian $H_u(\alpha)$,

$$H_u(\alpha) \Psi_u(\alpha) = E_u(\alpha) \Psi_u(\alpha), \quad (4.13)$$

$$H_u(\alpha) = H_u + \alpha [V_{ee} - \sum_i u(\mathbf{r}_i)]. \quad (4.14)$$

The zeroth-order Hamiltonian is H_u : it belongs in the same class of Hamiltonians as H_v (4.10), with a local potential u (different in general from v) that simulates the electron interactions in a mean-field way. The fully interacting Hamiltonian H is obtained for $\alpha = 1$.

If we search for the potential that minimizes the energy difference (4.9) for the non-interacting state $\Psi_u(0) = \Phi_u$, the minimizing potential is clearly $u = v$, since this makes $T_{\Psi_u(0)}[v] = 0$. Hence, for small α , we expect that the potential which minimizes $T_{\Psi_u(\alpha)}[v]$ will be close to u , and we therefore set

$$v(\mathbf{r}) = u(\mathbf{r}) + \alpha v'(\mathbf{r}). \quad (4.15)$$

With the above form for v , the leading term in the energy difference $T_{\Psi_u(\alpha)}[u + \alpha v']$ turns out to be of second order,

$$T_{\Psi_u(\alpha)}[u + \alpha v'] = \alpha^2 T_u[u + v'] + \mathcal{O}(\alpha^3); \quad (4.16)$$

where

$$T_u[w] = \sum_{n \neq \text{g.s.}} \frac{|\langle \Phi_{u,n} | V_{ee} - \sum_i w(\mathbf{r}_i) | \Phi_u \rangle|^2}{E_{u,n} - E_u}, \quad (4.17)$$

with $\Phi_{u,n}$ and $E_{u,n}$ being respectively the n th eigenstate and energy eigenvalue of the effective Hamiltonian H_u .

The second-order energy difference $T_u[w]$ is a functional of both the potentials u and w , but for now we take u to be fixed and minimize $T_u[u + v']$ over v' : this is equivalent to minimizing $T_u[w]$ over w , because $w = u + v'$ and u is fixed. The functional derivative of $T_u[w]$ with respect to w , at fixed u , is given by

$$\frac{\delta T_u[w]}{\delta w(\mathbf{r})} = \sum_{i,a} \frac{\langle \phi_{u,i} | \mathcal{J}_u - \mathcal{K}_u - w | \phi_{u,a} \rangle}{\epsilon_{u,i} - \epsilon_{u,a}} \phi_{u,a}^*(\mathbf{r}) \phi_{u,i}(\mathbf{r}) + \text{c.c.} \quad (4.18)$$

\mathcal{J}_u is the direct Coulomb (or Hartree) local potential operator and \mathcal{K}_u is the Coulomb exchange non-local operator. $\phi_{u,i}$ and $\phi_{u,a}$ are respectively occupied and unoccupied orbitals in the Slater determinant Φ_u , with $\epsilon_{u,i}$ and $\epsilon_{u,a}$ their corresponding eigenvalues.

Optimization over w of the second-order energy difference (4.17), by setting the functional derivative (4.18) equal to zero (for fixed u), yields the first order KS potential. We denote by $w_0[u]$ the minimizing potential of $T_u[w]$ for fixed u ,

$$\min_w T_u[w] = T_u[w_0[u]]. \quad (4.19)$$

From the expansion (4.15), the first-order term $v'[u]$, which denotes the optimized v' for fixed u , can be obtained from

$$w_0[u](\mathbf{r}) = u(\mathbf{r}) + v'[u](\mathbf{r}). \quad (4.20)$$

The expansion of the KS potential to first order is therefore

$$v_s[u](\mathbf{r}) = v_{en}(\mathbf{r}) + u(\mathbf{r}) + \alpha v'[u](\mathbf{r}) + \mathcal{O}(\alpha^2). \quad (4.21)$$

We denote the exact KS potential as v_s , since this is of course independent of u ; at finite order, however, the expansion of the KS potential depends on u and we write $v_s[u]$ to denote the KS potential up to first-order. We also denote by $\Phi_s[u]$ the ground-state of $v_s[u]$, i.e. the KS determinant of the first-order KS potential $v_s[u]$.

In theory, there are an infinite number of choices for u , each of which corresponds to a KS potential $v_s[u]$. We discuss how to make an appropriate choice for u , i.e. one that leads to a rapidly-converging expansion of the KS potential and energy difference, in the next section. For now, it is interesting to note that, by setting $w = u$ in the functional derivative (4.18), we retrieve the OEP equation for exact exchange (xOEP) (3.64,3.65). This particular choice of u will be discussed in more detail in § 4.4.1; for now, we see how it also arises from an alternative perspective.

The density $\rho_{\Psi_u(\alpha)}(\mathbf{r})$ of the weakly interacting state $\Psi_u(\alpha)$ is given by

$$\rho_{\Psi_u(\alpha)}(\mathbf{r}) = \rho_u(\mathbf{r}) + \alpha \left. \frac{\delta T_u[w]}{\delta w(\mathbf{r})} \right|_{w=u} + \mathcal{O}(\alpha^2), \quad (4.22)$$

where $\rho_u(\mathbf{r})$ is the density of the zeroth-order state Φ_u . The density $\rho_{\Psi_u(\alpha)}(\mathbf{r})$ of the weakly interacting system differs from the zeroth-order density $\rho_u(\mathbf{r})$ by a charge density equal (up to first order) to the functional derivative (4.18), where the latter is evaluated at $w = u$. Therefore, the search for the zeroth order potential u for which the ground-state density does not change to first order yields the exact exchange potential, as observed by Bartlett and coworkers [215].

Furthermore, the density $\rho_{\Psi_u(\alpha)}$ is related to the density $\rho_{u+\alpha v'}(\mathbf{r})$ as follows:

$$\rho_{\Psi_u(\alpha)}(\mathbf{r}) = \rho_{u+\alpha v'}(\mathbf{r}) + \alpha \left. \frac{\delta T_u[w]}{\delta w(\mathbf{r})} \right|_{w=u+v'} + \mathcal{O}(\alpha^2). \quad (4.23)$$

Hence, the density $\rho_{\Psi_u(\alpha)}$ of the weakly interacting state differs from the density $\rho_{u+\alpha v'}(\mathbf{r})$ of the non-interacting state by a charge density equal (up to first order) to the functional derivative (4.18), where the latter is evaluated at $w = u + v'$. Therefore, these densities are equal if the potential w is equal to the minimizing potential $w_0[u]$ (4.20); this minimizing potential defines the KS potential $v_s[u]$ (4.21). In other words, for any u , the density of the KS state is equal to the density of the weakly-interacting state (to first order),

$$\rho_s[u](\mathbf{r}) = \rho_{\Psi_u(\alpha)}(\mathbf{r}) + \mathcal{O}(\alpha^2), \quad (4.24)$$

where $\rho_s[u](\mathbf{r}) = \rho_{u+\alpha v'[u]}(\mathbf{r})$. This implies that, if the weakly-interacting state $\Psi_u(\alpha)$ is well-converged when truncated at finite order, then so will be the KS determinant. We explore physical arguments to choose u appropriately in the next section.

4.2 Reference determinants with minimum correlation energy

We now explore the relationship between the perturbative expansion of the energy difference (4.16) and perturbative expansions of correlation energy expressions, which will guide our choice of zeroth-order Hamiltonian H_u . As a prelude to this discussion, we first consider the relationship between the xOEP and correlation energy. Historically, the xOEP is given by a minimization of the total energy expression

$$E_{\text{EXX}} = \min_v \langle \Phi_v | H | \Phi_v \rangle, \quad (4.25)$$

where the Slater determinant Φ_v belongs in the class of Hamiltonians (4.10). Since the exact energy $\langle \Psi | H | \Psi \rangle$ does not depend on v , the minimization of the energy is

equivalent to the minimization over v of the magnitude of the correlation energy from the reference Slater determinant Φ_v ,

$$E_H^c[v] \doteq \langle \Psi | H | \Psi \rangle - \langle \Phi_v | H | \Phi_v \rangle < 0; \quad (4.26)$$

In the above expression it is clear that this correlation energy depends on the interacting Hamiltonian H and the local potential v . Hence, another interpretation of the xOEP follows:

Corollary. *xOEP is that effective potential $v(\mathbf{r})$ with weakest correlation energy from its ground state Φ_v .*

The implication is that if we want to treat the interacting Hamiltonian perturbatively to *all* orders, then the effective Hamiltonian with the xOEP is the best zeroth-order Hamiltonian, as the remaining correlation energy to be treated perturbatively is smallest. This is perhaps not surprising, as the first order term in the expansion of the KS potential in DFT PT is the xOEP.

However, we are typically unable to access all orders of perturbation theory, and thus we are usually interested in the lowest orders of perturbative expansions. Hence, we consider the partially interacting system described by the perturbative Hamiltonian $H_u(\alpha)$ in (4.14) where the zeroth-order potential $u(\mathbf{r})$ will later be determined in an optimal way. In analogy to the xOEP corollary, we make the following statement for the weakly interacting system with Hamiltonian $= H_u(\alpha)$, in the limit $\alpha \rightarrow 0$ and for any u :

Lemma. *The KS potential $v_s[u](\mathbf{r})$ is that effective potential with weakest correlation energy from its ground state $\Phi_s[u]$.*

In this statement, the KS potential $v_s[u]$ is given to first order and the correlation energy to second order (the leading order term).

Proof. The correlation energy for the *partially* interacting system (4.13), with non-interacting reference state Φ_v , is defined as

$$E_{H_u(\alpha)}^c[v] = E_u(\alpha) - \langle \Phi_v | H_u(\alpha) | \Phi_v \rangle < 0. \quad (4.27)$$

For fixed u , the potential that minimizes the magnitude of the correlation energy $E_{H_u(\alpha)}^c[v]$ over v is the same as the potential that minimizes the expectation value $\langle \Phi_v | H_u(\alpha) | \Phi_v \rangle$ over v , since $E_u(\alpha)$ does not depend on v . This minimizing potential v depends on the parameters u and α characterising the weakly-interacting state $\Psi_u(\alpha)$ and thus it is in general different from the xOEP.

Let us expand the correlation energy (4.27) in powers of α and obtain the dominant term. When $\alpha = 0$, the potential which minimizes the magnitude of $E_{H_u(\alpha)}^c[v]$ is $v = u$, since Φ_v is the ground-state of $H_u(0)$. Hence, for small α , we substitute expansion (4.15) into the correlation energy (4.27) and expand the latter,

$$E_{H_u(\alpha)}^c[u + \alpha v'] \doteq E_u(\alpha) - \langle \Phi_{u+\alpha v'} | H_u(\alpha) | \Phi_{u+\alpha v'} \rangle, \quad (4.28)$$

to second order in α to obtain

$$E_{H_u(\alpha)}^c[u + \alpha v'] = -\alpha^2 T_u[u + v'] + \mathcal{O}(\alpha^3), \quad (4.29)$$

with $T_u[w]$ being the second-order energy difference (4.17).

Up to second order in α , the correlation energy (4.29) is thus equal to minus the energy difference (4.17):

$$E_{H_u(\alpha)}^c[u + \alpha v'] = -T_{\Psi_u(\alpha)}[u + \alpha v']. \quad (4.30)$$

Given that the KS potential $v_s[u]$ is the minimizing potential of the energy difference (4.17), it is therefore also the potential which minimizes the magnitude of $E_{H_u(\alpha)}^c$, completing the proof. \square

It follows that when we minimize $T_u[w]$ over w to obtain the first order KS potential $v_s[u]$, its KS ground-state $\Phi_s[u]$ not only has the same density as $\Psi_u(\alpha)$ to first order, but $v_s[u]$ also has the following unique properties among other effective local potentials:

- it best adopts $\Psi_u(\alpha)$ (to first order) as its own approximate ground state and
- $\Phi_s[u]$ has the lowest magnitude of correlation energy to second order.

Let us denote by $E_u^c[w]$ the negative of the energy difference $T_u[w]$,

$$E_u^c[w] = -T_u[w]. \quad (4.31)$$

$E_u^c[w]$ is a second order correlation energy expression. It is useful to use this notation to represent the total energy of the weakly interacting system using three different references: the zeroth-order state Φ_u , the perturbative state $\Phi_{u+\alpha v'}$, and the KS determinant $\Phi_s[u]$. Keeping up to second order, we have in the limit $\alpha \rightarrow 0$:

$$E_u(\alpha) = \langle \Phi_u | H_u(\alpha) | \Phi_u \rangle + \alpha^2 E_u^c[u] + \mathcal{O}(\alpha^3) \quad (4.32)$$

$$= \langle \Phi_{u+\alpha v'} | H_u(\alpha) | \Phi_{u+\alpha v'} \rangle + \alpha^2 E_u^c[u + v'] + \mathcal{O}(\alpha^3) \quad (4.33)$$

$$= \langle \Phi_s[u] | H_u(\alpha) | \Phi_s[u] \rangle + \alpha^2 E_u^c[u + v'[u]] + \mathcal{O}(\alpha^3). \quad (4.34)$$

The difference between the energies (4.33) and (4.34) is that in the latter, the second order correlation energy has already been minimized with respect to v' , whereas it is unoptimized in the former.

4.3 Comparison of DFT perturbation theory and present method

4.3.1 Traditional DFT PT method

In traditional DFT PT, the total energy is expanded in a perturbative manner. The KS potential, which is the functional derivative of the total energy, is thus given to the same order of perturbative expansion as the total energy. The first order term in the energy expansion is the (exact) exchange energy, and thus the first order term in the expansion of the KS potential is the exchange-only potential. Higher orders of the total energy expansion yield the correlation energy; in practise,

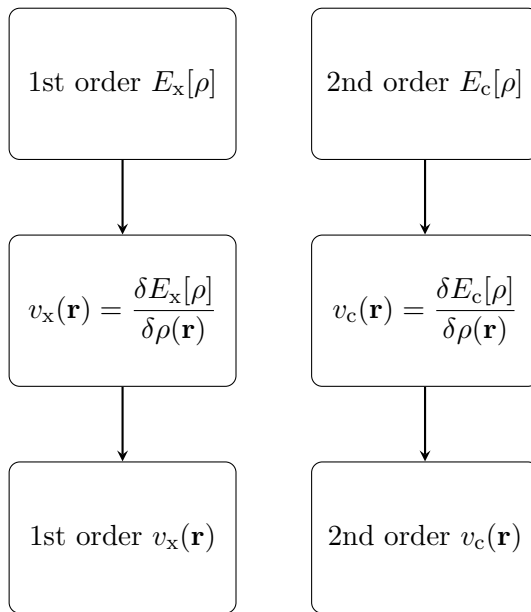


Figure 4.1: Illustration of the traditional DFT PT scheme: first and second order energy expressions yield, respectively, first order exchange and second order correlation potentials.

the expansion is truncated at second-order [192, 194, 196], yielding a second-order correlation potential. This scheme is illustrated in Fig. 4.1.

The first-order exchange and second-order correlation energies are only implicit functionals of the density, through their explicit dependence on the KS orbitals and their eigenvalues. Thus, the functional derivatives in Fig. 4.1 cannot be computed directly and the exchange and correlation potentials must be obtained by solving OEP equations. However, this does not change the fact that these potentials are still the functional derivatives of energy expressions with respect to the density.

4.3.2 Present WFT-DFT method

In the present method, there are no density-functional expressions to minimize; the connection to DFT is that the KS potential emerges from the minimization of the energy difference (4.9). The exchange and correlation potentials are hence not obtained by taking functional derivatives of total energy expansions up to

second order, but instead come from the minimization of the second-order energy correlation energy $E_u^c[w]$ over the potential w .

The minimizing potential $w_0[u](\mathbf{r})$ is equal to $u(\mathbf{r}) + \alpha v'[u](\mathbf{r})$ for $\alpha = 1$, and therefore it represents the Hxc-potential in KS theory. To obtain the xc-potential, we subtract the Hartree potential of the KS system with density $\rho_s[u]$. This gives the xc-potential up to first order; note that, in general, the xc-potential potential in our method is given as a single quantity and not separable into separate exchange and correlation components, in contrast to DFT PT. We emphasize again the conceptual difference between the two methods, namely that in our method we not minimize total energy expansions which are functionals of the density; rather we minimize the second-order energy difference $T_u[w]$ (4.17), or equivalently the magnitude of the second-order correlation energy $E_u^c[w]$ (4.6), which are WFT expressions. This scheme is summarized in Fig. 4.2.

4.4 Local exchange potentials

In this section, we explore approximations for the wave-function Ψ in the energy difference (4.9) which yield potentials with exchange only character. The first choice is based on a particular choice of u for the perturbative expansion $\Psi_u(\alpha)$ that has been considered in the previous two sections; this yields the well-known exact exchange potential (xOEP). We already saw in § 4.1.2 how the xOEP comes from the potential u for which the ground-state density does not change to first order (4.22); we now see it arises from the perspective of minimizing a correlation energy.

We also briefly discuss using the first-order Møller-Plesset expansion [40] for Ψ , which turns out to be equivalent to choosing Ψ to be the Hartree–Fock determinant. This yields the so-called local Fock exchange potential, as discussed in Ref. [190], which has been considered elsewhere in the literature as an accurate approximation for the xOEP potential [50, 189, 216, 217].

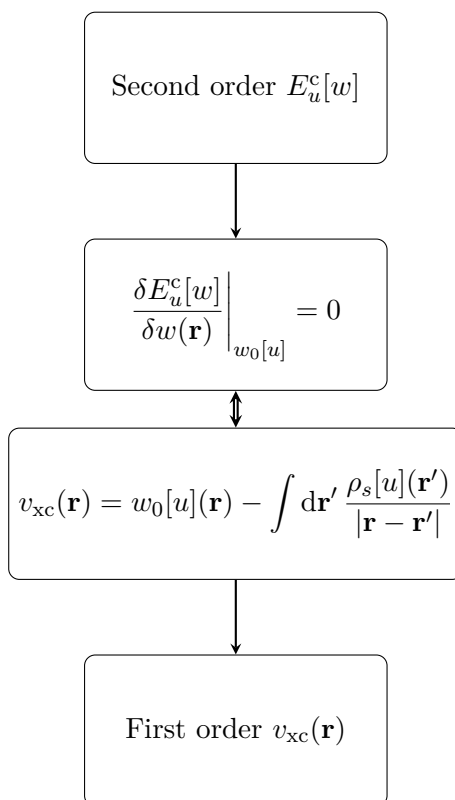


Figure 4.2: Illustration of the present WFT-DFT scheme: the magnitude of the second-order correlation energy $E_u^c[w]$ is minimized to yield a first-order exchange and correlation potential.

4.4.1 Exact exchange potential

Based on the discussion in § 4.2, we anticipate that a good choice for u in the expansion of $\Psi_u(\alpha)$ will be the potential u which minimizes the magnitude of the second-order correlation energy $|E_u^c[u]|$. Of course, this assumes the perturbative expansion (4.32) behaves ‘normally’ and higher order terms give successively smaller contributions; but this is generally a safe assumption to make.

Mathematically, the problem of finding

$$\min_u |E_u^c[u]| = \min_u T_u[u] \quad (4.35)$$

is a challenging one and we shall not attempt to find this minimizing potential. However, we present an argument to choose u that makes $T_u[u]$ small if not minimal.

For any choice of u , it holds that

$$\min_w T_u[w] \leq T_u[u], \quad (4.36)$$

where we have not performed any optimization over u . This inequality holds because the search for the minimizing potential w includes u , and thus $\min_w T_u[w]$ cannot exceed the value of $T_u[u]$. It follows that, if we first minimize $T_u[w]$ over w ,

$$\min_w T_u[w] = T_u[u + v'[u]] \leq T_u[u], \quad (4.37)$$

then this makes the magnitude of the correlation energy $E_u^c[u]$ small, regardless of the choice of u .

We shall choose u such that, after $T_u[w]$ has been optimized over w , $v'[u] = 0$. This choice, which we denote u_{Hx} as it will give the (Hartree and) exchange-only KS potential, yields equality in inequality (4.37),

$$T_{u_{\text{Hx}}}[u_{\text{Hx}} + v'[u_{\text{Hx}}]] \stackrel{0}{=} T_{u_{\text{Hx}}}[u_{\text{Hx}}]. \quad (4.38)$$

This choice for u leads to the well-known equation for the xOEP (with additional Hartree term),

$$\left\{ \sum_{i,a} \frac{\langle \phi_{u,i} | \mathcal{J}_u - \mathcal{K}_u - u | \phi_{u,a} \rangle}{\epsilon_{u,i} - \epsilon_{u,a}} \phi_{u,a}^*(\mathbf{r}) \phi_{u,i}(\mathbf{r}) + \text{c.c.} \right\} \Big|_{u=u_{\text{Hx}}} = 0. \quad (4.39)$$

In our method and DFT PT, the xOEP (and the KS orbitals) are identical if the perturbative expansion in DFT PT is truncated at first order, ie contains no correlation energy. If second-order correlation energy is included in DFT PT then the self-consistent KS orbitals are altered away from their exchange-only character, and the exchange potential will also be modified. By contrast, in our method, one can define a second-order correlation energy from the KS potential with exchange-only character (the solution of the xOEP equation (4.39)): it is given by $E_{u_{\text{Hx}}}^c = -T_{u_{\text{Hx}}}[u_{\text{Hx}}]$.

4.4.2 Local Fock exchange potential

We now consider a different approximation for the interacting wave-function Ψ in the energy difference (4.9), which does not involve the perturbative expansion discussed thus far. Instead, we consider a Møller-Plesset expansion for Ψ , whose zeroth-order term is the Hartree-Fock determinant, Φ_{HF} .

Considering only this zeroth-order term in the expansion for Ψ initially, the energy difference to be minimized is

$$T_{\Psi}[v] = \langle \Phi_{\text{HF}} | H_v | \Phi_{\text{HF}} \rangle - E_v. \quad (4.40)$$

When this expression is minimized with respect to v its functional derivative becomes equal to zero, ie

$$\rho_{\text{HF}} - \rho_v(\mathbf{r}) = 0. \quad (4.41)$$

The potential $v(\mathbf{r})$ is therefore the effective (KS) potential that yields the HF density. Since HF is an exchange-only theory, the local potential with the HF density is expected to have exchange-only character, but be different from the EXX potential in KS theory. We follow the nomenclature in Ref. [190] and denote this potential the Local Fock exchange (LFX) potential.

Analytically, it was shown that the LFX and EXX potentials obey different virial relations [190]; but that the difference between these vanishes up to second-order in an adiabatic connection expansion, and thus we expect the LFX potential to be a close approximation of the EXX potential. The similarity of results from the two potentials was demonstrated for a range of periodic systems in Refs. [190] and [218], and for finite systems in Refs. [189] and [217]. In Fig. 4.3, we demonstrate the qualitative similarity of the two potentials for the Neon and Beryllium atoms, using the method from Ref. [219] and described in Chapter 5 to obtain the LFX potentials, and the approach presented in § 6.3.2 for the EXX potentials. As discussed in Ref. [190], the differences between LFX and EXX results are more significant in systems where correlation is important, which is as expected.

Much like in our expansion of $\Psi_u(\alpha)$, we can include higher-order terms in the MP expansion of the wave-function Ψ_{MP} , which give rise to expansions of the KS potential. We note that, from Brillouin's theorem [39], singly excited Slater determinants do not couple directly to their zeroth-order HF determinant, and thus the density of Ψ_{MP} does not change to first order. Therefore, the potential which minimizes the energy difference

$$T_{\Psi_{\text{MP1}}}[v] = \langle \Psi_{\text{MP1}} | H_v | \Psi_{\text{MP1}} \rangle - E_v, \quad (4.42)$$

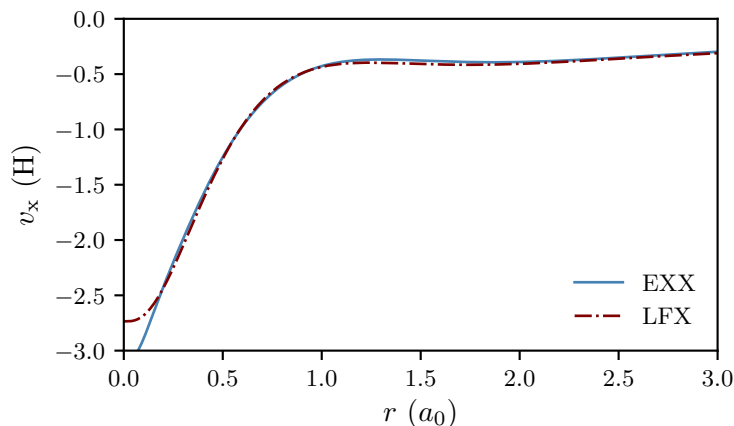
is the same potential as that which minimizes the energy difference (4.40) for the HF determinant.

We draw a further analogy here with the xOEP. Including first-order corrections to the MP wave-function does not change the density $\rho_{\Psi_{\text{MP}}}$ or the KS potential. For the expansion Ψ_{MP} , the LFX potential is thus the zeroth-order term in the expansion of the KS potential for which the density and KS potential are unchanged when first-order electron interactions are switched on. Likewise, for the expansion $\Psi_u(\alpha)$, the xOEP is that potential for which the density (4.22) and KS potential (4.21) are unchanged when first-order electron interactions are switched on.

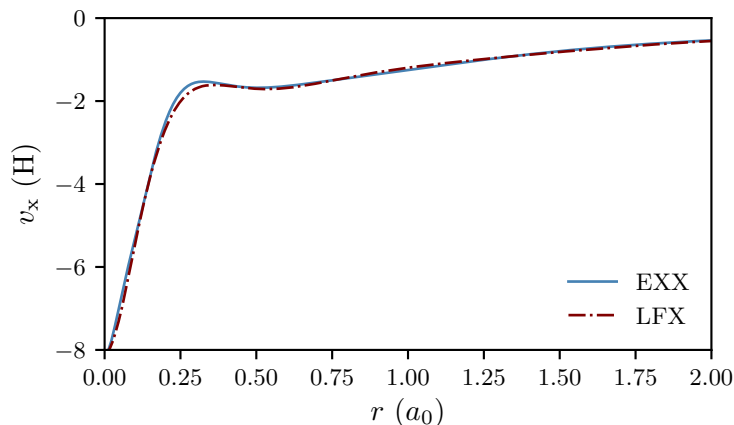
This concludes our discussion of the EXX and LFX potentials, which follow different derivations but share many similar characteristics. In the next section, we construct an expansion for $\Psi_u(\alpha)$ which leads to a KS potential with exchange and correlation character [220].

4.5 First order exchange and correlation potential

In the previous section, we argued that the potential that minimizes the magnitude of the second-order correlation energy $|E_u^c[u]|$ (4.32) is an energetically good choice of u . As discussed, the mathematical complexity of finding this u led us instead to consider a different choice which made $|E_u^c[u]|$ small but not minimal, yielding the



(a) Beryllium. The LFX potential is contaminated by some finite basis set effects near the origin.



(b) Neon

Figure 4.3: Comparison of LFX (calculation details in Chapter 5) and EXX (calculation details in § 6.3.2) potentials.

Hartree and exact exchange potential. In this section, we want to go further by deriving an expression with correlation character in addition to exact exchange.

In § 4.2, we drew the link between the second-order energy difference $T_u[w]$, and the second-order correlation energy $E_u^c[w]$. Moreover, we argued that minimizing the magnitudes of the second-order correlation energies (4.32) and (4.33) leads to fast-converging expansions of the KS potential, or in other words defines energetically good choices for u . Now, rather than trying to minimize $|E_u^c[u]|$, we shall instead minimize $|T_u[w]|$, which is equal to the second-order energy difference $T_u[w]$ (4.17).

In principle, the minimization of $T_u[w]$ over the two potentials u and w is an equally complicated procedure as minimizing $|E_u^c[u]|$. However, we can decouple the minimization which significantly simplifies the procedure. To start, we split $T_u[w]$ into two terms $S_u[w]$ and $D[u]$:

$$T_u[w] = S_u[w] + D[u], \quad (4.43)$$

with

$$S_u[w] = \sum_{n \text{ single}} \frac{|\langle \Phi_{u,n} | V_{ee} - \sum_i w(\mathbf{r}_i) | \Phi_u \rangle|^2}{E_{u,n} - E_u} \quad (4.44)$$

and

$$D[u] = \sum_{n \text{ double}} \frac{|\langle \Phi_{u,n} | V_{ee} | \Phi_u \rangle|^2}{E_{u,n} - E_u}. \quad (4.45)$$

The first term $S_u[w]$ is a sum is over singly excited determinants from Φ_u , while the second term $D[u]$ is a sum over doubly excited determinants. Higher-order excitations from the ground-state vanish.

The potential w appears in $S_u[w]$ but not in $D[u]$. Hence the minimizing potential $w_0[u]$ of $T_u[w]$ also minimizes $S_u[w]$ but leaves $D[u]$ unaffected.

In practice, we find that for any reasonable u , the minimization of $T_u[w]$ over w reduces $S_u[w]$ to very small values, compared with $D[u]$:

$$0 < S_u[w_0[u]] \ll D[u]. \quad (4.46)$$

Some example calculations are shown in Table 4.1. These results demonstrate that after $S_u[w]$ has been minimized over w for various choices of u , $S_u[w_0]$ is consistently smaller than $D[u]$ by approximately two orders of magnitude.

Therefore, the dominant term in $T_u[w_0[u]]$ is $D[u]$, and the minimum of the energy difference $T_u[w]$ over w is approximately equal to $D[u]$,

$$T_u[w_0[u]] \simeq D[u]. \quad (4.47)$$

u	$D[u]$ (eV)	$S_u[w_0]$ (eV)
Ne*		
LDA	2.70	1.91×10^{-2}
PBE	2.67	1.88×10^{-2}
B3LYP	2.51	1.81×10^{-2}
EXX	2.58	1.85×10^{-2}
Avg.	2.62	1.87×10^{-2}
Avg. per elec.	0.262	1.87×10^{-3}
HF*		
LDA	2.87	3.15×10^{-2}
PBE	2.85	3.21×10^{-2}
B3LYP	2.63	2.97×10^{-2}
EXX	2.73	2.89×10^{-2}
Avg.	2.77	3.06×10^{-2}
Avg. per elec.	0.277	3.06×10^{-3}
H ₂ O*		
LDA	2.76	3.90×10^{-2}
PBE	2.72	4.01×10^{-2}
B3LYP	2.49	3.69×10^{-2}
EXX	2.62	2.68×10^{-2}
Avg.	2.65	3.57×10^{-2}
Avg. per elec.	0.265	3.57×10^{-3}
CO*		
LDA	4.47	9.66×10^{-2}
PBE	4.42	9.51×10^{-2}
B3LYP	3.89	8.46×10^{-2}
EXX	4.08	9.23×10^{-2}
Avg.	4.22	9.22×10^{-2}
Avg. per elec.	0.301	6.58×10^{-3}
C ₂ H ₄ [†]		
LDA	2.87	8.25×10^{-2}
PBE	2.83	8.18×10^{-2}
B3LYP	2.51	7.34×10^{-2}
EXX	2.73	7.97×10^{-2}
Avg.	2.74	7.94×10^{-2}
Avg. per elec.	0.171	4.96×10^{-3}
Tot. avg. per elec.	0.255	4.01×10^{-3}

* cc-pVTZ/cc-pVTZ-RIFIT orbital/auxiliary basis sets

† cc-pVDZ/cc-pVDZ-RIFIT orbital/auxiliary basis sets

Table 4.1: Example values for $S_u[w_0]$ and $D[u]$ (4.43). The potential u is the converged KS potential for the set of functionals demonstrated. We observe that $D[u] \gg S_u[w_0]$, regardless of the system or the potential u .

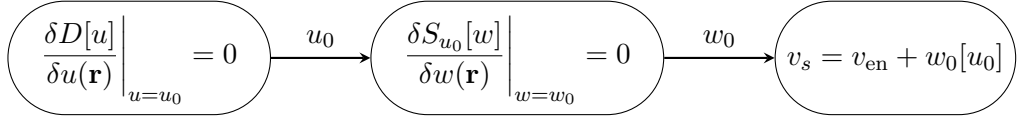


Figure 4.4: Schematic demonstrating the decoupled minimization procedure for $T_u[w]$ after splitting it into the terms $S_u[w]$ and $D[u]$.

Given the above reasoning, we conclude it is safe to decouple the minimization of $T_u[w]$ in order to find the optimal values u_0 and $w_0[u_0]$. First, we minimize $D[u]$ over u to find the potential u_0 which corresponds to the best zeroth-order Hamiltonian H_{u_0} in the perturbative expansion $H_u(\alpha)$ (4.14). Then, we minimize $S_{u_0}[w]$ over w to find the optimal w_0 . This procedure is illustrated in Fig. 4.4. We note that, based on this argument, it is clear that $w = u_{\text{Hx}}$ is not the energetically optimal choice of u , because it does not minimize in any sense the dominant term $D[u]$.

To minimize $D[u]$, we first compute its functional derivative,

$$\int d\mathbf{r} \delta u(\mathbf{r}) \frac{\delta D[u]}{\delta u(\mathbf{r})} = \lim_{\lambda \rightarrow 0} \frac{D[u + \lambda \delta u] - D[u]}{\lambda}. \quad (4.48)$$

Hence we need to determine how $D[u]$ changes due to a perturbation $u \rightarrow u + \lambda \delta u$. To first order, this change is given by

$$D[u + \lambda \delta u] = \sum_{n \text{ double}} \frac{|(\Phi_n + \lambda \Phi_{\delta u, n}^{(1)} | \Phi_0 + \lambda \Phi_{\delta u, 0}^{(1)})|^2}{E_n + \lambda E_{\delta u, n}^{(1)} - E_0 - \lambda E_{\delta u, 0}^{(1)}}, \quad (4.49)$$

where the dependence on u is now assumed and Φ_0 labels the ground state. We use the notation $(\Phi_1 | \Phi_2) = \langle \Phi_1 | V_{ee} | \Phi_2 \rangle$. To write $D[u + \lambda \delta u]$ explicitly to first order in λ , we re-write it in the form

$$D[u + \lambda \delta u] = \sum_{n \text{ dbl}} \frac{|(\Phi_n + \lambda \Phi_{\delta u, n}^{(1)} | \Phi_0 + \lambda \Phi_{\delta u, 0}^{(1)})|^2}{E_n + \lambda E_{\delta u, n}^{(1)} - E_0 - \lambda E_{\delta u, 0}^{(1)}} \times \frac{E_n + \lambda E_{\delta u, n}^{(1)} - E_0 - \lambda E_{\delta u, 0}^{(1)}}{E_n + \lambda E_{\delta u, n}^{(1)} - E_0 - \lambda E_{\delta u, 0}^{(1)}}, \quad (4.50)$$

and then express both sides of the above expression as a power series in λ . Expanding the squared term yields the following expression for the functional deriv-

ative (4.48),

$$\lim_{\lambda \rightarrow 0} \frac{D[u + \lambda \delta u] - D[u]}{\lambda} = \sum_{n \text{ dbl}} \frac{(\Phi_n | \Phi_u)}{E_n - E_0} \left\{ (\Phi_0 | \Phi_{\delta u, n}^{(1)}) + (\Phi_{\delta u, 0}^{(1)} | \Phi_n) - \frac{1}{2} \frac{E_{\delta u, n}^{(1)} - E_{\delta u, 0}^{(1)}}{E_n - E_0} (\Phi_0 | \Phi_n) \right\} + \text{c.c.} \quad (4.51)$$

We must now determine the perturbed states and energies. We begin with the perturbed state $|\Phi_{\delta u, n}^{(1)}\rangle$; from Rayleigh-Schrödinger perturbation theory, this is given by

$$|\Phi_{\delta u, n}^{(1)}\rangle = \sum_{m \neq n} \frac{\langle \Phi_m | \delta U | \Phi_n \rangle}{E_n - E_m} |\Phi_m\rangle, \quad (4.52)$$

where $\delta U \doteq \sum_i \delta u(\mathbf{r}_i)$.

The doubly occupied state $|\Phi_n\rangle$ can be written in the form $|\Phi_{ij}^{ab}\rangle$, where i, j denote occupied orbitals in the ground state and a, b denote unoccupied orbitals. The matrix element, $|\Phi_{\delta u, n}^{(1)}\rangle$, is evaluated using Slater-Condon rules and is given by

$$|\Phi_{\delta u, n}^{(1)}\rangle = \sum_c \sum_k \frac{\langle c | \delta u | k \rangle}{\epsilon_k - \epsilon_c} |\Phi_{ijk}^{abc}\rangle, \quad (4.53)$$

where $k \in |\Phi_{ij}^{ab}\rangle$, and $c \notin |\Phi_{ij}^{ab}\rangle$. The possible combinations for the pair (k, c) are therefore

$$(a, i); (a, j); (b, i); (b, j); (\mu, i); (\mu, j); (a, \nu); (b, \nu), \quad (4.54)$$

where $\mu \neq (i, j)$, $|\mu\rangle \in |\Phi\rangle$ and $\nu \neq (a, b)$, $|\nu\rangle \notin |\Phi\rangle$. Any other permissible combination of (k, c) represents a triple excitation which will vanish in the final expression.

We now determine the state $|\Phi_{ijk}^{abc}\rangle$ based on these possible combinations. We write

$$|\Phi_{ijk}^{abc}\rangle = \hat{c}_c^\dagger \hat{c}_k \hat{c}_b^\dagger \hat{c}_j \hat{c}_a^\dagger \hat{c}_i |\Phi\rangle, \quad (4.55)$$

where \hat{c}^\dagger and \hat{c} are fermion creation and annihilation operators. Using the anti-commutator properties of these operators, namely

$$\{\hat{c}_i^\dagger, \hat{c}_j^\dagger\} = \{\hat{c}_i, \hat{c}_i\} = 0; \{\hat{c}_i^\dagger, \hat{c}_j\} = \delta_{ij}, \quad (4.56)$$

and the fact that

$$\hat{c}_n^\dagger \hat{c}_n |\Phi\rangle = \begin{cases} |\Phi\rangle, & |n\rangle \in |\Phi\rangle; \\ |0\rangle, & |n\rangle \notin |\Phi\rangle, \end{cases} \quad (4.57)$$

the following combinations for the state $|\Phi_{ijk}^{abc}\rangle$ are possible:

$$|\Phi_{ijk}^{abc}\rangle = \begin{cases} |\Phi_{ijb}^{abj}\rangle & = |\Phi_i^a\rangle, \\ |\Phi_{ija}^{abi}\rangle & = |\Phi_j^b\rangle, \\ |\Phi_{ija}^{abj}\rangle & = -|\Phi_i^b\rangle, \\ |\Phi_{ijb}^{abi}\rangle & = -|\Phi_j^a\rangle, \\ \sum_\nu |\Phi_{ija}^{ab\nu}\rangle & = -\sum_\nu |\Phi_{ij}^{b\nu}\rangle, \\ \sum_\nu |\Phi_{ijb}^{ab\nu}\rangle & = \sum_\nu |\Phi_{ij}^{a\nu}\rangle, \\ \sum_\mu |\Phi_{ijk}^{ab\mu}\rangle & = \sum_\mu |\Phi_{j\mu}^{ab}\rangle, \\ \sum_\mu |\Phi_{ijk}^{ab\mu}\rangle & = -\sum_\mu |\Phi_{i\mu}^{ab}\rangle. \end{cases} \quad (4.58)$$

We are now able to compute the matrix element $(\Phi_0|\Phi_{\delta u,n}^{(1)})$ in the functional derivative (4.51) (relabelling μ as k and ν as c),

$$\begin{aligned} (\Phi_0|\Phi_{\delta u,n}^{(1)}) &= \frac{\langle j|\delta u|b\rangle}{\Delta_{bj}}(\Phi_0|\Phi_i^a) + \frac{\langle i|\delta u|a\rangle}{\Delta_{ai}}(\Phi_0|\Phi_j^b) \\ &\quad - \frac{\langle j|\delta u|a\rangle}{\Delta_{aj}}(\Phi_0|\Phi_i^b) - \frac{\langle i|\delta u|b\rangle}{\Delta_{bi}}(\Phi_0|\Phi_j^a) \\ &\quad + \sum_{\substack{unocc \\ c \neq (a,b)}} \left\{ \frac{\langle c|\delta u|b\rangle}{\Delta_{bc}}(\Phi_0|\Phi_{ij}^{ac}) - \frac{\langle c|\delta u|a\rangle}{\Delta_{ac}}(\Phi_0|\Phi_{ij}^{bc}) \right\} \\ &\quad + \sum_{\substack{occ \\ k \neq (i,j)}} \left\{ \frac{\langle i|\delta u|k\rangle}{\Delta_{ki}}(\Phi_0|\Phi_{jk}^{ab}) - \frac{\langle j|\delta u|k\rangle}{\Delta_{kj}}(\Phi_0|\Phi_{ik}^{ab}) \right\}, \end{aligned} \quad (4.59)$$

where $\Delta_{\alpha\beta} = \epsilon_\alpha - \epsilon_\beta$. The matrix element $(\Phi_{\delta u,0}^{(1)}|\Phi_n)$ is likewise given by

$$\begin{aligned} (\Phi_{\delta u,0}^{(1)}|\Phi_n) &= \frac{\langle j|\delta u|b\rangle}{\Delta_{jb}}(\Phi_j^b|\Phi_{ij}^{ab}) + \frac{\langle i|\delta u|a\rangle}{\Delta_{ia}}(\Phi_i^a|\Phi_{ij}^{ab}) \\ &\quad - \frac{\langle j|\delta u|a\rangle}{\Delta_{ja}}(\Phi_j^a|\Phi_{ji}^{ab}) - \frac{\langle i|\delta u|b\rangle}{\Delta_{ib}}(\Phi_i^b|\Phi_{ij}^{ba}) \\ &\quad + \sum_{\substack{unocc \\ c \neq (a,b)}} \left\{ \frac{\langle i|\delta u|c\rangle}{\Delta_{ic}}(\Phi_i^c|\Phi_{ij}^{ab}) - \frac{\langle j|\delta u|c\rangle}{\Delta_{jc}}(\Phi_j^c|\Phi_{ji}^{ab}) \right\} \\ &\quad + \sum_{\substack{occ \\ k \neq (i,j)}} \left\{ \frac{\langle k|\delta u|a\rangle}{\Delta_{ka}}(\Phi_k^a|\Phi_{ij}^{ab}) - \frac{\langle k|\delta u|b\rangle}{\Delta_{kb}}(\Phi_k^b|\Phi_{ij}^{ba}) \right\}. \end{aligned} \quad (4.60)$$

Finally, we compute the perturbed energy levels $E_{\delta u, n}^{(1)}$ and $E_{\delta u, 0}^{(1)}$ and hence the difference $E_{\delta u, n}^{(1)} - E_{\delta u, 0}^{(1)}$,

$$E_{\delta u, n}^{(1)} - E_{\delta u, 0}^{(1)} = \langle \Phi_{ij}^{ab} | \delta U | \Phi_{ij}^{ab} \rangle - \langle \Phi_0 | \delta U | \Phi_0 \rangle \quad (4.61)$$

$$= \int d\mathbf{r} \delta u(\mathbf{r}) \left(|\phi_a(\mathbf{r})|^2 + |\phi_b(\mathbf{r})|^2 - |\phi_i(\mathbf{r})|^2 - |\phi_j(\mathbf{r})|^2 \right). \quad (4.62)$$

We collate these terms to determine the functional derivative (4.51). Let us first consider what happens to the first four terms in each of the matrix elements (4.59) and (4.60) in the context of the functional derivative (4.51). The contribution from the very first term in each expression is given by

$$\sum_{\substack{occ \\ i, j \\ i \neq j}} \sum_{\substack{unocc \\ a, b \\ a \neq b}} (\Phi_{ij}^{ab} | \Phi_0) \frac{\langle j | \delta u | b \rangle}{\Delta_{jb}} \left[\frac{(\Phi_0 | \Phi_i^a) - (\Phi_j^b | \Phi_{ij}^{ab})}{\Delta_{ai} + \Delta_{bj}} \right], \quad (4.63)$$

where

$$(\Phi_0 | \Phi_i^a) - (\Phi_j^b | \Phi_{ij}^{ab}) = \left(\sum_{k \in \Phi_u} - \sum_{k \in \Phi_i^a} \right) \langle ik || ak \rangle = \langle ij || aj \rangle - \langle ib || ab \rangle, \quad (4.64)$$

with $\langle ij || ab \rangle = \langle ij | V_{ee} | ab \rangle - \langle ij | V_{ee} | ba \rangle$. The remaining three terms in the matrix elements (4.59) and (4.60) involving a single-orbital substitution can be evaluated in a similar manner, and by relabelling dummy indices these terms turn out to be identical. The total contribution from these terms is therefore

$$4 \sum_{\substack{occ \\ i, j \\ i \neq j}} \sum_{\substack{unocc \\ a, b \\ a \neq b}} (\Phi_{ij}^{ab} | \Phi_0) \frac{\langle i | \delta u | a \rangle}{\Delta_{ai}} \frac{\langle ji || bi \rangle - \langle ja || ba \rangle}{\Delta_{ai} + \Delta_{bj}}. \quad (4.65)$$

We note that several of the other terms in the matrix elements (4.59) and (4.60) are duplicates of each other, which again can be seen by relabelling dummy indices. After expanding all the remaining terms in expressions (4.59), (4.60) and (4.63) in terms of KS orbitals, the functional derivative of the double excitations term is

given by

$$\begin{aligned}
 \frac{\delta D[u]}{\delta u(\mathbf{r})} = & 2 \sum_{\substack{i,j \\ i \neq j}}^{occ} \sum_{\substack{a,b \\ a \neq b}}^{unocc} \frac{\langle ab || ij \rangle}{\Delta_{ai} + \Delta_{bj}} \\
 & \times \left\{ 2\phi_i^*(\mathbf{r})\phi_a(\mathbf{r}) \frac{\langle ji || bi \rangle - \langle ja || ba \rangle}{\Delta_{ai}} \right. \\
 & + \sum_{c \neq (a,b)}^{unocc} \phi_c^*(\mathbf{r})\phi_b(\mathbf{r}) \frac{\langle ij || ac \rangle}{\Delta_{bc}} + \phi_i^*(\mathbf{r})\phi_c(\mathbf{r}) \frac{\langle cj || ab \rangle}{\Delta_{ic}} \\
 & + \sum_{k \neq (i,j)}^{occ} \phi_i^*(\mathbf{r})\phi_k(\mathbf{r}) \frac{\langle jk || ab \rangle}{\Delta_{ki}} - \phi_k^*(\mathbf{r})\phi_a(\mathbf{r}) \frac{\langle ij || kb \rangle}{\Delta_{ka}} \\
 & \left. - \frac{1}{2} [|\phi_a(\mathbf{r})|^2 - |\phi_i(\mathbf{r})|^2] \frac{\langle ij || ab \rangle}{\Delta_{ai} + \Delta_{bj}} \right\} + \text{c.c.} \quad (4.66)
 \end{aligned}$$

The above expression is equal to zero at the minimizing potential, $u(\mathbf{r}) = u_0(\mathbf{r})$.

This result is reminiscent of the derivative of the double-excitations part of the second-order correlation energy in traditional DFT PT. In Ref. [192], in which the KS potential is partially expanded in an auxiliary basis set $\{g_t\}$,

$$v_s(\mathbf{r}) = v_{\text{en}}(\mathbf{r}) + v_0(\mathbf{r}) + \sum_t b_t^\sigma g_t(\mathbf{r}), \quad (4.67)$$

the derivative of the doubly-excited correlation energy term with respect to b_t^σ can be expressed as

$$\frac{\partial E_d^{(2)}}{\partial b_t^\sigma} = - \int d\mathbf{r} g_t(\mathbf{r}) \frac{\delta D[u]}{\delta u(\mathbf{r})}, \quad (4.68)$$

with $\delta D[u]/\delta u(\mathbf{r})$ given by (4.66). However, as previously stressed, in Ref. [192] and other works in DFT PT, the minimization is carried out over the total energy, which is unbound from below. We discuss the issues with a total energy minimization involving a second-order correlation energy in § 4.6.

We can re-express the functional derivative $\delta D[u]/\delta u(\mathbf{r})$ (4.66) to make it more convenient to apply the KLI or CEDA approximations [144–147]. We note that some terms contain a denominator of mixed sign, which yields less accurate results if we approximate the denominators with a constant. Consider the complex conjugate

of the expression

$$\begin{aligned}
 & \left[\sum_{\substack{i,j \\ i \neq j}}^{\text{occ}} \sum_{\substack{a,b,c \\ a \neq b \neq c}}^{\text{unocc}} \phi_c^*(\mathbf{r}) \phi_b(\mathbf{r}) \frac{\langle ab||ij \rangle}{\Delta_{ai} + \Delta_{bj}} \frac{\langle ij||ac \rangle}{\Delta_{bc}} \right]^* \\
 &= \sum_{\substack{i,j \\ i \neq j}}^{\text{occ}} \sum_{\substack{a,b,c \\ a \neq b \neq c}}^{\text{unocc}} \phi_c(\mathbf{r}) \phi_b^*(\mathbf{r}) \frac{\langle ij||ab \rangle}{\Delta_{ai} + \Delta_{bj}} \frac{\langle ac||ij \rangle}{\Delta_{bc}} \\
 &= \sum_{\substack{i,j \\ i \neq j}}^{\text{occ}} \sum_{\substack{a,b,c \\ a \neq b \neq c}}^{\text{unocc}} \phi_c^*(\mathbf{r}) \phi_b(\mathbf{r}) \frac{\langle ab||ij \rangle}{\Delta_{ai} + \Delta_{cj}} \frac{\langle ij||ac \rangle}{\Delta_{cb}}, \quad (4.69)
 \end{aligned}$$

where in the last step we have just swapped the labels of the dummy indices b and c . This term plus its complex conjugate is therefore equal to

$$\begin{aligned}
 & \sum_{\substack{i,j \\ i \neq j}}^{\text{occ}} \sum_{\substack{a,b,c \\ a \neq b \neq c}}^{\text{unocc}} \phi_c^*(\mathbf{r}) \phi_b(\mathbf{r}) \langle ab||ij \rangle \frac{\langle ij||ac \rangle}{\Delta_{bc}} \left[\frac{1}{\Delta_{ai} + \Delta_{bj}} - \frac{1}{\Delta_{ai} + \Delta_{cj}} \right] \\
 &= - \sum_{\substack{i,j \\ i \neq j}}^{\text{occ}} \sum_{\substack{a,b,c \\ a \neq b \neq c}}^{\text{unocc}} \phi_c^*(\mathbf{r}) \phi_b(\mathbf{r}) \frac{\langle ab||ij \rangle \langle ij||ac \rangle}{(\Delta_{ai} + \Delta_{bj})(\Delta_{ai} + \Delta_{cj})}, \quad (4.70)
 \end{aligned}$$

where the denominator is now of fixed (positive) sign. Likewise the term in $\delta D[u]/\delta u(\mathbf{r})$ (4.66) with denominator Δ_{ki} with its complex conjugate becomes

$$- \sum_{\substack{i,j,k \\ i \neq j,k}}^{\text{occ}} \sum_{\substack{a,b \\ a \neq b}}^{\text{unocc}} \phi_i^*(\mathbf{r}) \phi_k(\mathbf{r}) \frac{\langle ab||ij \rangle \langle jk||ab \rangle}{(\Delta_{ai} + \Delta_{bj})(\Delta_{ak} + \Delta_{kj})}. \quad (4.71)$$

Using the above expressions (4.70) and (4.71), we can rewrite $\delta D[u]/\delta u(\mathbf{r})$ (4.66)

as

$$\begin{aligned}
 \frac{\delta D[u]}{\delta u(\mathbf{r})} &= \sum_{i,j}^{\text{occ}} \sum_{a,b}^{\text{unocc}} \frac{\langle ab||ij \rangle}{\Delta_{ai} + \Delta_{bj}} \\
 &\times \left\{ 4\phi_i^*(\mathbf{r}) \phi_a(\mathbf{r}) \frac{\langle ji||bi \rangle - \langle ja||ba \rangle}{\Delta_{ai}} \right. \\
 &- \sum_{c \neq (a,b)}^{\text{unocc}} \left[\phi_c^*(\mathbf{r}) \phi_b(\mathbf{r}) \frac{\langle ij||ac \rangle}{\Delta_{ai} + \Delta_{cj}} - 2\phi_i^*(\mathbf{r}) \phi_c(\mathbf{r}) \frac{\langle cj||ab \rangle}{\Delta_{ci}} \right] \\
 &- \sum_{k \neq (i,j)}^{\text{occ}} \left[\phi_i^*(\mathbf{r}) \phi_k(\mathbf{r}) \frac{\langle jk||ab \rangle}{\Delta_{ak} + \Delta_{bj}} + 2\phi_k^*(\mathbf{r}) \phi_a(\mathbf{r}) \frac{\langle ij||kb \rangle}{\Delta_{ak}} \right] \\
 &\left. - [|\phi_a(\mathbf{r})|^2 - |\phi_i(\mathbf{r})|^2] \frac{\langle ij||ab \rangle}{\Delta_{ai} + \Delta_{bj}} \right\} + \text{c.c.} \quad (4.72)
 \end{aligned}$$

If desired, it is now straightforward to use the Unsöld approximation [148] and remove the summations over the unoccupied orbitals using the completeness relation.

Setting $\delta D[u]/\delta u(\mathbf{r})$ (4.66,4.72) equal to zero defines the minimizing potential u_0 ,

$$\left. \frac{\delta D[u]}{\delta u(\mathbf{r})} \right|_{u=u_0} = 0. \quad (4.73)$$

As $\delta D[u]/\delta u(\mathbf{r})$ depends implicitly on u , the above equation to determine u_0 must be solved iteratively with an energy minimization algorithm such as steepest descent. At the i^{th} iteration, $u(\mathbf{r})$ is updated as

$$u^{(i)}(\mathbf{r}) = u^{(i-1)}(\mathbf{r}) - \epsilon \left. \frac{\delta D[u]}{\delta u(\mathbf{r})} \right|_{u=u^{(i-1)}}, \quad (4.74)$$

with ϵ some small positive number (determined for example by a line search). We iterate until $D[u]$ and its functional derivative are converged.

Once the optimal potential u_0 has been found, together with its single-particle orbitals $\phi_{u_0,p}$ and energies $\epsilon_{u_0,p}$, we may proceed to determine the first-order KS potential by minimizing $S_{u_0}[w]$ over w , keeping u_0 fixed.

The minimizing potential $w_0[u_0] = u_0 + v'[u_0]$ (4.20) is given by (for fixed u_0)

$$\begin{aligned} 0 &= \left. \frac{\delta S_{u_0}[w]}{\delta w(\mathbf{r})} \right|_{w=u_0+v'[u_0]} \\ &= \sum_{i,a} \frac{\langle \phi_{u_0,i} | \mathcal{J}_{u_0} - \mathcal{K}_{u_0} - u_0 - v'[u_0] | \phi_{u_0,a} \rangle}{\epsilon_{u_0,i} - \epsilon_{u_0,a}} \phi_{u_0,a}^*(\mathbf{r}) \phi_{u_0,i}(\mathbf{r}) + \text{c.c.} \end{aligned} \quad (4.75)$$

The above equality is a standard OEP equation for the potential $v'[u_0]$; however, it needs only to be solved once to determine $v'[u_0]$, as the orbitals ϕ_{i,u_0} and their energies depend only on the already determined u_0 .

Finally, the KS potential to first order is given by

$$v_s[u_0](\mathbf{r}) = v_{en}(\mathbf{r}) + u_0(\mathbf{r}) + \alpha v'[u_0](\mathbf{r}) + \mathcal{O}(\alpha^2); \quad (4.76)$$

the correlation energy corresponding to the KS potential is

$$E_{u_0}^c[u_0 + v'[u_0]] = -S_{u_0}[u_0 + v'[u_0]] - D[u_0]. \quad (4.77)$$

In summary, by minimizing $T_u[w]$ over u and w , not only is the magnitude of the correlation energy the smallest possible over all u and w , leading to a fast converging expansion of the KS potential, but the resulting first order KS potential $v_s[u_0]$ also has both exchange and correlation character, rather than just exchange.

4.6 Analysis of variational collapse in DFT PT

In this section, we analyse the tendency towards variational collapse that is observed in DFT PT. By exploring the relationship between the second-order correlation energies in DFT PT, and the second-order correlation energy expressions in our work, we gain further insights into the liability of DFT PT to suffer from variational collapse.

Using the notation of the energy difference (4.17) and correlation energy (4.27), the second-order correlation energy in DFT PT, $E_c[\rho]$, is given by

$$E_c[\rho] = E_{v_{\text{Hxc}[\rho]}}^c[v_{\text{Hx}}[\rho]]. \quad (4.78)$$

In the above expression, v_{Hxc} and v_{Hx} refer respectively to the Hartree, exchange and correlation, and the Hartree and exchange potentials, for the KS system with density ρ . We note that the above expression, which is equivalent to equation (4.6), contains an implicit dependence on the Hxc-potential (through the KS orbitals), and an explicit dependence on the Hx-only potential. Alternatively, some applications of DFT PT [192] have used the following simpler form for the second-order correlation energy, which we denote $\tilde{E}_c[\rho]$ to distinguish it from $E_c[\rho]$ in Eq. (4.78),

$$\tilde{E}_c[\rho] = E_{v_{\text{Hxc}[\rho]}}^c[v_{\text{Hxc}}[\rho]]. \quad (4.79)$$

In the above, v_{Hxc} appears explicitly in place of v_{Hx} in the second-order energy (4.6).

To proceed with the analysis and compare with our method, it is convenient to view the density functionals (4.78) and (4.79) as potential functionals. Hence, we consider the density, $\rho = \rho_u$, to be the ground-state density of an effective Hamiltonian H_u , with ground-state Slater determinant Φ_u (4.13); this defines the KS system for an interacting state with density ρ_u . In this system, the potential u represents the Hxc part of the KS potential, with $w_0[u]$ representing the Hx part

of the KS potential, as can be seen by setting the functional derivative of $T_u[w]$ (4.18) equal to zero.*

Using our notation, the second-order correlation energies $E_c[\rho]$ (4.78) and $\tilde{E}_c[\rho]$ (4.79) can thus be written as

$$E_c[\rho_u] = E_u^c[w_0[u]] = -S_u[w_0[u]] - D[u]; \quad (4.80)$$

$$\tilde{E}_c[\rho_u] = E_u^c[u] = -S_u[u] - D[u]. \quad (4.81)$$

Meanwhile the total energy functionals, written as potential-functionals, are given respectively by

$$E[\rho_u] = \langle \Phi_u | H | \Phi_u \rangle - S_u[w_0[u]] - D[u] = \langle \Phi_u | H | \Phi_u \rangle - T_u[w_0[u]]; \quad (4.82)$$

$$\tilde{E}[\rho_u] = \langle \Phi_u | H | \Phi_u \rangle - S_u[u] - D[u] = \langle \Phi_u | H | \Phi_u \rangle - T_u[u]. \quad (4.83)$$

In DFT PT, the minimization over the total energy (truncated at second-order) with respect to the density ρ_u is equivalent to the minimization over the potential u , when viewed through an OEP lens. Thus, in DFT PT the above energy functionals are minimized with respect to u . The minimization over only the first term $\langle \Phi_u | H | \Phi_u \rangle$ in these expressions is well-defined, and leads to the Hx-only potential.

However, the second-order terms $-T_u[w_0[u]]$ and $-T_u[u]$ are unbound from below; thus, during the minimization over the total energies these terms will blow up and lead to variational collapse. This will be observed for both $E_c[\rho_u]$ and $\tilde{E}_c[\rho_u]$, but the effect will be particularly strong for the latter because, in this case, there is no optimization over w to restrict the magnitude of $S_u[w]$.

In the above analysis, the difference between the present method and DFT PT is stark. In the present method, we minimize the magnitude of second-order correlation energies, tantamount to *minimizing* the energy differences $T_u[u]$ over u or $T_u[w]$ over u and w . By contrast, in DFT PT, the minimization of the total energies truncated at second-order is biased towards the *maximization* of these quantities.

* $w_0[u]$ also represents the Hxc part of the KS potential with density $\rho_s[u]$ (4.21)

This further emphasises that our method, applied in a fully self-consistent manner, will not be prone to the issue of variational collapse inherent to DFT PT.

4.7 Summary and discussion

In this chapter, we have built on previous work at the interface of density and wave-function theories [188]. In this earlier work, a link between WFT and DFT was established via the energy difference (4.9): it transpires that the potential which minimizes this energy difference, a WFT expression, is the KS potential from DFT. It was also postulated in this earlier work that a perturbative expansion (4.13,4.14), similar to expansions in MBPT, could be used to develop perturbative expansions for the KS potential.

In the research presented in this chapter, we have explored appropriate choices for the zeroth-order potential u in the weakly-interacting expansion $H_u(\alpha)$ (4.14). We established a link between the second-order energy difference $T_u[w]$ (4.17) and the second-order correlation energy between the partially-interacting system and the non-interacting reference state Φ_v (4.27). Using physically intuitive arguments and experience from WFT, we argued that minimizing the magnitude of the second-order correlation energies (4.32) and (4.34) leads to fast-converging expansions for the KS potential, and thus defines good choices for the potential u .

We explored three choices for the zeroth-order term in a weakly-interacting expansion for the wave-function. In the first two choices, the density of the weakly-interacting state does not change to first-order; respectively, these choices define two exchange-only potentials in DFT, the EXX and LFX potentials. The third and final choice, based on a minimization of $|E_u^c[w]|$ (4.6) over both u and w , leads to a potential previously unseen in the literature with both exchange and correlation character to first order. We claim this is an energetically more optimal choice for u than that which yields the EXX potential, because the choice of u which

defines the EXX potential leaves the energetically dominant term of $|E_u^c[w]|$ (4.45) unoptimized.

Finally, we also considered in detail the relationship between the present work linking WFT and DFT and traditional DFT PT. The tendency towards variational collapse in DFT PT was analysed using expressions from our work; this emphasised the differences between the two methods, and provided further evidence that our method will not be prone to variational collapse.

In the following chapter, we explore the integration of WFT and DFT in a different light, by developing a method to obtain numerically the KS potential from a given density.

Density-to-potential inversion: role of the screening density

In this chapter, we present a method to accurately obtain the KS potential from a given density. The problem of inverting a density to find its KS potential has a long history in the DFT literature; in the first section of this chapter we explore the motivation for an accurate density-to-potential inversion procedure and review some of the methods that have been developed.

In our method, the screening density (introduced in § 3.7.1) plays a fundamental role in ensuring the KS potential has correct profile. The method, and the particulars of the algorithm employed, is described in § 5.2. Following this, we show that the method can be applied to a variety of different systems and target densities in § 5.3. Finally, we draw comparison with the related and well-known density-inversion method of Zhao, Morrison and Parr [221, 222] in § 5.4, before finishing with a brief summary and discussion.

5.1 Motivation and review of existing methods

As discussed in Chapter 3, commonly-used functionals in DFT have various qualitative failings, such as the self-interaction error and closely-linked delocalization

error, and the static correlation error. These qualitative failings hinder the predictive power of DFT in various applications such as charge-transfer processes [223] and molecular dissociation [121]; there are many research groups developing new methods and functionals to overcome these difficulties [97, 109, 224–226].

In order to gauge the accuracy of new approaches in DFT, it is important to have an accurate reference against which to benchmark results. Commonly, this is achieved by comparing results with experiment or a higher-level theory such as coupled cluster or quantum Monte-Carlo. However, it is also useful to have an accurate reference KS potential, which can be obtained (in theory) by inverting the density from a higher-level calculation to obtain the local (KS) potential which reproduces that density. Further applications of density-to-potential inversion algorithms include density-dependent embedding schemes [227], partition DFT [228], machine learning the xc-potential from inverted densities [229, 230], and quantifying ‘density-dependent’ errors in DFT [231].

In contrast to the usual problem in DFT, in which the KS equations are solved self-consistently given an input xc-functional to determine the ground-state density, a reliable numerical framework for the inverse problem remains an active area of research. For one or two* electron densities, the effective potential can be directly obtained through the formula

$$v_s(\mathbf{r}) = \frac{\nabla^2 \phi_1(\mathbf{r})}{2\phi_1(\mathbf{r})}. \quad (5.1)$$

However, for systems with $N > 2$, the inverse problem is challenging and as such a plethora of methods has been developed.

Early algorithms for the density-inversion problem were limited to few-electron or spherically symmetric systems; these include the parameter-based approach by Almbladh and Pedroza [232], or the method by Aryasetiawan and Stott [233], later extended by various others [234–237], based on solving $N - 1$ differential equations. Since then, more generally applicable methods have been developed; we briefly

*for a closed-shell system in the restricted KS formalism

describe two of the most famous approaches. The first is the Zhao-Morrison-Parr scheme [221, 222], in which the following KS equation is solved

$$\left\{ -\frac{\nabla^2}{2} + v_{\text{en}}(\mathbf{r}) + \left(1 - \frac{1}{N}\right) v_{\text{H}}^t(\mathbf{r}) + v_{\text{ZMP}}(\mathbf{r}) \right\} \phi_i(\mathbf{r}) = \epsilon_i \phi_i(\mathbf{r}), \text{ with} \quad (5.2)$$

$$v_{\text{ZMP}}(\mathbf{r}) = \lambda \int d\mathbf{r}' \frac{\rho(\mathbf{r}') - \rho_t(\mathbf{r}')}{|\mathbf{r} - \mathbf{r}'|}, \quad (5.3)$$

in the limit that $\lambda \rightarrow \infty$. The second is the direct optimization method by Wu and Yang [238], in which the objective functional

$$W_s[\Psi, v] = 2 \sum_{i=1}^{N/2} \langle \phi_i | \hat{T} | \phi_i \rangle + \int d\mathbf{r} v(\mathbf{r}) \{ \rho(\mathbf{r}) - \rho_t(\mathbf{r}) \} \quad (5.4)$$

is maximised wrt the potential $v(\mathbf{r})$; $W_s[\Psi, v]$ attains its maximum value when the KS density $\rho(\mathbf{r})$ and target density $\rho_t(\mathbf{r})$ are equal, ie when $v(\mathbf{r})$ is the KS potential for the system with density $\rho_t(\mathbf{r})$.

Various other methods have been developed for the inverse problem [190, 239–245], most of which follow an iterative scheme in which the potential is updated as

$$v_s^{(i)}(\mathbf{r}) = v_s^{(i-1)}(\mathbf{r}) + \Delta v_s^{(i)}[\rho^{(i)}, \rho_t](\mathbf{r}) \quad (5.5)$$

until some objective functional $S[\rho^{(i)}, \rho_t]$ depending on both the density at the i th iteration and the target density ρ_t is minimized. In Ref. [246], the authors establish a link between these methods based on the Levy–Perdew–Sahni equation [247]. Recently, more sophisticated approaches, based on partial differential equations and careful tuning of the input density, have been implemented [248, 249]; algorithms have also been developed for the time-dependent inverse problem [250, 251].

Despite the multitude of methods for the density-to-potential inversion problem in DFT, it remains an interesting and open-ended research problem; see Ref. [248] for a review of the difficulties in obtaining an accurate KS potential from a given density. The popularity of KS-DFT is driven, in part, by the balance between accuracy and ease-of-use; this balance is not so well-maintained in the inverse problem, in which more accurate methods are often more challenging to implement.

The method we present in this chapter, based on the approach in Ref. [190], is designed to be conceptually simple and straightforward to implement in Gaussian basis set codes. In our method, which uses the concept of screening density (3.45), the value of the screening charge (3.46) is fixed; this stabilizes the minimization procedure and ensures the KS potential has the correct asymptotic behaviour, as we observe that multiple potentials can arise from the same density. We always apply our method to the widely-used correlation-consistent basis sets [163, 164], to understand what level of accuracy can be expected for a particular basis set.

5.2 Method

Our method falls within the general class of iterative methods described by equation (5.5). Our objective functional is given by the Coulomb energy $U[\rho - \rho_t]$ of the density difference $\rho_v - \rho_t$,

$$U[\rho_v - \rho_t] = \frac{1}{2} \int d\mathbf{r} \int d\mathbf{r}' \frac{[\rho_v(\mathbf{r}) - \rho_t(\mathbf{r})][\rho_v(\mathbf{r}') - \rho_t(\mathbf{r}')] }{|\mathbf{r} - \mathbf{r}'|}, \quad (5.6)$$

where ρ_v is the density of a non-interacting N -electron system with KS potential $v_{\text{en}} + v$. This effective potential v mimics the electronic repulsion; at the minimum of the Coulomb energy U , with $\rho_t = \rho_v$, this effective potential is equal to the Hxc-potential for the system with density ρ_t , which is the potential we seek.

Clearly, the Coulomb objective functional (5.6) is strictly non-negative, and is equal to zero when non-interacting density ρ_v is identical to the target density ρ_t . We represent the effective potential $v(\mathbf{r})$ using a screening density $\rho_{\text{scr}}(\mathbf{r})$, which integrates to a screening charge Q_{scr} :

$$v(\mathbf{r}) = \int d\mathbf{r}' \frac{\rho_{\text{scr}}(\mathbf{r}')}{|\mathbf{r} - \mathbf{r}'|}, \quad (5.7)$$

$$\int d\mathbf{r} \rho_{\text{scr}}(\mathbf{r}) = Q_{\text{scr}}. \quad (5.8)$$

As discussed in § 3.7.1, we argue that the value of the screening charge Q_{scr} is a measure of self-interactions. In theory, its value lies anywhere in the range

$$N - 1 \leq Q_{\text{scr}} \leq N, \quad (5.9)$$

with $Q_{\text{scr}} = N - 1$ being a necessary condition for the method to be fully self-interaction free. As the value of Q_{scr} does not change in the algorithm we use, it is important to start with a screening density that is consistent with the screening charge of the target density.

When we vary the potential $v(\mathbf{r})$ as

$$v(\mathbf{r}) \rightarrow v(\mathbf{r}) + \epsilon \int d\mathbf{r}' \frac{\delta\rho_{\text{scr}}(\mathbf{r}')}{|\mathbf{r} - \mathbf{r}'|}, \quad (5.10)$$

the change in the objective functional $\delta U[v]^*$ is given by

$$\delta U[v] = \epsilon \int d\mathbf{r} \int d\mathbf{r}' \delta\rho_{\text{scr}}(\mathbf{r}) \tilde{\chi}_v(\mathbf{r}, \mathbf{r}') \delta\rho(\mathbf{r}') + \mathcal{O}(\epsilon^2), \quad (5.11)$$

with

$$\delta\rho(\mathbf{r}) = \rho_v(\mathbf{r}) - \rho_t(\mathbf{r}) \quad (5.12)$$

and

$$\tilde{\chi}_v(\mathbf{r}, \mathbf{r}') = \int d\mathbf{x} \int d\mathbf{y} \frac{\chi_v(\mathbf{x}, \mathbf{y})}{|\mathbf{r} - \mathbf{x}| |\mathbf{r}' - \mathbf{y}|}. \quad (5.13)$$

$\chi_v(\mathbf{r}, \mathbf{r}')$ is the density-density response function (3.62) for the KS system described by the effective potential $v(\mathbf{r})$. Since it is a negative semi-definite operator, if we vary $\rho_{\text{scr}}(\mathbf{r})$ in the direction

$$\rho_{\text{scr}}(\mathbf{r}) \rightarrow \rho_{\text{scr}}(\mathbf{r}) + \epsilon\delta\rho(\mathbf{r}), \quad \text{with } \epsilon > 0 \quad (5.14)$$

then U will decrease, with the change δU equal to

$$\delta U[v] = -\epsilon \int d\mathbf{r} \int d\mathbf{r}' \delta\rho(\mathbf{r}) \tilde{\chi}_v(\mathbf{r}, \mathbf{r}') \delta\rho(\mathbf{r}') + \mathcal{O}(\epsilon^2). \quad (5.15)$$

We can therefore use a gradient-descent based algorithm to minimize U . We note that during the minimization procedure, the screening charge Q_{scr} remains equal to the value prescribed by the initial guess for ρ_{scr} , since $\int d\mathbf{r} \delta\rho(\mathbf{r}) = 0$.

As an aside, we note that this algorithm to minimize the Coulomb objective functional will also minimize the energy difference $T_{\Psi}[v]$ as seen in Chapter 4,

$$T_{\Psi}[v] = \langle \Psi | H_v | \Psi \rangle - E_v, \quad (5.16)$$

* $U[\rho_v - \rho_t]$ is a functional of ρ_v and the target density ρ_t ; since the target density is fixed and ρ_v depends on v , we denote U more simply as a functional of v , $U = U[v]$.

given that the functional derivative of $T_\Psi[v]$ is equal to $-\delta\rho(\mathbf{r})$. However, the Coulomb energy is a more straightforward quantity to evaluate than $T_\Psi[v]$; it requires only the density, rather than the wave-function, for the target system.

5.2.1 Algorithm

We have implemented the method described above in the HIPPO code. The algorithm is described below.

1. Initialize the screening density as follows:

$$\rho_{\text{scr}}^{(0)}(\mathbf{r}) = \frac{N - \alpha}{N} \rho^{(0)}(\mathbf{r}), \quad (5.17)$$

where $\alpha \in [0, 1]$ depends on the target density, and thus $Q_{\text{scr}} = N - \alpha$. $\rho^{(0)}$ can be any function which integrates to N ; in practise, we choose it to be the density from an LDA calculation because this is computationally cheap to obtain and typically seems to be a reasonable starting point.

The screening density is expanded in an auxiliary basis,

$$\rho_{\text{scr}}(\mathbf{r}) = \sum_k^{n_{\text{aux}}} \rho_k^{\text{s}} \theta_k(\mathbf{r}). \quad (5.18)$$

For the auxiliary basis, we use the density-fitted basis set [252] corresponding to the choice of orbital basis. Analysis and justification for this choice of auxiliary basis set is presented in the following section.

2. Solve the single-particle KS equations

$$\left[-\frac{\nabla^2}{2} + v_{\text{en}}(\mathbf{r}) + v(\mathbf{r}) \right] \phi_{v,i}(\mathbf{r}) = \epsilon_{v,i} \phi_{v,i}(\mathbf{r}) \quad (5.19)$$

to update the density $\rho_v(\mathbf{r})$.

3. Update the screening density at the i th iteration as follows,

$$\delta\rho_{\text{scr}}^{(i)}(\mathbf{r}) = \rho_{\text{scr}}^{(i-1)}(\mathbf{r}) + \epsilon[\rho_v^{(i-1)}(\mathbf{r}) - \rho_t(\mathbf{r})]. \quad (5.20)$$

For any ϵ where $0 < \epsilon \ll 1$, the above step is guaranteed to decrease U (except in the limit $U = 0$). The value of ϵ in steepest-descent algorithms is usually chosen by a line-search routine, of which there are several flavours. We use a quadratic line search to pick the optimal ϵ : this procedure is described in Appendix A.

In the above step, we observe that it is convenient to expand the target density in the same orbital basis as the KS density, because the density difference is given without further computation. It is then straightforward to make the following transformation from the density difference in the orbital basis to the change in $\delta\rho_{\text{scr}}$ in the auxiliary basis*,

$$\delta\rho_p^{\text{S}} = - \sum_q^{n_{\text{aux}}} \sum_{k,l}^{n_{\text{orb}}} \delta\rho_{kl} \langle \theta_p | \tilde{\theta}_q \rangle^{-1} \langle \tilde{\theta}_q | \xi_k \xi_l \rangle, \text{ with} \quad (5.21)$$

$$\tilde{\theta}_q(\mathbf{r}) = \int d\mathbf{r}' \frac{\theta_q(\mathbf{r}')}{|\mathbf{r} - \mathbf{r}'|}. \quad (5.22)$$

4. Repeat steps 2 and three until either

- i U and δU are converged to within some chosen tolerance, or;
- ii The amount, or the rate of increase, of *negative* screening charge,

$$Q_{\text{neg}} = \frac{1}{2} \left\{ \left(\int d\mathbf{r} |\rho_{\text{scr}}(\mathbf{r})| \right) - Q_{\text{scr}} \right\} \quad (5.23)$$

exceeds a chosen amount.

Condition (ii) is a kind of *regularization* [248, 253]. It has been observed [248, 249] that the density-to-potential inversion problem in KS-DFT is ill-posed, in that the potential obtained from an inversion may be non-unique and contain unphysical (discontinuous and oscillatory) features. This is largely due to errors or missing information in the input density; Gaussian-basis set densities lack the correct cusp near the nuclei, as well as incorrect decay in the asymptotic region [249]. Additional factors that may adversely affect the

*In fact, it is cheaper still to expand the screening density in products of the orbital basis, eliminating the need for this additional computational step. We discuss later why we use an auxiliary basis for the screening density.

KS potential include finite basis set effects due to the interplay between the orbital and auxiliary basis sets [173, 178, 179] and possible issues related to non-interacting v -representability [50, 254–259].

In our method, the fixed nature of the screening charge restricts the freedom of the KS potential, reducing the prevalence of the above issues. Furthermore, the update step for the screening density (5.20) is quite restrictive and usually prevents the potential from developing spurious oscillations. However, we are still restricted by the quality of the input density, and thus issues of over-converging to the input density tend to emerge. This problem is reflected, for example, in the quality of the KS eigenvalues or the appearance of the KS potential. We have observed that these issues are often correlated with a large or rapid build up of negative screening charge. Thus, a simple criterion to avoid over-convergence is simply to stop the optimization procedure when Q_{neg} or δQ_{neg} surpasses a certain threshold. Specific details of the convergence criteria used are discussed in § 5.2.3.

5.2.2 Choice of basis set representation for the screening density

As discussed in the prior section, we choose to expand the screening density $\rho_{\text{scr}}(\mathbf{r})$ in the density-fitted basis which corresponds to the orbital basis used in the calculation. This is an intuitive choice, because it seems sensible to expand a the screening density in a basis set designed for density-like quantities; it is also a convenient choice, because density-fitted basis sets are frequently used in the computation of two-electron integrals in quantum chemistry codes (see § 3.9.1).

To justify this choice quantitatively, we recall (§ 3.9.1) that in typical DFT calculations the xc-potential is represented on a grid. This grid, unlike the Gaussian representation for the Hxc-potential we use (5.7,5.18), is specifically optimized to accurately represent the xc-potential, with the Hartree potential represented using the orbital basis. The natural choice of criteria for the auxiliary basis set

$U[\rho_{\text{ga}} - \rho_{\text{gr}}]$	orbital	uncontracted	ρ -fitted
He	2.3×10^{-7}	2.1×10^{-7}	1.2×10^{-8}
Be	7.0×10^{-4}	5.5×10^{-9}	4.2×10^{-10}
Ne	9.0×10^{-5}	1.8×10^{-6}	3.4×10^{-10}
HF	9.0×10^{-5}	2.9×10^{-7}	7.5×10^{-9}
H ₂ O	1.2×10^{-4}	2.2×10^{-7}	8.5×10^{-9}
H ₂	7.0×10^{-8}	1.6×10^{-7}	6.0×10^{-8}
CO	3.5×10^{-4}	2.7×10^{-7}	1.6×10^{-9}

Table 5.1: Values of $U[\rho_{\text{ga}} - \rho_{\text{gr}}]$ for LDA potentials in different Gaussian basis sets. All bases cc-pVTZ.

will therefore be that which accurately reproduces the Hxc-potential as it is normally expressed. The xc-potential can be transformed from the grid to Gaussian based representation using the relation (with $\rho_{\text{xc}}(\mathbf{r})$ representing the xc-part of the screening density),

$$v_{\text{xc}}(\mathbf{r}) = \sum_k^{n_{\text{aux}}} \rho_l^{\text{xc}} \int d\mathbf{r}' \frac{\theta_k(\mathbf{r}')}{|\mathbf{r} - \mathbf{r}'|}, \text{ with} \quad (5.24)$$

$$\rho_k^{\text{xc}} = \sum_l^{n_{\text{aux}}} \langle \tilde{\theta}_k | \theta_l \rangle^{-1} \langle \theta_l | v_{\text{xc}} \rangle. \quad (5.25)$$

To quantify the accuracy of representing the screening density in a particular Gaussian basis set, we use the Coulomb energy $U[\rho_{\text{ga}} - \rho_{\text{gr}}]$ (5.6), where ρ_{ga} and ρ_{gr} are the densities arising from defining the potential in a Gaussian basis set (integrated over $|\mathbf{r} - \mathbf{r}'|^{-1}$) and on the grid respectively. The smaller the value of $U[\rho_{\text{ga}} - \rho_{\text{gr}}]$, the better one might expect the Gaussian representation to be. In Table 5.1, we compare the values of $U[\rho_{\text{ga}} - \rho_{\text{gr}}]$ for three choices of basis functions for the screening density: the orbital basis, the density-fitted basis, and the uncontracted orbital basis, which is a common choice for the potential [108–110, 173]. We observe that the density-fitted sets give the closest fit to the grid representation based on this criterion, which is perhaps not surprising as they are specifically optimized for this purpose.

In Fig. 5.1, we plot the LDA xc-potentials for these basis set choices. In contrast to the above-mentioned analysis, the uncontracted sets seem to give the best fit to the

grid potential, but we note that the density-fitted sets give a close fit everywhere except the nuclear positions; it is also clear from these plots that the contracted orbital basis is a completely inadequate representation for the xc-potential*. In our experience, the algorithm works more smoothly for the density-fitted sets than the uncontracted ones. Given that we minimize $U[\rho_v - \rho_t]$, it makes sense to choose a representation that also minimizes this expression. The gradient-descent algorithm also struggles to reproduce the target density near the nuclei regardless of the auxiliary basis chosen, so the lack of accuracy of the density-fitted sets in this region is not so important in our method.

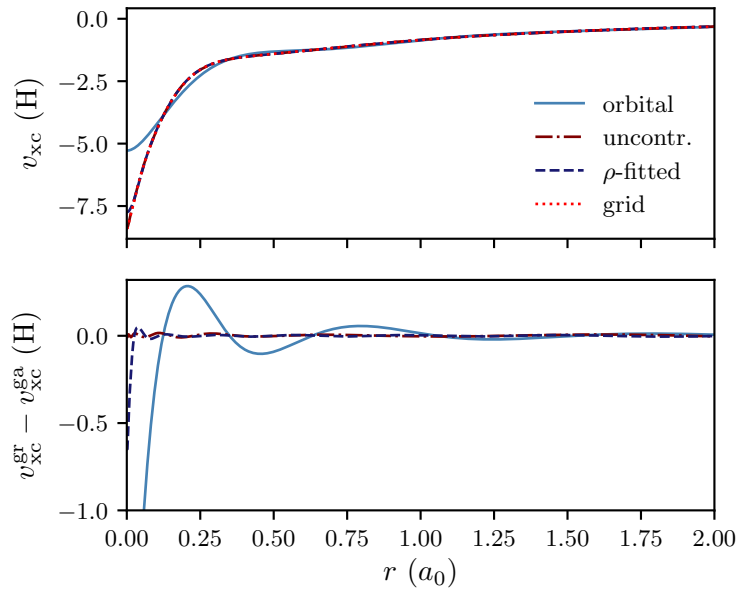
5.2.3 Convergence criteria

The tolerances for the objective functional U , and the change in the objective functional δU , are chosen to be 5×10^{-9} and 5×10^{-11} per electron, respectively. We have observed that, in the inversion of a density that comes from a DFT calculation (such as LDA), satisfying the above criteria does not lead to any issues regarding over-convergence. However, we see that these tolerances are often too strict for the inversion of densities from wave-function theories (Hartree–Fock and coupled cluster), as the quality of the potential starts to deteriorate before convergence is reached.

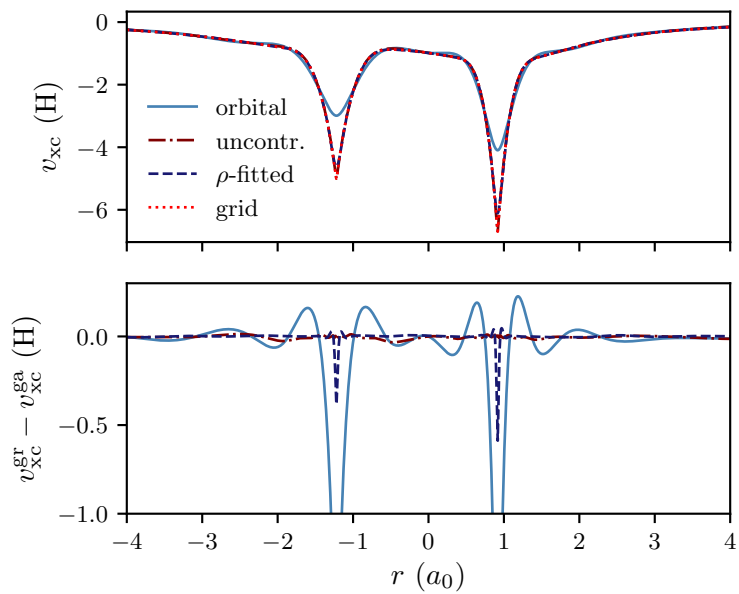
As discussed in § 5.2.1, we monitor the amount of negative screening charge to avoid over-convergence. The onset of negative screening charge is dependent on several factors, including

- i the number of electrons, N ,
- ii the size of the basis set, and
- iii the nature of the target density,

*In Ref. [219], when the Hxc-potential was separated into Hartree and xc-components for plotting purposes, the Hartree part was computed using the orbital basis. In this thesis, the Hartree potential is transformed into the auxiliary basis representation in the same manner as the xc-potential (5.25) to maintain consistency, and thus the plots look different.



(a) Ne (cc-pVTZ)



(b) CO (cc-pVTZ)

Figure 5.1: Comparison of the LDA xc-potential on a grid, against various Gaussian basis set representations. Lower images show the differences between the grid and Gaussian representation.

Q_{neg}	cc-pVDZ	cc-pVTZ
He	0.0	9.88×10^{-3}
Be	5.81×10^{-2}	7.65×10^{-2}
Ne	0.0	3.30×10^{-4}
HF	4.50×10^{-2}	8.18×10^{-2}
H ₂ O	3.03×10^{-2}	1.15×10^{-1}
H ₂	6.55×10^{-3}	6.35×10^{-2}
CO	1.09×10^{-2}	3.51×10^{-4}

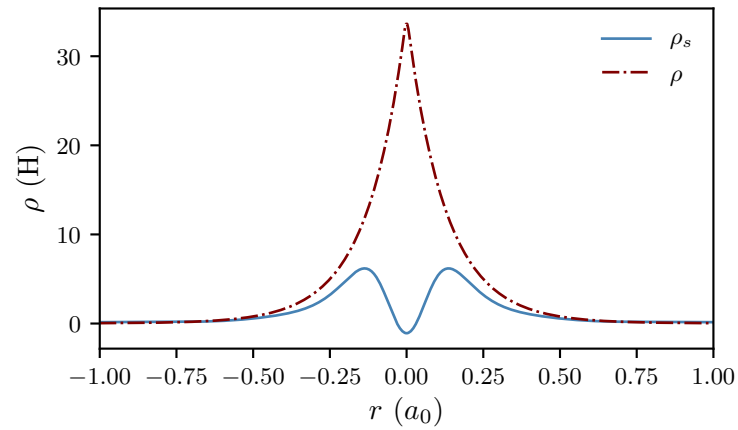
Table 5.2: Amount of negative screening charge, Q_{neg} , for exact LDA screening densities.

in addition to other (hard to quantify) factors related to the system under consideration. An example of the correlation between negative screening charge and the accuracy of the inverted KS potential is seen in Table 5.3. As we later argue, the energy eigenvalue of the highest-occupied molecular orbital (HOMO) is a reliable indicator of the quality of the inverted potential; for the example in the table, we see that the HOMO value becomes worse as Q_{neg} increases.

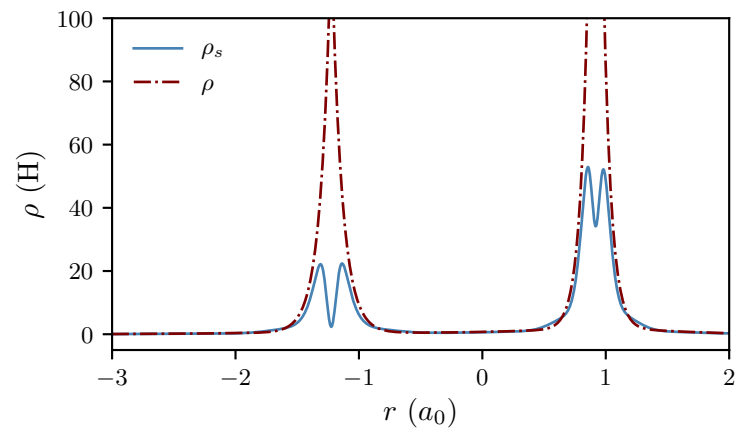
To guide our intuition regarding how much negative screening charge to allow, we recall that we can determine the ‘exact’ screening density for an LDA calculation via the relations (5.24-5.25). In Table 5.2, we see that a small amount of negative screening charge is typically present for the LDA effective screening density. In Fig. 5.2, we see this negative screening density is usually present near the nuclei. There is no reason to expect significantly dissimilar behaviour for different target densities, and therefore it seems judicious to allow a small amount of negative screening charge to manifest itself in the inversion procedure.

With the above arguments in mind, we monitor the following variables during the inversion procedure:

- i Soft limit, $Q_{\text{neg}}^{\text{soft}}$;
- ii Change in Q_{neg} , δQ_{neg} between iterations;
- iii Hard limit, $Q_{\text{neg}}^{\text{hard}}$;



(a) Be (cc-pVTZ)



(b) CO (cc-pVTZ)

Figure 5.2: Effective screening densities, $\rho_s(\mathbf{r})$, for LDA densities, with the actual densities for comparison. We observe the tendency for a small amount of negative screening charge near the nuclei.

If both conditions (i) and (ii) are satisfied, or just condition (iii), the calculation stops. For the sake of consistency, we use the same values for all calculations shown in this chapter:

- i $Q_{\text{neg}}^{\text{soft}} = 0.01$;
- ii $\delta Q_{\text{neg}} = 0.005$;
- iii $Q_{\text{neg}}^{\text{hard}} = 0.05$;

CCSD(T)				HF			
U (H)	Q_{neg}	$-\epsilon_{\text{H}}$ (eV)	% err	U (H)	Q_{neg}	$-\epsilon_{\text{H}}$ (eV)	% err
1.09×10^{-4}	0.00	8.71	6.5%	1.32×10^{-4}	0.00	8.28	1.5 %
2.31×10^{-5}	0.221	9.34	0.2%	4.69×10^{-5}	0.112	8.97	6.7%
1.36×10^{-5}	0.630	9.82	5.4%	3.33×10^{-6}	0.258	9.14	8.7%
1.29×10^{-5}	1.01	10.09	8.3%	5.03×10^{-8}	0.300	9.19	9.3%

Table 5.3: Values of the Coulomb objective functional $U[\rho_v - \rho_t]$, negative screening charge Q_{neg} , and HOMO eigenvalue ϵ_{H} , for inverted CCSD(T) and HF densities of the Beryllium atom. The final column shows, respectively, the percentage difference between ϵ_{H} and the experimental ionization potential of 9.32eV, and the Hartree–Fock value of 8.41eV.

where all the above values are quoted per electron. For the examples we have tested (atoms and small molecules at their equilibrium geometries), these values seem to be a reasonable choice. However, we note that there is a degree of arbitrariness in the specific numbers used and they may need to be adjusted in certain circumstances, such as molecules stretched beyond their equilibrium geometries.

5.3 Results

5.3.1 Inversion of LDA densities

To demonstrate the validity of our method, we first apply it to the inversion of LDA densities. In this case, we have an exact reference for the inverse potential, giving insight into the accuracy and limitations of the inversion procedure.

As discussed in § 5.2.1, it is important to initialize the inversion with the correct value of Q_{scr} since it does not change during the optimization cycle. As can be seen in Fig. 5.3, different values of Q_{scr} give rise to different xc-potentials (the difference is essentially a constant shift); this is for the same reason that the solution of the OEP equation has the freedom to vary by a constant (§ 3.9.3) [173, 174].

Since LDA is a method fully-contaminated by self-interactions, one would expect $Q_{\text{scr}} = N$ (§ 3.7.1). Indeed, this equality holds for the LDA potential expressed

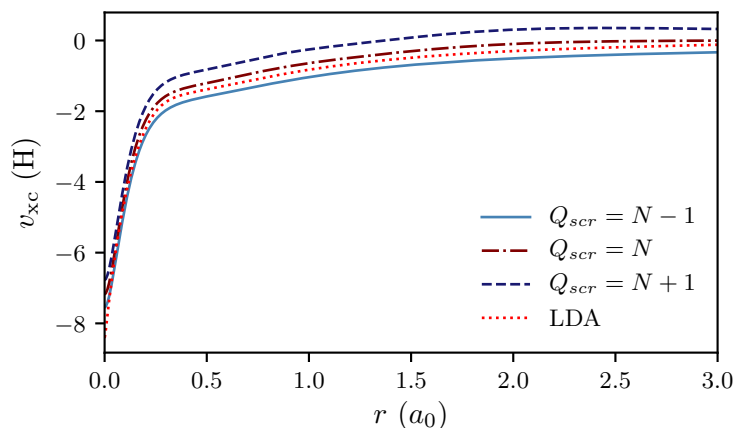


Figure 5.3: The inverted xc-potentials from the LDA density of Neon (cc-PVTZ), for different values of Q_{scr} . Each value of Q_{scr} yields a unique xc-potential.

	He		Be	
	α	$-\epsilon_{\text{H}}$ (eV)	α	$-\epsilon_{\text{H}}$ (eV)
cc-pVDZ	0.479	15.15	0.207	4.50
cc-pVTZ	0.214	14.82	0.148	4.81
cc-pVQZ	0.301	15.41	0.185	5.29
cc-pV5Z	0.256	15.89	0.165	5.41

Table 5.4: Values of α , where $Q_{\text{scr}} = N - \alpha$, and ionization potentials (IPs) as the negative of the HOMO energies, for He and Be with increasing basis set size.

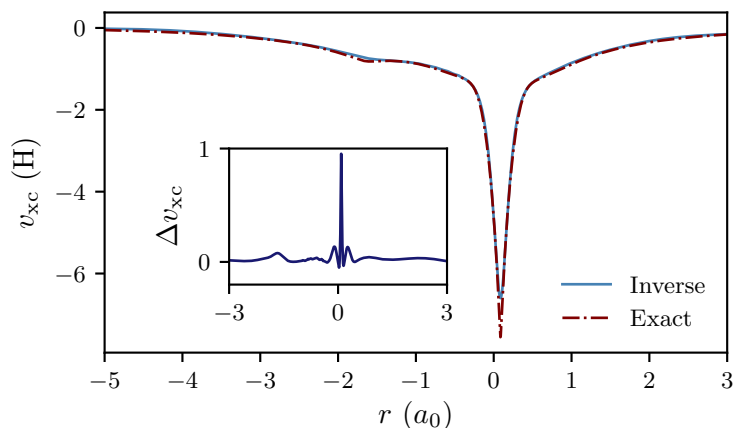
on the grid. However, when the potential is transformed into a Gaussian basis set representation (5.24-5.25), $Q_{\text{scr}} \neq N$. This is because typical Gaussian basis sets are insufficient to fully describe the character of the xc-potential on the grid; if we were to approach the complete basis set limit, we would see that $Q_{\text{scr}} \rightarrow N$ in this limit. Table 5.4 shows some example values of Q_{scr} as we increase the basis set size; even for very large basis sets, we see that the value of Q_{scr} differs significantly from N . We have observed that, if desired, it is possible to more cheaply approach the limit of $Q_{\text{scr}} = N$ by adding one or two diffuse basis functions to the auxiliary basis. For the results presented in this chapter, we choose not to modify the well-known cc-pVXZ basis functions, but in principle the modification of these basis sets is necessary without *a priori* knowledge of the precise value of Q_{scr} .

$-\epsilon_{\text{H}}$ (eV)	cc-pVDZ			cc-pVTZ			cc-pVQZ		
	Inverse	LDA	% err	Inverse	LDA	% err	Inverse	LDA	% err
He	15.15	15.14	0.1	14.82	15.47	4.2	15.41	15.37	0.6
Be	4.50	5.62	19.9	4.81	5.60	14.1	5.29	5.60	5.5
Ne	6.69	12.24	45.3	10.56	13.17	19.8	11.75	13.40	12.3
HF	7.18	8.45	15.0	8.91	9.38	5.0	9.37	9.64	2.8
H ₂ O	5.71	6.23	8.3	6.67	7.00	4.7	6.86	7.21	4.4
H ₂	9.53	10.12	5.8	10.00	10.25	2.4	10.02	10.26	2.3
CO	6.16	8.71	29.3	7.73	9.07	14.8	8.82	9.11	3.2
Avg % err			17.7			9.3			4.5

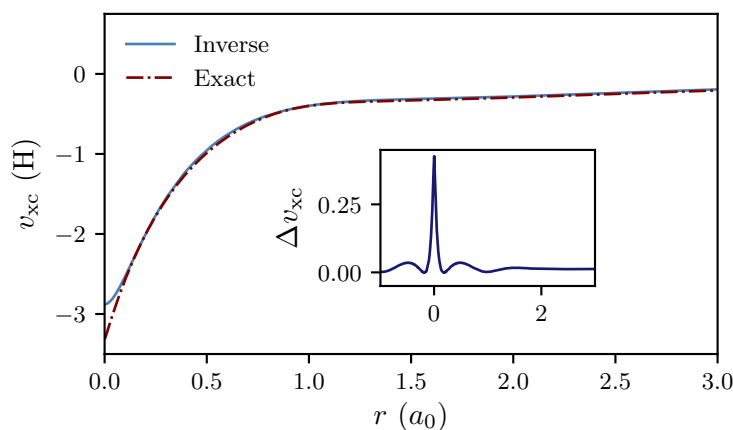
Table 5.5: Comparison of the HOMO eigenvalues ϵ_{H} from inverted LDA densities and the actual LDA eigenvalues.

With a method to calculate the appropriate value of Q_{scr} for LDA densities, we now demonstrate the accuracy of our method when applied to LDA densities and the convergence with an increase in the basis set size. In Fig. 5.4, we see the qualitative similarities between the actual LDA potential, and the inverted xc-potential from and LDA density, for the HF molecule and the Be atom. The region of biggest difference is near the nuclei; this is due in part to the deficiency of the input density, which lacks the correct cusp near the nucleus. If this region is considered important, it is important to use a larger basis set or modify the input density in some way, such as the method described in Ref. [249].

The KS eigenvalues from the inverted LDA density, compared with the actual LDA eigenvalues, can be used as a quantitative measure of the accuracy of the inversion procedure. We focus specifically on the HOMO energy level ϵ_{H} ; Table 5.5 compares the values of ϵ_{H} for the inverted system with the actual LDA values. These results show approximately what level of accuracy can be expected with a given basis set, with a clear convergence towards the correct LDA values as the basis set size is increased.



(a) HF (cc-pVTZ)



(b) Be (cc-pVQZ)

Figure 5.4: Comparison between the xc-potential from inverted LDA densities, and actual LDA results.

5.3.2 Constrained inversion of LDA densities

As discussed in the previous subsection, it is important to initialize correctly the screening charge in order to accurately obtain the xc-potential from the inversion of a density. Conversely, we can exploit the freedom of being able to choose the screening charge to mitigate against self-interaction errors. As discussed, the screening charge can be used as a measure of self-interactions, and thus by initializing with a screening charge of $N - 1$,

$$Q_{\text{scr}} = N - 1, \quad (5.26)$$

to reduce self-interaction effects, in particular the incorrect asymptotic behaviour of the (H)xc-potential, in common functionals such as LDA.

This concept has already been explored in a different context [108, 109], by minimizing the total energy functional for a DFA such as LDA, under the constraint (5.26) and also under the additional constraint that

$$\rho_{\text{scr}}(\mathbf{r}) \geq 0. \quad (5.27)$$

The above constraint was applied both as a form of regularization for the OEP equation, and to ensure the screening density did not develop a ‘hole’ with charge -1 in the far-field region. However, this positivity constraint is a computational bottleneck; it is not required under the density inversion procedure since there is no OEP equation to be solved and the update step (5.20) does not allow screening charge to develop in regions of zero density.

In exact KS theory, the ionization potential (IP) is formally equal to the negative of the KS HOMO eigenvalue (3.49). A systematic failing of common DFT functionals is that they significantly underestimate IPs using this relationship. This is largely attributed to the SI error inherent in these functionals. In Table 5.6, we compare LDA IPs with IPs obtained under the constraint $Q_{\text{scr}} = N - 1$, which we denote ‘constrained’ LDA (CLDA). We see that the IPs demonstrate systematic improvement relative to the experimental IPs under this constraint, as had been observed in Refs. [108] and [109]. We see that the IPs obtained via the density inversion method are in close agreement compared to those from the original method [108]. In Chapter 7, we relax the positivity constraint for the original CLDA method, using the more rigorous solution to the OEP equation described in § 3.9.3.

5.3.3 Inversion of densities from wave-function theories

The main aim of any density-inversion scheme is of course to obtain the KS potentials corresponding to densities from theories other than DFT. In this chapter, we have applied our method to densities from two theories: Hartree–Fock (HF) and

IP (eV)	LDA	CLDA (inv)	CLDA [108]	Expt. [260]
He	15.47	23.12	23.82	24.59
Be	5.60	8.48	8.65	9.32
Ne	13.17	18.85	18.89	21.56
HF	9.38	14.08	14.17	16.03
H ₂ O	6.83	11.10	11.04	12.62
H ₂	10.25	15.15	15.64	15.43
CO	8.97	12.50	12.84	14.01

Table 5.6: Comparison of IPs (from HOMO energies) for constrained-LDA using the inversion of density, and the previous implementation of CLDA. All basis sets are cc-pVTZ.

coupled cluster theory, specifically CCSD(T). We focus on these theories specifically because HF is an exchange only method, whose inversion yields the exchange-only Local Fock exchange (LFX) potential (§ 4.4.2) [190]; meanwhile CCSD(T) densities [45, 261] are very accurate even for strongly-correlated systems, and hence it should provide an indication of what to expect from the ‘exact’ KS potential.

As demonstrated in the inversion of LDA densities, it is important to choose the correct screening charge. As HF and CCSD(T) are both self-interaction free theories, in a complete basis set we would expect $Q_{\text{scr}} = N - 1$. Unlike the LDA case, there is no way to determine whether this value varies due to finite basis set effects; however, our results strongly suggest it is a good choice and hence we always use this value. We focus again on the HOMO eigenvalue ϵ_{H} : due to Koopman’s theorem [24] and its equivalent in KS-DFT (3.49), the LFX value of ϵ_{H} should equal its HF value. Likewise, $-\epsilon_{\text{H}}$ from an inverted CCSD(T) density should be approximately equal to the experimental IP*.

Table 5.7 shows a comparison between HF and LFX IPs for increasing basis set size. Like in the LDA case, the method is demonstrably more accurate for larger basis sets; we see that it is important to use at least a cc-pVTZ basis set to obtain meaningful results, with this basis set yielding a reasonable average error of 3.8%. We see a similar picture emerge for the CCSD(T) examples in Table 5.8; in this

*We cannot expect to approach equality with the experimental IP except in the complete basis set limit.

IP (eV)	cc-pVDZ			cc-pVTZ			cc-pVQZ		
	Inverse	HF	% err	Inverse	HF	% err	Inverse	HF	% err
He	25.23	24.88	1.4	24.97	24.97	0.0	24.98	24.98	0.0
Be	8.96	8.41	6.5	8.42	8.42	0.0	8.37	8.42	0.6
Ne	17.57	22.65	22.4	22.19	23.01	3.6	24.40	23.10	5.6
HF	14.21	17.12	17.0	16.57	17.52	5.4	17.23	17.64	2.3
H ₂ O	12.03	13.44	10.5	12.99	13.76	5.6	13.40	13.85	3.2
H ₂	16.13	16.10	0.2	16.16	16.16	0.0	16.17	16.17	0.0
CO	11.65	14.96	22.1	13.74	15.09	8.9	14.03	15.11	7.1
Avg % err			11.5			3.4			2.7

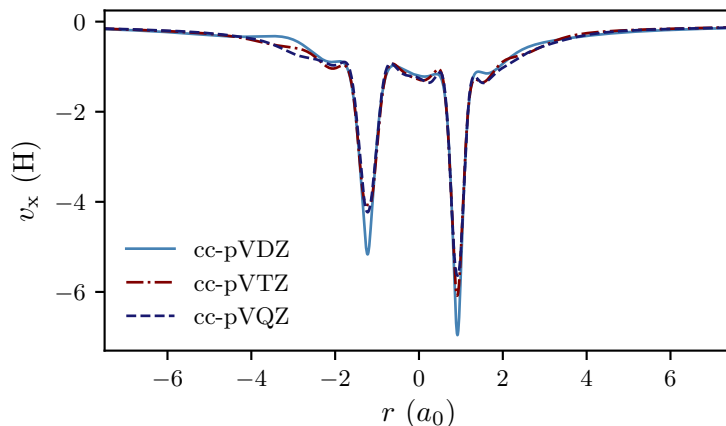
Table 5.7: Comparison of IPs for the local potential of an HF density with the actual HF IPs.

IP (ev)	cc-pVDZ		cc-pVTZ		Expt [260]
	Inverse	% err	Inverse	% err	
He	24.94	1.4	24.57	0.1	24.59
Be	9.13	2.0	9.12	2.0	9.32
Ne	12.09	43.9	20.41	5.3	21.56
HF	11.34	29.3	15.43	3.7	16.03
H ₂ O	10.01	20.7	12.28	2.7	12.62
H ₂	15.91	3.1	16.45	6.6	15.43
CO	10.01	28.6	13.18	5.9	14.01
Avg % err		18.4		3.8	

Table 5.8: Comparison of IPs for the local potential of a CCSD(T) density with experimental IPs.

case, the cc-pVQZ results have not been computed due the computational expense of obtaining the input densities. However, the average error of 3.8% for the cc-pVTZ results is similar to the HF result.

Besides the comparisons of IPs, it is insightful to plot the xc-potentials from the inversion procedure. In Fig. 5.5, we plot the xc-potentials for various basis sets. From this figure, we see that the xc-potentials are smooth and converge with increasing basis set size. These plots emphasize the importance of using at least a cc-pVTZ basis set to obtain qualitatively accurate potentials. Like in the LDA case, we observe the inverse potentials are least consistent near the nuclei, but away from this region their behaviour is more reliable.



(a) CO (inverted HF density)

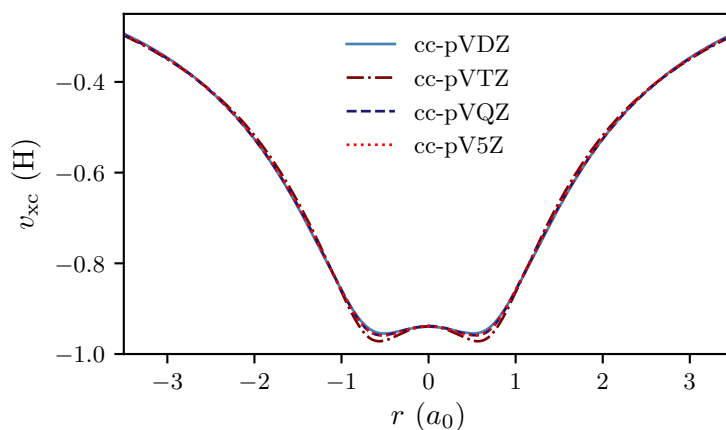
(b) H₂ (inverted CCSD(T) density)

Figure 5.5: x(c)-potentials from HF and CCSD(T) densities for various basis sets

On account of the similarity between the LFX and EXX potentials, particularly for weakly-correlated systems (§ 4.4.2), the inversion of HF densities offers a route to obtain exchange-only potentials without needing to solve the OEP equation. This similarity can be further exploited to obtain approximate correlation potentials, by taking the difference between an inverted CCSD(T) density and an LFX potential. This provides an important reference in the development of new functionals with accurate correlation character, as it has been observed that the correlation potentials of typical DFT functionals are quite poor [100]. In Fig. 5.6, we have plotted the correlation potential for the Argon atom using this method, with the

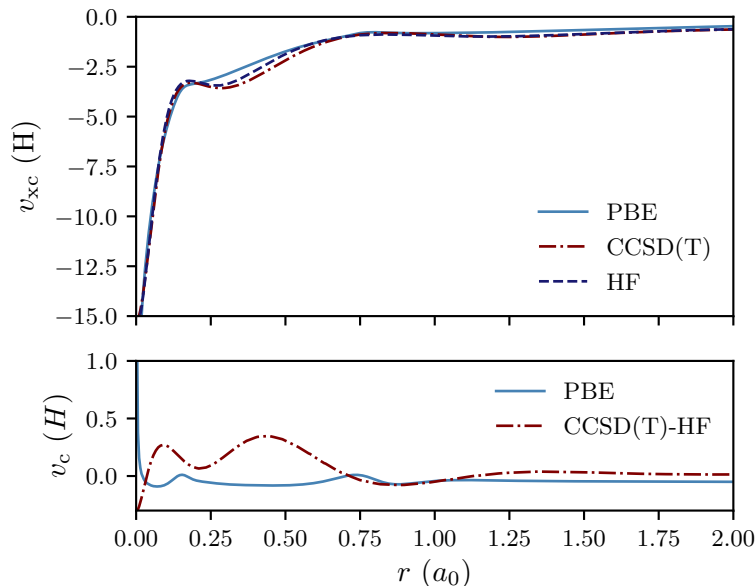


Figure 5.6: Top: Ar (cc-pvTZ) xc-potentials from inverted HF and CCSD(T) densities, and PBE; bottom: correlation potentials from the difference of CCSD(T) and HF inverted xc-potentials, and PBE.

PBE correlation potential also shown for comparison.

5.4 Comparison with the method by Zhao, Morrison and Parr

Our density-inversion method invites a comparison with the well-known method by Zhao, Morrison and Parr (ZMP) [222], since this method also features the Coulomb energy of the difference between the KS and target densities (5.6). In the ZMP method, rather than minimizing $U[\rho_v - \rho_t]$, they impose the condition that it vanishes in the minimization of the total energy functional. This leads to the following definition of the KS potential,

$$v_s^\lambda(\mathbf{r}) = v_{\text{en}}(\mathbf{r}) + \left(1 - \frac{1}{N}\right) v_{\text{H}}^t(\mathbf{r}) + \lambda \int d\mathbf{r}' \frac{\rho_v(\mathbf{r}') - \rho_t(\mathbf{r}')}{|\mathbf{r} - \mathbf{r}'|}, \quad (5.28)$$

where λ is a Lagrange multiplier used to enforce $U[\rho_v - \rho_t] = 0$. The densities ρ_v and ρ_t become equal in the limit $\lambda \rightarrow \infty$; computationally, this is done by solving

the KS equations for increasingly large values of λ and extrapolating to the limit of infinite λ .

In the ZMP method, it is commented that the Fermi-Amaldi term in the potential $(1 - 1/N)v_{\text{H}}^t(\mathbf{r})$ is present primarily to aid convergence, but also to obtain accurately the KS orbital energies. As noted in the ZMP paper, replacement of this term with just $v_{\text{H}}^t(\mathbf{r})$ leads to an arbitrary shift in the eigenvalue spectrum. In our analysis using the screening density, it is clear why the Fermi-Amaldi term must be included: without it, the electrons experience a repulsive field from a net charge of N electrons, whereas for an SI-free input density they should experience a field from a net charge of $N - 1$ electrons.

In some sense, the connection between the ZMP method and our approach is like the connection between the direct minimization of an energy density-functional, and the indirect minimization using the OEP method. In the ZMP method, the total energy is minimized directly wrt the density, with the “xc”-functional given by

$$E_{\text{xc}}^{\text{ZMP}}[\rho_v] = \lim_{\lambda \rightarrow \infty} \lambda U[\rho_v - \rho_t] - \frac{1}{N} U[\rho_v]. \quad (5.29)$$

In practise, the limit $\lambda \rightarrow \infty$ is reached approximately by doing separate calculations for several values of λ and extrapolating to the infinite limit. In our method, we minimize only the Coulomb energy $U[\rho_v - \rho_t]$, which is equivalent to minimizing the total ZMP energy functional with $\lambda = \infty$. This can only be done by minimizing $U[\rho_v - \rho_t]$ indirectly wrt the density (over the potential $v(\mathbf{r})$) in an OEP-like manner.

5.5 Summary and discussion

In this chapter, we have considered the problem of density-to-potential inversion in KS-DFT. Our method is based on the algorithm in Ref. [190] but applied here to a finite basis set code with a wider variety of target densities. It is simple to implement in any standard Gaussian-basis set code, with both the objective functional

(5.6) and the update step for the screening density (5.20) being straightforward to obtain. The inverted potentials are unique (for the correctly chosen screening charge) and continuous, making the inversion procedure well-posed. We also see clear convergence with basis set size, with meaningful accuracy obtained for moderately-large cc-pVTZ basis sets.

In our analysis, we have seen the importance of the role played by the screening density. It is an important practical feature, as without a constraint on the screening charge the inverted potential is undetermined up to a constant; it is also a useful tool in understanding SI effects.

We have observed that our method is limited both by the basis set used to generate the target density, and by the auxiliary basis set used for the screening density. These problems are not easily solved using larger basis sets from the standard cc-pVXZ family: as such, future work for this density-inversion method would likely focus on how to modify these basis sets in a minimal way to yield systematic improvements.

Open-shell systems in Kohn–Sham theory via implicit density functionals

The treatment of open-shell systems is an enigmatic problem in DFT. Typically, the spin-DFT formalism is applied to open-shell systems. Although this often yields good energetics, it should not be formally required in the absence of a magnetic field; besides, adopting this formalism leads to a so-called ‘spin-symmetry dilemma’ in DFT [262]. However, the naive closed-shell-like approximation for the exchange energy of open-shell systems, which assumes (incorrectly) half the electrons are spin-up and the other half spin-down, causes a ‘ghost’ exchange error due to the exchange of fractional opposite-spin electrons.

In this chapter, we consider how to treat open-shell systems within the restricted KS formalism without incurring this ghost exchange error. We start (§ 6.1) by considering the motivation for such a formalism, and in particular the origins of the ghost exchange error. Then in § 6.2, we discuss our approach, in which the xc-functional is considered an implicit functional of the density, which leads naturally to an OEP equation for the KS potential. In § 6.3 we then explain how the OEP method described in § 3.9.3 is applied to DFAs and the exact exchange

(EXX) functional. Following that, we present results to demonstrate we can reliably solve the OEP equation for both DFAs (§ 6.4.1) and EXX (§ 6.4.2) and compare our results with unrestricted KS theory. Finally, we briefly summarize our findings and discuss their significance in § 6.5; additionally, we see how the unrestricted KS equations, until now derived from a spin-DFT perspective, arise from the generalized KS (GKS) formalism in the absence of an external magnetic field.

6.1 Motivation and the ‘ghost’ exchange error

The standard, or spin-restricted, KS formalism is the *de facto* approach for closed shell systems in DFT [263]. However, as touched on in § 3.5, there isn’t a unanimously favoured approach for the treatment of open-shell systems [67]. Most commonly, open-shell systems are treated within the spin-DFT formalism, otherwise known as spin-unrestricted or just unrestricted KS (UKS) theory.

UKS theory often yields good results, not only for open-shell systems, but also improving on RKS results for closed-shell systems in certain situations [264]. However, the fundamental variable of spin-DFT is not the density but the spin-density; in the true spirit of DFT, the spin-density should not be required in the absence of a magnetic field. Furthermore, having the spin-density as the fundamental variable can cause a conundrum known as the ‘spin-symmetry dilemma’ [262], in which spin-DFT yields the correct total energy but the wrong spin-density. We return to this dilemma in the discussion in § 6.5.

Alternatively, one can use the standard (restricted) KS theory for open-shell systems, as is routinely done for closed-shell systems. In this case, the exchange* energy is typically written as an explicit functional of the density and its gradient (for the most popular semi-local approximations). For example, the LDA exchange

*and correlation, though we focus here on the more conceptually straightforward exchange error

energy is given by

$$E_x^{\text{LDA}} = C \int d\mathbf{r} \rho^{4/3}(\mathbf{r}); \quad (6.1)$$

the exchange potential is then given directly by the functional derivative with respect to the density.

Recalling that the KS system represents an auxiliary system of non-interacting electrons, we see why the LDA exchange (6.1) and similar GGA expressions are problematic. The exchange energy in this auxiliary system ought to be consistent with Pauli’s exclusion principle, which forbids same spin-electrons from occupying the same spatial position, but there is no exchange force between opposite-spin electrons. Density functionals approximations which depend only on the density, and do not account for the spin-density, are liable to violate Pauli’s exclusion principle for open-shell systems*. This violation is because the density alone cannot account for the fact that the spin-densities are different for open-shell systems.

The tacit assumption in the LDA exchange approximation (6.1) and other DFAs is that the spin-densities are equal to each other and to half the total density. For open-shell systems, this assumption is incorrect and leads to an exchange energy between fractional charges of opposite-spin electrons. This error has also been observed for the exact exchange functional in ensemble calculations, when the KS orbitals are fractionally occupied [265]. We call this spurious exchange energy the ‘ghost’ exchange error, in analogy to the ghost interaction of Ref. [266]. We note that this error is not limited to approximate density-functionals, and is also observed in the exact exchange functional if fractional spin-densities are introduced.

We define the ghost-exchange error by the difference of the exchange energy with mixed spin-densities, and the reference exchange energy in which the spin densities

*The exact density functional, if it existed, would not violate Pauli’s exclusion principle if it had no spin-density dependence, as the density alone is in principle sufficient for an exact description. However, such a functional would have a highly non-local density dependence, in contrast to typical (semi)-local DFAs.

are separate*, as they must be to form a Slater determinant. In other words,

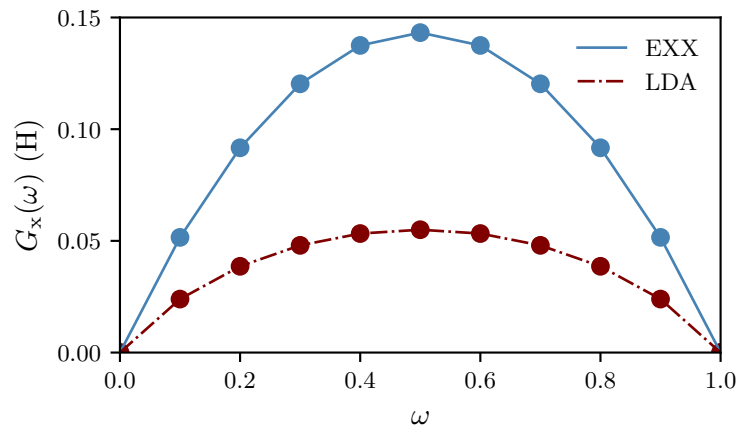
$$G_x(\omega) = E_x[(1 - \omega)\rho^\uparrow + \omega\rho^\downarrow, (1 - \omega)\rho^\uparrow + \omega\rho^\downarrow] - E_x[\rho^\uparrow, \rho^\downarrow], \text{ with} \quad (6.2)$$

$$0 \leq \omega \leq 1 \quad \text{and} \quad \rho^\sigma(\mathbf{r}) = \sum_{i=1}^{N_\sigma} |\phi_i(\mathbf{r})|^2. \quad (6.3)$$

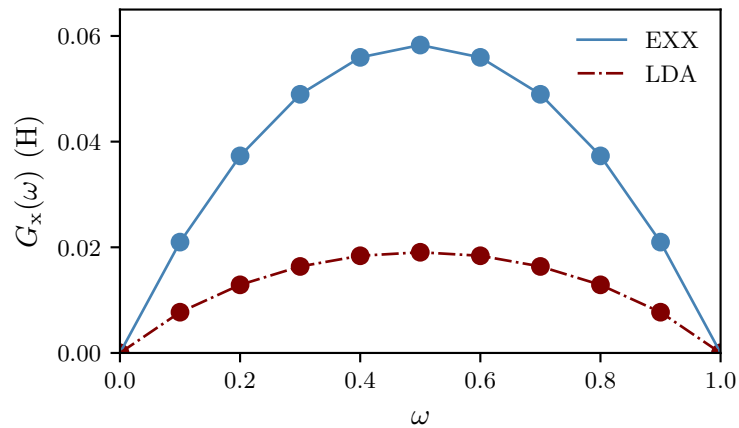
In Fig. 6.1, we see the effect of the ghost exchange error for the Hydrogen and Lithium atoms, for both the approximate LDA exchange functional and the exact exchange functional. In fact, the error is larger for the exact functional, but it is sizeable in either case. From this we conclude that the exchange functional in KS theory must account for any differences in the spin densities, making the usual closed-shell approach inaccurate.

We note that there exist other approaches for open-shells in KS theory. These have largely been developed with the goal of computing energy differences between different multiplet states, because UKS theory suffers from spin contamination issues [267–269], making it unreliable for computing these differences. The most well-known method is the so-called restricted open-shell KS method (ROKS) [270, 271]. In this method, the spin-up and down-orbitals have the same spatial wavefunction; however, it is not strictly within KS theory, as it uses a linear combination of KS determinants to satisfy symmetry constraints in a similar spirit to the ROHF method [27]. A related approach is the restricted open-shell singlet (ROSS) method [272], which is applicable specifically to open-shell singlets. Additionally, there is the so-called symmetrized approach by Görling [273, 274]; like ROKS, this uses a linear combination of Slater determinants to satisfy symmetry arguments, and thus is not formally within standard KS theory. In fact, it is an extension of DFT, as the fundamental variable is not the density or even the spin-density, but the totally symmetric contribution to the spin-density.

*An alternative interpretation for the mixing of spin-densities is that the up- and down-spin densities are partially constructed from fractionally occupied KS orbitals.



(a) Hydrogen



(b) Lithium

Figure 6.1: Illustration of the ghost exchange error, $G_x(\omega)$, as a function of the mixing fraction ω of the up- and down-spin densities. There is no ghost exchange error when there is no mixing ($\omega = 0, 1$) and it is maximised for equal mixing ($\omega = 0.5$).

6.2 Theory

We propose a method to treat open-shell systems within the standard KS formalism, without incurring a ghost-exchange error. In this new approach, the exchange (and by extension correlation) functional depends implicitly on the density through its explicit dependence on the spin densities, which themselves are implicit functionals of the density. In this sense, the theory is formally within DFT and not spin-DFT as the density is the fundamental variable; however, there is no ghost-exchange error as there is no mixing of spin-densities in the exchange functional.

We begin with some basic theory regarding the properties that should be satisfied by the exchange energy functional. The exact exchange energy in KS theory is given by

$$E_x[\rho^\uparrow, \rho^\downarrow] = -\frac{1}{2} \int d\mathbf{r} \int d\mathbf{x} \left\{ \frac{|\rho^\uparrow(\mathbf{r}, \mathbf{x})|^2}{|\mathbf{r} - \mathbf{x}|} + \frac{|\rho^\downarrow(\mathbf{r}, \mathbf{x})|^2}{|\mathbf{r} - \mathbf{x}|} \right\}. \quad (6.4)$$

It is clear that the above expression is separable into the separate exchange energies of the up and down spin-densities,

$$E_x[\rho^\uparrow, \rho^\downarrow] = E_x[\rho^\uparrow, 0] + E_x[0, \rho^\downarrow]. \quad (6.5)$$

Any approximate exchange functional should satisfy the above additive relation in order to avoid the ghost exchange error. As discussed, semi-local functionals depending only on the density and its gradient do not satisfy this additive property for open-shell systems. However, the local spin-density approximation (LSDA) for exchange does explicitly satisfy this relation,

$$E_x^{\text{LSDA}}[\rho^\uparrow, \rho^\downarrow] = \tilde{C} \int d\mathbf{r} [\rho^\uparrow(\mathbf{r})]^{4/3} + [\rho^\downarrow(\mathbf{r})]^{4/3}. \quad (6.6)$$

Spin-dependent GGAs are parameterized to satisfy the spin-scaling relation [275],

$$E_x[\rho^\uparrow, \rho^\downarrow] = \frac{1}{2} \left(E_x[2\rho^\uparrow, 0] + E_x[0, 2\rho^\downarrow] \right) \quad (6.7)$$

which is equivalent to satisfying the relation (6.5).

We must therefore use density-functionals that depend explicitly on the spin-density in order to satisfy the additive relation (6.5). During the KS procedure, we still minimize with respect to the total density, and not the separate spin-densities, which yields a common effective potential for all the orbitals. We are therefore still within ordinary KS theory and do not invoke spin-DFT; the exchange functional becomes an implicit functional of the density through its explicit spin-density dependence. An alternative way of framing this argument is by considering the exchange functional as an orbital dependent functional depending implicitly on the density, just as the kinetic energy functional is an orbital-dependent functional.

Given that the exchange-functional is an implicit density-functional, the corresponding correlation-functional should also be considered an implicit density-functional. It is logical to use the spin-parameterized correlation energy functionals, which like the exchange functionals are explicit functionals of the spin-density and implicit functionals of the total density, because xc-functionals usually benefit from error cancellation between the exchange and correlation contributions. We typically observe a modest gain in accuracy using the spin-dependent correlation functionals, which is smaller in magnitude than the ghost-exchange error. The xc-functional is thus given by

$$E_{\text{xc}}^{\text{iDFA}} = E_{\text{xc}}^{\text{SDFA}}[\rho^\uparrow[\rho], \rho^\downarrow[\rho]], \quad (6.8)$$

where the acronym iDFA stands for *implicit* DFA. We have stressed that the spin-densities are implicit functionals of the total energy in the above expression.

The total energy functional is thus given by

$$E^{\text{iDFA}}[\rho] = T_{\text{s}}[\rho] + \int d\mathbf{r} v_{\text{en}}(\mathbf{r})\rho(\mathbf{r}) + U[\rho] + E_{\text{xc}}^{\text{iDFA}}[\rho]. \quad (6.9)$$

This leads to the normal KS equations, with the xc-potential given by the functional derivative

$$v_{\text{xc}}[\rho](\mathbf{r}) = \frac{\delta E_{\text{xc}}^{\text{iDFA}}[\rho]}{\delta \rho(\mathbf{r})} = \frac{\delta E_{\text{xc}}^{\text{SDFA}}[\rho^\uparrow[\rho], \rho^\downarrow[\rho]]}{\delta \rho(\mathbf{r})}. \quad (6.10)$$

As the xc-functional is an implicit density-functional, the functional derivative cannot be directly computed and must be determined via the OEP method. It is

given by

$$\int d\mathbf{r}' \sum_{\sigma} \chi^{\sigma}(\mathbf{r}, \mathbf{r}') v_{xc}[\rho](\mathbf{r}') = \int d\mathbf{r}' \sum_{\sigma} \chi^{\sigma}(\mathbf{r}, \mathbf{r}') \frac{\delta E_{xc}^{\text{SDFA}}[\rho^{\uparrow}, \rho^{\downarrow}]}{\delta \rho^{\sigma}(\mathbf{r}')}, \quad \text{with} \quad (6.11)$$

$$\chi^{\sigma}(\mathbf{r}, \mathbf{r}') = \sum_{i=1}^{N_{\sigma}} \sum_{a=N_{\sigma}+1}^{\infty} \frac{\phi_i^*(\mathbf{r}) \phi_i(\mathbf{r}') \phi_a(\mathbf{r}) \phi_a^*(\mathbf{r}')}{\epsilon_i - \epsilon_a} + \text{c.c.} \quad (6.12)$$

Thus far, we have focussed on developing a restricted KS formalism for approximate (semi-local) density-functionals which avoids the ghost-exchange error. Although this error is not inherently present in the exact exchange functional (6.4), the method is equally applicable to EXX for both open and closed-shell systems. Most applications of the OEP method for EXX in finite basis set codes have been for closed-shell systems. This may be because it has been tacitly assumed that one would typically need to solve separate OEP equations for each spin-channel (a notable exception being the symmetrized LHF (CEDA) approach by Della Salla and Görling [276]), as is usually done for approximate functionals; given the mathematical and numerical difficulties in solving the OEP equation for a single KS potential (§ 3.9.3), this may seem to be a daunting task. However, from our analysis it is clear that there is no need to invoke spin-DFT equations for open-shell systems. In fact, for exact exchange, open-shell systems can be solved just as straightforwardly as closed-shell systems as the OEP equation to be solved is fundamentally the same in either case.

During the minimization of the energy with respect to the density, we seek only the absolute ground-state energy; this is unlike most other KS schemes for open-shell systems which target the ground-state energy for a given symmetry to obtain different spin multiplet energies. We note that the density is constructed according to

$$\rho(\mathbf{r}) = \sum_k^{n_{\text{orb}}} f_k |\phi_k(\mathbf{r})|^2, \quad (6.13)$$

where $f_k \in \{0, 1, 2\}$ is the occupation number. Typically in closed-shell theory, the orbitals are occupied according to the Aufblau principle, but this is not a formal requirement and we are free to search over any f_k which yield the lowest

total energy. Although it is not practical to search over all possible values of f_k , there are situations where it is energetically favourable to adopt a slightly different configuration to what might be expected, both for systems with even and odd numbers of electrons. We explore examples of when this occurs in § 6.4.1.

Since we are strictly limited to searching for the ground-state energy, we are not formally justified in using terminology (for example ‘singlet’) which refers to the spin-eigenstate of the system. However, for the sake of convenience, we use this terminology in a colloquial manner to denote the difference between the number of spin-up and spin-down orbitals that are occupied. For example, when we refer to a state as a ‘triplet’ we simply mean that

$$N_{\uparrow} - N_{\downarrow} = \Delta N_{\uparrow\downarrow} = 2, \quad (6.14)$$

and likewise for other multiplet states.

6.3 Implementation of the OEP equation

We follow the general procedure for solving the OEP equation described in § 3.9.3. The OEP equation to be solved (6.11) is for the xc (or x-only for exact exchange) potential only, and thus the effective density in which we expand our potential represents only the x(c)-part of the potential, not the full Hxc-potential as we saw in the previous chapter. We denote this effective density $\rho_{xc}(\mathbf{r})$ to differentiate it from the Hxc-screening density $\rho_{scr}(\mathbf{r})$.

The OEP equation we solve falls within the general class of OEP equations in equation (3.86), with the full response function $\chi(\mathbf{r}, \mathbf{r}')$ in this equation equal to the sum over the spin-separated response functions,

$$\chi(\mathbf{r}, \mathbf{r}') = \sum_{\sigma} \chi^{\sigma}(\mathbf{r}, \mathbf{r}'); \quad (6.15)$$

and the right-hand side $b(\mathbf{r})$ is

$$b(\mathbf{r}) = \int d\mathbf{r}' \sum_{\sigma} \chi^{\sigma}(\mathbf{r}, \mathbf{r}') \frac{\delta E_{xc}^{SDFA}[\rho^{\uparrow}, \rho^{\downarrow}]}{\delta \rho^{\sigma}(\mathbf{r}')}. \quad (6.16)$$

Computationally, solving the OEP equation amounts to solving equations (3.95-3.96) to determine the effective density $\rho_{xc}(\mathbf{r})$. The matrix A_{kl} is derived from the response function $\chi(\mathbf{r}, \mathbf{r}')$ and is thus invariant to the precise problem. The vector b_k , which comes from $b(\mathbf{r})$, and the screening charge* Q_{scr} , are specific to the problem being solved; we discuss the details of their implementation for (i) approximate density functionals and (ii) the exact exchange functional in the proceeding sub-sections.

6.3.1 Implementation for (semi)-local density-functionals

We seek the vector $b_k = \langle \tilde{\theta}_k | b \rangle$, with $b(\mathbf{r})$ defined by equation (6.16). The functional derivative of the spin-dependent energy functional is computed using the LIBXC package, which given inputs such as the spin-densities and their gradients on the grid, returns the following quantities:

$$v_1^\sigma(\mathbf{r}) = \frac{\partial e_{xc}[\rho^\uparrow, \rho^\downarrow]}{\partial \rho^\sigma(\mathbf{r})}, \quad (6.17)$$

$$v_2^{\sigma, \sigma'}(\mathbf{r}) = \frac{\partial e_{xc}[\rho^\uparrow, \rho^\downarrow]}{\partial f^{\sigma, \sigma'}(\mathbf{r})}, \quad \text{with } f^{\sigma, \sigma'}(\mathbf{r}) = \nabla \rho^\sigma(\mathbf{r}) \cdot \nabla \rho^{\sigma'}(\mathbf{r}). \quad (6.18)$$

From the above quantities, we can obtain the spin-dependent xc-potentials $v_{xc}^\sigma(\mathbf{r})$ on the grid. For the LSDA case, v_{xc}^σ is simply equal to $v_1^\sigma(\mathbf{r})$ (6.17). For GGA functionals, $v_{xc}^\sigma(\mathbf{r})$ is given by

$$v_{xc}^\sigma(\mathbf{r}) = \frac{\partial e_{xc}[\rho^\uparrow, \rho^\downarrow]}{\partial \rho^\sigma(\mathbf{r})} - \nabla \cdot \frac{\partial e_{xc}[\rho^\uparrow, \rho^\downarrow]}{\partial \nabla \rho^\sigma(\mathbf{r})} \quad (6.19)$$

$$= v_1^\sigma(\mathbf{r}) - 2\nabla \cdot \left\{ \nabla \rho_\sigma(\mathbf{r}) v_2^{\sigma, \sigma}(\mathbf{r}) + \nabla \rho_{\sigma'}(\mathbf{r}) v_2^{\sigma, \sigma'}(\mathbf{r}) \right\}, \quad (6.20)$$

where the chain rule is used to transform from equation (6.19) to (6.20). In typical DFT calculations, the gradient in the above equation (6.20) is not directly computed: since the xc-potential is always integrated over products of basis functions (3.80), the product rule is used to transform the gradient to act on the basis functions. This is because there are numerical issues associated with taking

*in this case the x(c)-only screening charge

the Laplacian of Gaussian basis functions. Despite these issues, we compute the xc-potential directly on the grid from equation (6.20) since there is no clear alternative for calculating $b(\mathbf{r})$ in the OEP equation (6.11); we are exploring approaches to avoid computing $\nabla^2 \rho^\sigma(\mathbf{r})$, one of which is described in Appendix B.

Having obtained the spin-dependent xc-potentials from LIBXC, we first transform them from the grid into the auxiliary basis. In other words,

$$v_{\text{xc}}^\sigma(\mathbf{r}) = \sum_k^{n_{\text{aux}}} \rho_k^{\text{xc},\sigma} \tilde{\theta}_k(\mathbf{r}) \quad (6.21)$$

$$\Rightarrow \rho_k^{\text{xc},\sigma} = \sum_l^{n_{\text{aux}}} \langle \tilde{\theta}_k | \theta_l \rangle^{-1} \langle \theta_l | v_{\text{xc}}^\sigma \rangle. \quad (6.22)$$

The vector b_k is then given by

$$b_k = \sum_\sigma \sum_l^{n_{\text{aux}}} \rho_l^{\text{xc},\sigma} \langle \tilde{\theta}_k | \chi^\sigma | \tilde{\theta}_l \rangle \quad (6.23)$$

$$= \sum_\sigma \sum_k^{n_{\text{aux}}} \rho_k^{\text{xc},\sigma} A_{kl}^\sigma = \sum_\sigma \sum_k^{n_{\text{aux}}} \rho_k^{\text{xc},\sigma} \left[A_{kl}^{0,\sigma} + \alpha \bar{A}_{kl}^\sigma \right], \quad (6.24)$$

with

$$A_{kl}^{0,\sigma} = 2 \sum_{i=1}^{N_\sigma} \sum_{a=N_\sigma+1}^{n_{\text{orb}}} \frac{\langle \phi_i | \tilde{\theta}_k | \phi_a \rangle \langle \phi_i | \tilde{\theta}_l | \phi_a \rangle}{\epsilon_i - \epsilon_a}, \quad (6.25)$$

$$\bar{A}_{kl}^\sigma = - \sum_{i=1}^{N_\sigma} \left\{ \langle \phi_i | \tilde{\theta}_k \tilde{\theta}_l | \phi_i \rangle - \sum_{j=1}^{N_\sigma} \langle \phi_i | \tilde{\theta}_k | \phi_j \rangle \langle \phi_i | \tilde{\theta}_l | \phi_j \rangle \right\}. \quad (6.26)$$

In the above, we have decomposed the spin-dependent response matrix A_{kl}^σ into its main part $A_{kl}^{0,\sigma}$ and complement \bar{A}_{kl}^σ , in the same manner as the decomposition of the full matrix A_{kl} .

During the KS-SCF procedure, we note that the computationally dominant step is not the solving of the OEP equation, but rather the diagonalization of the Fock matrix, as also observed by Görling and co-workers [173]. The cost can be reduced further using CEDDA (§ 3.8.1), which amounts to replacing the matrix A_{kl} and vector b_k by their complement terms only,

$$A_{kl} = \bar{A}_{kl}; \quad b_k = \bar{b}_k, \quad (6.27)$$

and then solving the OEP equation as normal. In § 6.4.1, we compare results using CEDA with the full OEP solution (with small finite α).

We have also explored an alternative construction for the vector b_k , which in theory is equivalent and thus should yield the same xc-potential. However, this is not the case in practise due to finite basis set effects. In Appendix B, we describe this alternative method and compare potentials and total energies between the two constructions; as discussed in this appendix, the construction described above is both computationally cheaper and arguably yields slightly more reliable results, and hence we use this construction by default.

The final remaining quantity to be determined is the charge of the effective xc-density,

$$Q_{\text{xc}} = \int \mathbf{dr} \rho_{\text{xc}}(\mathbf{r}) \quad (6.28)$$

which is required to prevent the xc-potential varying by an arbitrary constant. As discussed in § 5.3.1, for L(S)DA and most GGAs one would expect $Q_{\text{xc}} = 0$, since the effective density represents only the xc-potential here. However, the representation of the potential via the effective density in a finite basis set cannot fully represent the xc-potential in its grid representation, and thus $Q_{\text{xc}} \neq 0$.

Obtaining the precise value of Q_{xc} in a finite basis set for open-shell systems is something of a dark art. We can obtain Q_{xc}^σ for each of the spin-potentials via the following relation,

$$Q_{\text{xc}}^\sigma = \rho_k^{\text{xc},\sigma} X_k \quad (6.29)$$

with $\rho_k^{\text{xc},\sigma}$ determined from Eq. (6.22), X_k defined in Eq. (3.94), and v_{xc}^σ the spin xc-potentials obtained from LIBXC on the grid. Although this does not define Q_{xc} for the common xc-potential that we seek, we typically find that $Q_{\text{xc}}^\uparrow \approx Q_{\text{xc}}^\downarrow$; some examples are shown in Table 6.1. We conclude that it is reasonable to take Q_{scr} as the average of its spin-values,

$$Q_{\text{xc}} = \frac{1}{2} [Q_{\text{xc}}^\uparrow + Q_{\text{xc}}^\downarrow]. \quad (6.30)$$

	Q_{xc}^\uparrow	Q_{xc}^\downarrow	$\Delta Q_{xc}^{\uparrow\downarrow}$
Li	-0.2769	-0.2615	0.0154
LiH ⁺	-0.0465	-0.0401	0.0063
Si	-0.4672	-0.3917	0.0755
O ₂	-0.5953	-0.5613	0.0340
OH	-0.3040	-0.2932	0.0108
NH ₄	-0.6123	-0.4616	0.1507
Na	-0.2387	-0.2389	0.0002
$\langle \Delta Q_{xc}^{\uparrow\downarrow} \rangle$			0.0134

Table 6.1: Comparison of Q_{xc}^\uparrow and Q_{xc}^\downarrow (6.29). Right-hand column shows the absolute difference $\Delta Q_{xc}^{\uparrow\downarrow} = |Q_{xc}^\uparrow - Q_{xc}^\downarrow|$; $\langle \Delta Q_{xc}^{\uparrow\downarrow} \rangle$ is the geometric mean of $|Q_{xc}^\uparrow - Q_{xc}^\downarrow|$.

6.3.2 Implementation of exact exchange energy functional

The exact exchange functional is not an explicit functional of the spin-densities, and hence the functional derivative of the exact exchange energy with respect to the spin-densities cannot be directly computed (6.11). Instead, the right-hand side $b(\mathbf{r})$ of the OEP equation is given by

$$b(\mathbf{r}) = \frac{\delta E_x[\{\phi_i^\uparrow\}, \{\phi_i^\downarrow\}]}{\delta v(\mathbf{r})} = \sum_{\sigma} \frac{\delta \tilde{E}_x[\{\phi_i^\sigma\}]}{\delta v(\mathbf{r})}, \quad (6.31)$$

where $\tilde{E}_x[\{\phi_i^\sigma\}]$ denotes the exchange energy for just the spin-up or spin-down system. The functional derivative (§ 3.8) is equal to

$$\frac{\delta \tilde{E}_x[\{\phi_i^\sigma\}]}{\delta v(\mathbf{r})} = 2 \sum_{i=1}^{N_\sigma} \sum_{a=N_\sigma+1}^{\infty} \int \int d\mathbf{r}' d\mathbf{x} \frac{\phi_i(\mathbf{r})\phi_i(\mathbf{x})\phi_a(\mathbf{r})\phi_a(\mathbf{r}')}{\epsilon_i - \epsilon_a} \frac{\rho_\sigma(\mathbf{x}, \mathbf{r}')}{|\mathbf{r}' - \mathbf{x}|}, \quad (6.32)$$

which leads to the following expression for vector b_k ,

$$b_k = 2 \sum_{\sigma} \sum_{i=1}^{N_\sigma} \sum_{a=N_\sigma+1}^{\infty} \frac{\langle \phi_i | \tilde{\theta}_k | \phi_a \rangle}{\epsilon_i - \epsilon_a} \int \int d\mathbf{r}' d\mathbf{x} \frac{\phi_i(\mathbf{x})\rho_\sigma(\mathbf{r}', \mathbf{x})\phi_a(\mathbf{r}')}{|\mathbf{r}' - \mathbf{x}|}. \quad (6.33)$$

We decompose this term in the usual way into a main part b_k^0 and complement \bar{b}_k . In order to make the computation of these terms more efficient, particularly for the complement term, we make a transformation from the orbital to the auxiliary

basis in the above integral. We first re-express this integral in the following way,

$$\int \int d\mathbf{r}' d\mathbf{x} \frac{\phi_i(\mathbf{x}) \rho_\sigma(\mathbf{r}', \mathbf{x}) \phi_a(\mathbf{r}')}{|\mathbf{r}' - \mathbf{x}|} = \sum_{j=1}^{N_\sigma} \int \int d\mathbf{r}' d\mathbf{x} \frac{\phi_i(\mathbf{x}) \phi_j(\mathbf{x}) \phi_j(\mathbf{r}') \phi_a(\mathbf{r}')}{|\mathbf{r}' - \mathbf{x}|} \quad (6.34)$$

$$= \sum_{j=1}^{N_\sigma} \int d\mathbf{r}' \phi_a(\mathbf{r}') \phi_j(\mathbf{r}') \int d\mathbf{x} \frac{\phi_i(\mathbf{x}) \phi_j(\mathbf{x})}{|\mathbf{r}' - \mathbf{x}|}. \quad (6.35)$$

For the latter integral in the above equation, we first expand the KS orbitals in the orbital basis set, and then transform the integral over a product of orbital basis functions into the integral over a single auxiliary basis function, using the transformation in equation (5.21). In other words,

$$\int d\mathbf{x} \frac{\phi_i(\mathbf{x}) \phi_j(\mathbf{x})}{|\mathbf{r}' - \mathbf{x}|} = \sum_{k,l}^{n_{\text{orb}}} c_{ik} c_{jl} \int d\mathbf{x} \frac{\xi_k(\mathbf{r}') \xi_l(\mathbf{x})}{|\mathbf{r}' - \mathbf{x}|} \quad (6.36)$$

$$= \sum_p^{n_{\text{aux}}} \bar{c}_{ijp} \tilde{\theta}_p(\mathbf{r}'). \quad (6.37)$$

Strictly, equality only holds in the above transformation if the product of the orbital basis can be represented fully in the auxiliary basis. However, we have found that even though this relation holds only approximately for finite basis sets, it is sufficiently accurate (using an uncontracted cc-pVDZ auxiliary basis set) to reliably obtain the exchange potential; we show some results in § 6.4.1.

The full vector b_k (in the complete basis set limit) is thus given by

$$b_k = 2 \sum_{\sigma} \sum_{i=1}^{N_\sigma} \sum_{a=N_\sigma+1}^{\infty} \frac{\langle \phi_i | \tilde{\theta}_k | \phi_a \rangle}{\epsilon_i - \epsilon_a} \left(\sum_{j=1}^{N_\sigma} \sum_p^{n_{\text{aux}}} \bar{c}_{ijp} \langle \phi_a | \tilde{\theta}_p | \phi_j \rangle \right). \quad (6.38)$$

In a finite basis set, this is decomposed in the usual way into a main part and complement term, $b_k = b_k^0 + \alpha \bar{b}_k$. The main term b_k^0 and complement \bar{b}_k are given by

$$b_k^0 = 2 \sum_{\sigma} \sum_{i=1}^{N_\sigma} \sum_{a=N_\sigma+1}^{n_{\text{orb}}} \frac{\langle \phi_i | \tilde{\theta}_k | \phi_a \rangle}{\epsilon_i - \epsilon_a} \left(\sum_{j=1}^{N_\sigma} \sum_p^{n_{\text{aux}}} \bar{c}_{ijp} \langle \phi_a | \tilde{\theta}_p | \phi_j \rangle \right) \quad (6.39)$$

$$\begin{aligned} \bar{b}_k = 2 \sum_{\sigma} \left\{ \sum_{i=1}^{N_\sigma} \sum_l^{N_\sigma} \frac{\langle \phi_i | \tilde{\theta}_k | \phi_l \rangle}{\epsilon_i - \epsilon_a} \left(\sum_{j=1}^{N_\sigma} \sum_p^{n_{\text{aux}}} \bar{c}_{ijp} \langle \phi_l | \tilde{\theta}_p | \phi_j \rangle \right) \right. \\ \left. - \int d\mathbf{r} \tilde{\theta}_k(\mathbf{r}) \sum_{i,j=1}^{N_\sigma} \left(\sum_p^{n_{\text{aux}}} \bar{c}_{ijp} \tilde{\theta}_p(\mathbf{r}) \right) \left(\sum_q^{n_{\text{aux}}} \bar{c}_{ijq} \theta_q(\mathbf{r}) \right) \right\}. \quad (6.40) \end{aligned}$$

In the second complement term, we have again made a transformation from the orbital to auxiliary basis to decrease the computational cost, in this case

$$\phi_i(\mathbf{r})\phi_j(\mathbf{r}) = \sum_q^{n_{\text{aux}}} \bar{c}_{ijq} \theta_q(\mathbf{r}). \quad (6.41)$$

The only remaining quantity required to solve the OEP equation is the screening charge Q_x . In a complete basis set limit, we would expect $Q_x = -1$ since the method is self-interaction free. As discussed during the inversion of HF densities in the previous chapter, there is no way to determine if this still holds when the effective density is expanded in a finite auxiliary basis set, and therefore the only sensible choice is to take the complete basis set limit $Q_x = -1$. We show some results in the following section which suggest this is a reasonable choice.

6.4 Results

We have implemented the algorithms described in the above sections in the HIPPO code, and applied the implementation to a variety of systems. A common feature of open-shell systems is degeneracy of the HOMO energy level, which can cause convergence issues. We have implemented the MOM method (§ 3.9.1) to overcome these difficulties and find that it works well even for solving the full OEP equation, despite the presence of the $\epsilon_i - \epsilon_a$ term in the denominator of both left and right hand sides of the equation. We have applied our method to a variety of systems and demonstrate some results in the upcoming sub-sections, first for DFAs and then for EXX.

6.4.1 (Semi)-local density-functionals

Primarily, we focus on the L(S)DA functional as a proof of concept, but our implementation can theoretically be applied equally well to GGAs. We first confirm that our method of solving the OEP equation, which includes the additional complement terms, yields converged and smooth potentials. In Figure 6.2, we observe for a few

systems the convergence of the xc-potential with respect to the size of the orbital basis. In three of these four examples, the potential is already well-converged with a contracted cc-pVDZ orbital basis, relative to an uncontracted cc-pVDZ auxiliary basis. The exception is the OH quadruplet, in which we observe some spurious oscillations for the cc-pVDZ orbital basis, with these being largely eliminated for the cc-pVTZ orbital basis.

Furthermore, in Table B.2 of Appendix B, we compare the KS HOMO eigenvalues obtained with our iDFA method with those from UKS theory for the LSDA functional. The iLDA eigenvalues are in relatively close agreement with the LSDA eigenvalues, which indicates the OEP results are reliable (since there is almost no spin-contamination for these systems). Additionally, we have observed the xc-potential is well-behaved using this method for many more examples in Ref. [277]*. We therefore conclude that our method of solving the OEP equation yields well-behaved potentials.

It is also informative to compare the approximate CEDA solution with the full OEP solution. As can be seen in Tables B.1 and B.2 of Appendix B, CEDA seems to be a very accurate approximation to the full OEP solution for iLDA, for both xc-potentials and total energies. This is further evidenced in Fig. 6.3, in which we have plotted the OEP and CEDA xc-potentials for two examples, alongside the spin-polarized potentials v^\uparrow and v^\downarrow for reference. For these examples we have used a cc-pVQZ orbital basis to ensure the full OEP solution is fully converged, and we observe that CEDA is almost indistinguishable from the full OEP in this instance. CEDA is mathematically guaranteed not to suffer from the instabilities of the full OEP solution; given that it seems to yield near-identical results for iLDA, and is computationally cheaper, it should be strongly considered as a viable alternative

*There are a couple of small differences between the current work and Ref. [277]. Firstly, a different screening charge constraint of $Q_{\text{scr}} = N - 1$, or equivalently $Q_{\text{xc}} = -1$, was used in that paper to mitigate against self-interaction errors. Secondly, the Hartree potential was absorbed into the right-hand-side of the OEP equation in Ref. [277], meaning the OEP equation determined the full Hxc-potential in that work rather than just the xc-potential in the current work. However, the latter change makes minimal difference to the results, and the former only shifts the xc-potential by a constant amount and therefore does not affect convergence arguments.

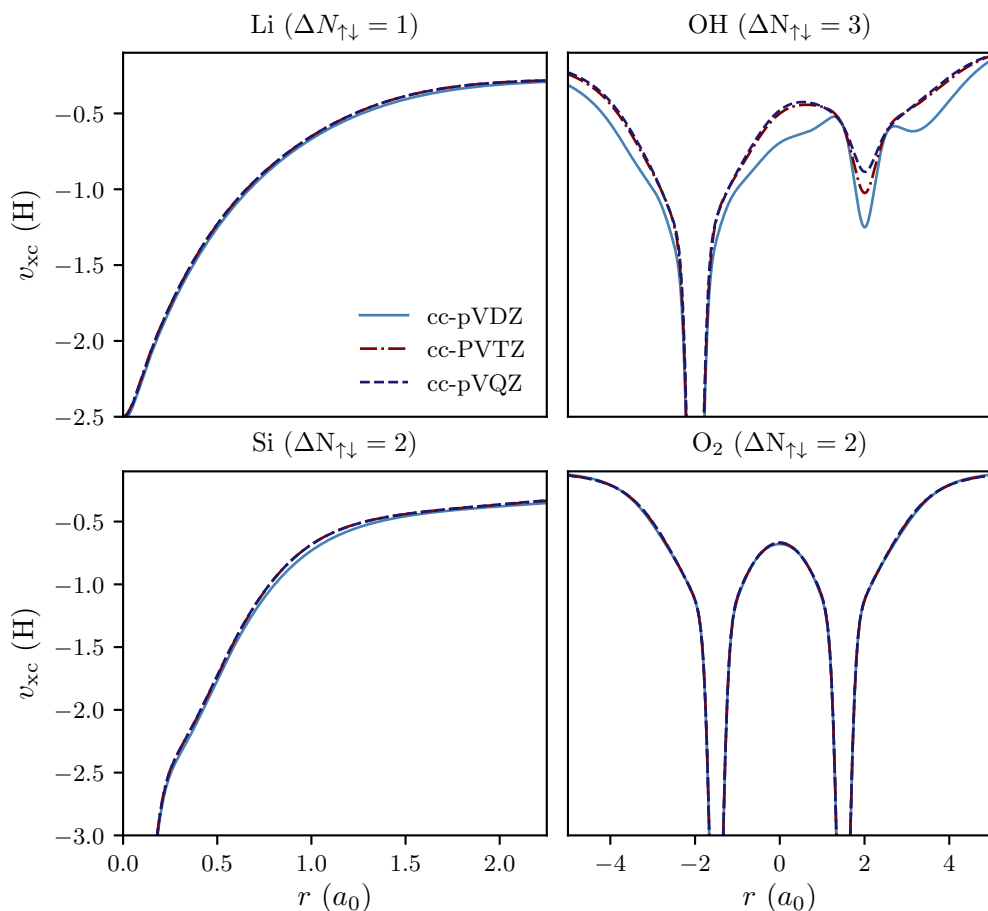


Figure 6.2: Convergence of iLDA xc-potentials wrt orbital basis set size for (i) Lithium (doublet), (ii) OH (quadruplet) with bond length $4.0a_0$, (iii) Si (triplet), and (iv) O_2 (triplet) with bond length $3.0a_0$. The auxiliary basis set is uncontracted cc-pVDZ for all calculations.

to the full OEP for iLDA. Nevertheless, we solve the full OEP equation for the remaining results in this sub-section.

With a reliable method for solving the OEP equation established, we now compare results from our implicit method with UKS theory, and also KS theory with the ghost exchange error. As can be seen in Table B.2 of Appendix B, the KS HOMO eigenvalues in our method yield similar results to UKS for L(S)DA; it is therefore not surprising that ground-state energies from the implicit method compare very favourably with those from UKS. This is demonstrated in Table 6.2, in which the iLDA results being almost identical to the UKS results, with the small differences

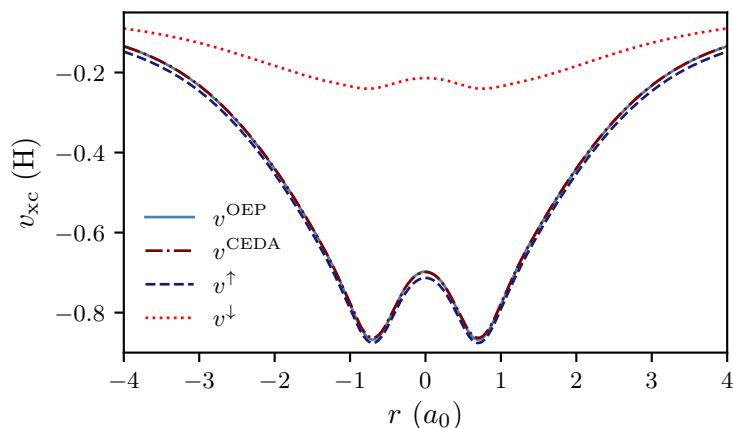
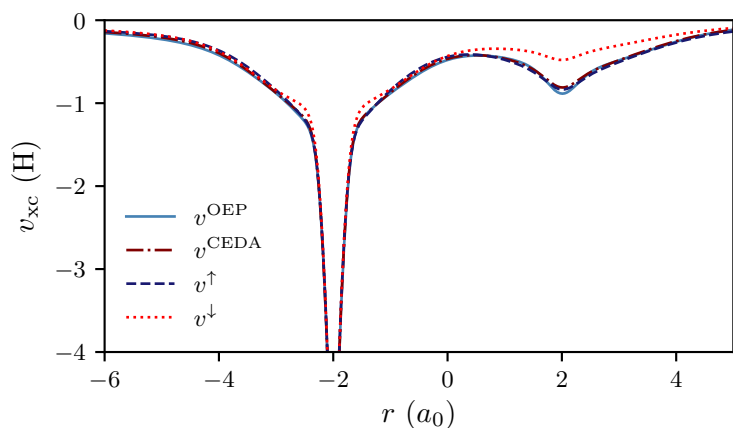
(a) H₂ triplet, bond length $3.78a_0$ (b) OH quadruplet, bond length $4a_0$

Figure 6.3: Comparison of iLDA xc-potentials between CEDA and the full OEP solution (with $\alpha = 10^{-2}$), with the spin-polarized xc-potentials also shown for reference. The orbital basis set is cc-pVQZ.

observed most likely due to the finite basis set representation of the xc-potential. In this table, we also see the effect of the ghost exchange (and correlation) error; although the absolute error in this case appears small, we shall see that it can play a significant role in physically meaningful situations.

A well-known problem for semi-local functionals in DFT is their qualitative failure to predict energy dissociation curves for diatomic molecules. The most famous example of this is the H₂ molecule [121]: as can be seen in Fig. 6.4, the H₂ molecule does not correctly dissociate into two Hydrogen atoms in the restricted KS

	E_{LDA} (H)	E_{iLDA} (H)	E_{LSDA} (H)	G_{xc} (H)
Li	-7.388721	-7.398133	-7.398155	0.00941
LiH ⁺	-7.652062	-7.685600	-7.685608	0.0335
Si*	-288.4505	-288.4503	-288.4505	-
Si [†]	-288.4640	-288.4904	-288.4910	0.0264
O ₂ *	-149.5825	-149.5821	-149.5825	-
O ₂ [†]	-149.6038	-149.6382	-149.6403	0.0344
OH	-75.34820	-75.37078	-75.37215	0.0226
NH ₄	-56.79800	-56.80390	-56.80404	0.00591
Na	-161.6491	-161.6571	-161.6572	0.00799
$\langle G_{\text{xc}} \rangle$				0.0200

*Singlet state
[†]Triplet state

Table 6.2: L(S)DA ground-state energies calculated with: (i) standard LDA, which includes the ghost exchange error, (ii) iLDA and (iii) spin-LDA (LSDA). The final column shows the ghost 'xc' error, defined here as the difference between the LDA and iLDA energies, with the main contribution to this error being the ghost exchange error. The discrepancy between LDA and iLDA singlet energies is because the iLDA xc-potential is expanded in a finite basis set. $\Delta N_{\uparrow\downarrow} = 2$ unless otherwise stated.

theory. The unrestricted (spin-DFT) solution does produce a qualitatively correct dissociation curve, but pays the price of the spin-symmetry dilemma in order to do so, which we discuss in more detail in § 6.5. The implicit LDA (iLDA) yields a different result still; there is a discontinuous transition at a bond length of about $4.2a_0$, at which point the triplet becomes lower in energy than the singlet, and the energy thus tends to the correct limit. There is no transition if the ghost exchange error is present: in this case the triplet energy is higher than the singlet at all bond distances.

We see a similar picture emerge for the OH radical, this time with the PBE functional, in Fig. 6.5. Just as for H₂, the normal PBE solution yields a qualitatively incorrect energy dissociation curve; however, the iPBE energy correctly becomes equal to the energy of the two separate atoms in the infinitely stretched limit, because there there is a crossing from the doublet to the quadruplet configuration at about $4a_0$. In both these examples, the transition region is interesting: the unrestricted solution yields a smooth dissociation curve due to the mixing of total-

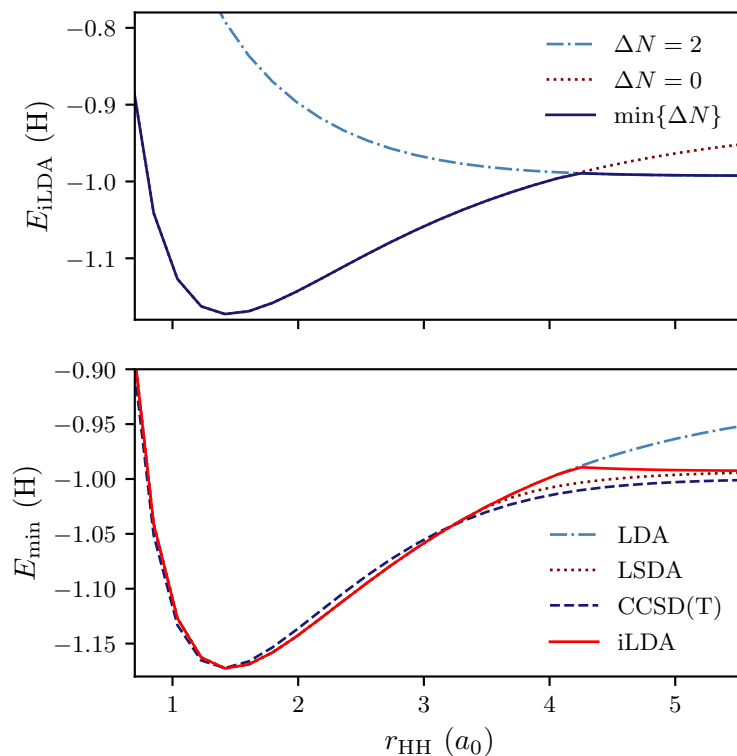


Figure 6.4: Energy dissociation curves for the H_2 molecule. Top, iLDA energies for different values of ΔN (singlet/triplet); bottom, comparison of LDA, spin-LDA (LSDA), CCSD(T) and iLDA minimum energies.

spin states, whereas in our single-determinant method the transition is abrupt. Of course, our method does not correct the ubiquitous inability of typical semi-local functionals to capture static correlation effects [138]; moreover, the spin-LDA/PBE energy surfaces are closer to the (highly accurate) CCSD(T) energy surfaces. Consequently, we do not expect our method to be used in place of UKS theory in typical calculations; rather, it is a tool to demonstrate the effect of the ghost-exchange error and the possibility of avoiding the spin-symmetry dilemma. Furthermore, it may be promising for applications where spin-contamination is significant.

*The CCSD(T) curve is shifted such that its minimum energy aligns with the SPBE minimum energy to make comparison easier.

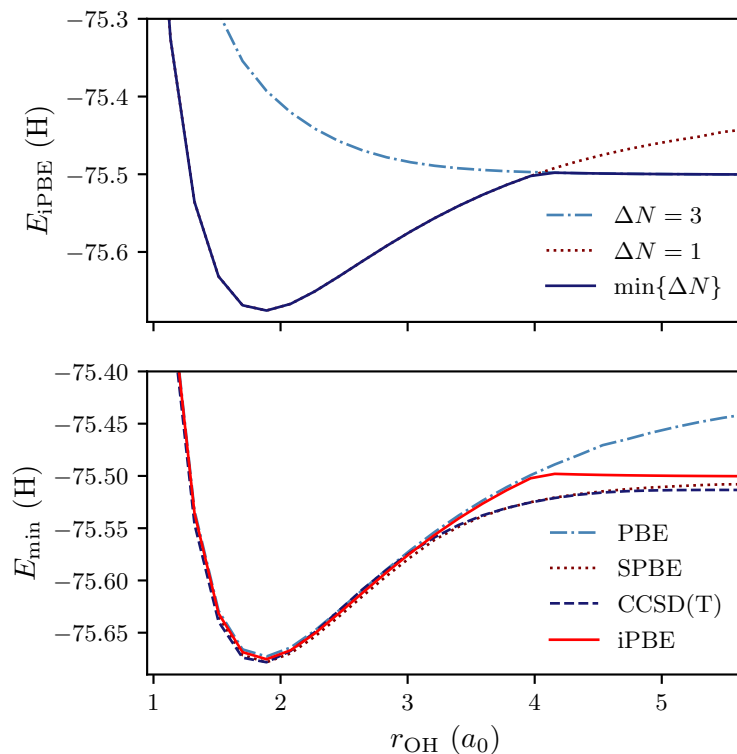


Figure 6.5: Energy dissociation curves for the OH radical. Top, iLDA energies for different values of ΔN (doublet/quadruplet); bottom, comparison of PBE, spin-PBE (SPBE), CCSD(T)* and iPBE minimum energies. We note that the iPBE results are computed using the alternative construction of b_k for the main part of the response matrix A_{kl}^0 described in Appendix B.

6.4.2 Exact exchange

We have applied the EXX implementation described in § 6.3.2 to compute ground-state energies and potentials for a variety of systems. This implementation is a novel way of solving the EXX OEP equation and therefore we present results for both open- and closed-shell examples.

As ever, to claim we can reliably solve the OEP equation we need to prove that the potential converges with respect to orbital basis set size, and does not display pathological behaviour. In Fig. 6.6, we demonstrate for a few systems the convergence of the exchange potential with respect to orbital basis set size, with fixed auxiliary (uncontracted cc-pVDZ) basis. In all cases, the potential clearly

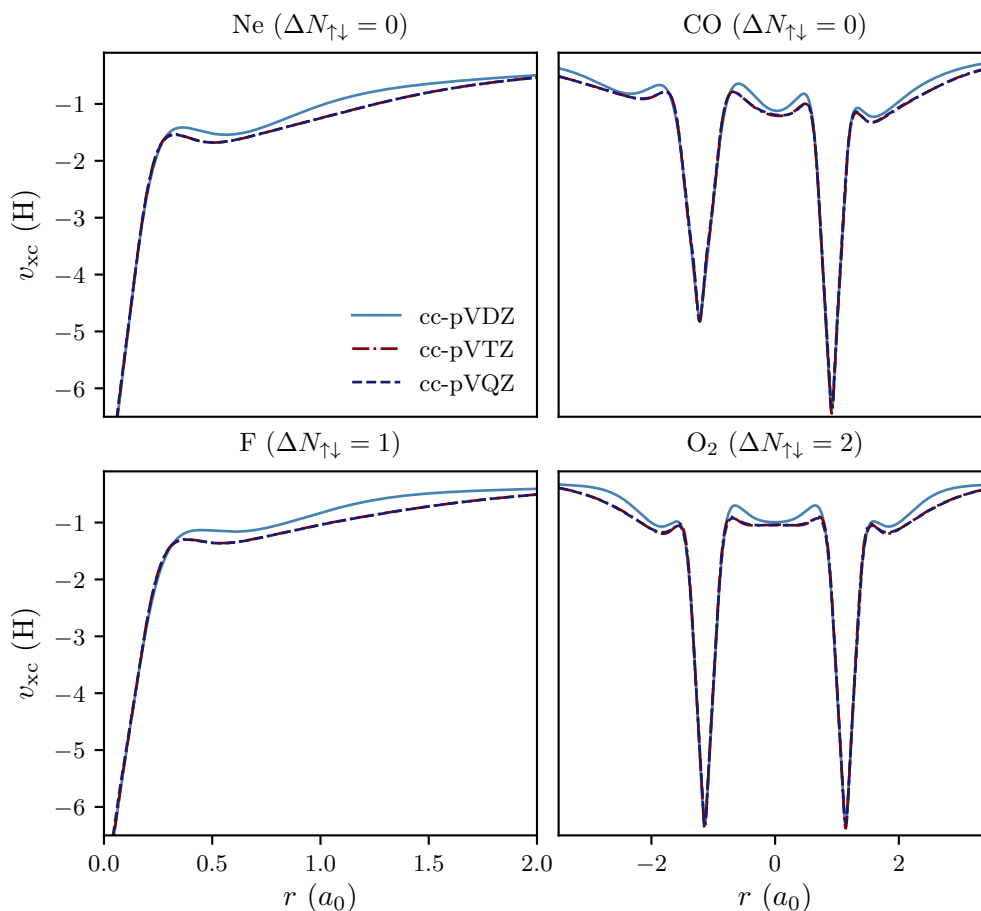


Figure 6.6: Convergence of EXX potentials wrt orbital basis set size for (i) Neon (singlet), (ii) CO (singlet) with bond length $2.14a_0$, (iii) F (doublet), and (iv) O₂ (triplet) with bond length $2.28a_0$. The auxiliary basis set is uncontracted cc-pVDZ for all calculations.

converges with respect to the orbital basis; however, it seems an orbital basis of at least cc-pVTZ size is required for the potential to be fully converged. This contrasts with the iLDA examples (Fig 6.2) in which a cc-pVDZ orbital basis was large enough in most examples. Possibly, this is due to the non-local nature of the right-hand side vector $b(\mathbf{r})$ of the EXX-OEP equation relative; however, more extensive testing would be required to verify this hypothesis.

The total energy of an EXX calculation is also a useful gauge of whether the OEP solution can be considered well-posed. The EXX potential is the local potential that minimizes the HF energy expression, and thus (being a more restricted solution

	Energy (H)			$-\epsilon_{\text{H}}$ (eV)		
	OEP	CEDA	HF	OEP	CEDA	HF
Li	-7.432438	-7.432270	-7.432706	5.32	5.18	5.34
LiH ⁺	-7.740910	-7.740830	-7.740966	16.69	16.66	20.27
Ne*	-128.5301	-128.5298	-128.5320	21.47	21.25	23.01
Si*	-288.7862	-288.7833	-288.7948	5.99	7.25	6.61
Si [†]	-288.8447	-288.8419	-288.8565	6.80	7.77	8.18
O ₂ *	-149.5734	-149.5716	-149.5825	10.45	10.39	12.77
O ₂ [†]	-149.6467	-149.6451	-149.6761	10.23	10.01	15.12
OH	-75.41144	-75.41054	-75.41947	13.16	14.21	15.14
NH ₄	-56.67656	-56.67444	-56.68041	2.92	3.65	3.54
Na	-161.8511	-161.8493	-161.8581	5.03	6.08	4.96
H ₂ O*	-76.05522	-76.05421	-76.05760	12.09	12.82	13.75
HF*	-100.0561	-100.0555	-100.0583	15.76	16.76	17.52
CO*	-112.7756	-112.7730	-112.7805	13.81	12.81	15.08
$\langle \Delta E^{\text{OEP}} \rangle$		0.00144	0.00688			

*Singlet state

[†]Triplet state

Table 6.3: EXX, CEDA and HF total energies and HOMO eigenvalues ϵ_{H} for a variety of systems. HF results are unrestricted for open-shell systems and restricted otherwise. $\Delta N_{\uparrow\downarrow} = 0$ unless otherwise stated. $\langle \Delta E^{\text{OEP}} \rangle$ is the average energy difference between the OEP, and respectively the CEDA and HF energies.

to the same minimization problem) the EXX total energy is expected to lie slightly above the self-consistent HF total energy: if this is not the case, it is an indication that the EXX solution is pathological, which has been observed in various OEP calculations [178]. In Table 6.3, we show EXX total energies alongside CEDA and HF total energies for various systems. The EXX energy is consistently higher than the HF energy in these systems, with an average difference of 0.00688 Hartree*; this strongly suggests the EXX solution is well-posed.

In Table 6.3, we also include a comparison of total energies between CEDA and the full OEP solution (with $\alpha = 10^{-2}$). The two are close, with an average difference of 0.00144 Hartree, but we note this is significantly larger than the difference between OEP and CEDA for the iLDA calculations. This suggests the EXX total energy

*This is several orders of magnitude larger than the difference between the iLDA and LSDA total energies, so it is more than just the effect of expanding the exchange potential in a finite basis set.

expression is more sensitive than L(S)DA to small variations in the orbitals, which is perhaps expected given that L(S)DA is a coarser approximation through its dependence on the (spin)-density rather than the KS orbitals. We also observe a noticeable difference in the potential between CEDA and the full OEP solution: this is reflected in the KS eigenvalues in Table 6.3 and also the exchange potentials, as can be seen in Fig. 6.7. In particular, the CEDA potential seems to lack some of the sharper features of the full OEP potential at the edges of the potential wells near the nuclei. The implication here is that CEDA is not such an accurate approximation to the full OEP as it is for (semi)-local functionals, as has been observed elsewhere for example Ref. [173].

6.5 Summary and discussion

In this chapter, we have shown that xc-functionals which depend only on the density and its derivatives, and not the spin-densities, are contaminated by a spurious exchange energy between fractional charges of opposite-spin electrons for open-shell systems. This ghost exchange error is usually avoided in practical calculations by adopting the formalism of spin-DFT, in which the spin-density rather than the density is considered the fundamental variable, leading to separate KS equations for the different spin systems. However, spin-DFT should not be formally required in the absence of a magnetic field. We have demonstrated how to avoid this ghost-exchange error within normal KS theory, by treating the xc-functional (which is an explicit functional of the spin-densities) as an implicit functional of the total density. This leads naturally to an OEP equation to determine the xc-potential; we have demonstrated for several examples that we can reliably solve the OEP equation, both for approximate functionals and the exact exchange functional.

One of the oft-cited issues with spin-DFT in the absence of a magnetic field is the spin-symmetry dilemma, so-called because spin-DFT can yield either accurate total energies but incorrect spin-densities; or correct spin-densities, but inaccurate

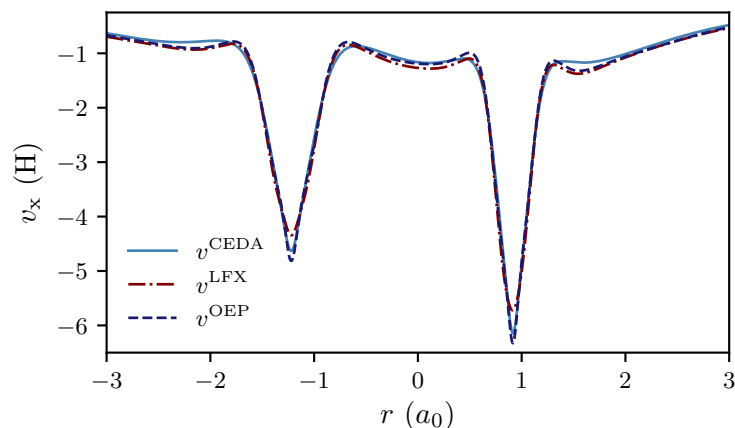
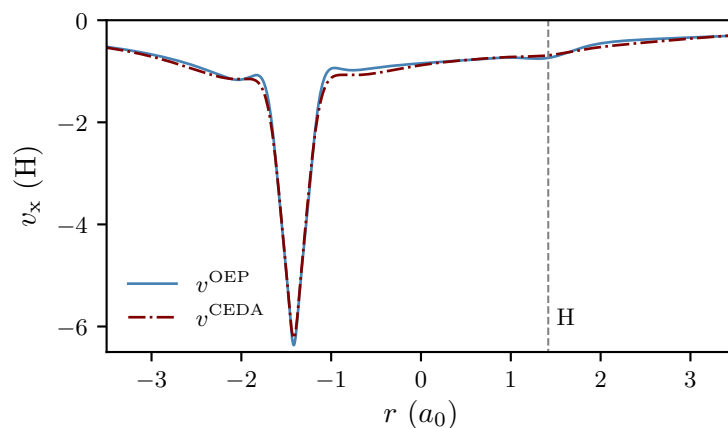
(a) CO singlet, bond length $2.14a_0$ (b) OH doublet, bond length $2.83a_0$

Figure 6.7: Comparison of EXX potentials between CEDA and the full OEP solution (with $\alpha = 10^{-2}$), with the LFX result (§ 5.3.3) also shown for comparison for CO*. The orbital basis set is cc-pVQZ.

*The density-inversion routine to calculate the LFX potential is currently only applicable for closed-shell systems.

total energies [79, 262, 273]. This is a dilemma in spin-DFT because the spin-density is the fundamental variable, and thus the theory is expected to yield both the correct energy and the correct spin-density. A famous example of the spin-symmetry dilemma is the dissociation of the H₂ molecule: this should dissociate into two Hydrogen atoms with total energy 1 Hartree and zero net spin-magnetization. As can be seen in Fig. 6.4, spin-DFT predicts the correct energy dissociation curve;

however, it dissociates into one spin-down Hydrogen atom and another spin-up Hydrogen atom. This ‘broken-symmetry’ solution therefore yields the wrong spin-density; however, if the correct spin-density (singlet state) is imposed through the restricted formalism, the total energy is wrong. This qualitative error is observed in the dissociation of other diatomic molecules and for most xc-functionals, such as the OH radical with the PBE functional in Fig. 6.5.

However, in DFT it is the total density rather than the spin-density which is the key variable. Our theory yields the correct ground-state energy and density in the dissociation limit, and thus there is no dilemma because the spin-density is unimportant. This perspective is discussed in the well-known paper by Perdew, Savin and Burke [262], who claim the spin-density is not an elementary quantity in the absence of a magnetic field; instead, they argue that the on-top electron pair density $P(\mathbf{r}, \mathbf{r}')$, alongside the total density, are the fundamental variables in this case. They propose an ‘alternative’ spin-density functional theory, in which they invoke the constrained search formalism to search for the anti-symmetric N -electron wave-function yielding a given $\rho(\mathbf{r})$ and $P(\mathbf{r}, \mathbf{r}')$, which minimizes the total energy. We share the philosophy of this paper, namely that the spin density is immaterial in the absence of a magnetic field*; but in our approach, there is no need to consider the auxiliary on-top pair density, with the density alone being sufficient to find the ground-state energy.

In the following sub-section, we show how the familiar equations of unrestricted KS theory can be derived without invoking spin-DFT, but rather through the generalized KS formalism.

6.5.1 Unrestricted KS equations from generalized KS theory

In generalized KS (GKS) theory, a general energy functional $S[\Phi]$ of an N -electron Slater determinant Φ , plays the role of the kinetic energy functional $T[\Phi]$ in KS

*‘Absence’ in this case meaning the absence of a magnetic field that is large enough to affect the quantities being calculated

theory. The total energy functional in GKS theory is given by

$$E[\{\phi_i\}; v_{\text{en}}] = S[\{\phi_i\}] + R^S[\rho[\{\phi_i\}]] + \int d\mathbf{r} v_{\text{en}}(\mathbf{r}) \rho[\{\phi_i\}](\mathbf{r}), \quad (6.42)$$

with $R^S[\rho]$ defined by

$$R^S[\rho] = F[\rho] - F^S[\rho], \quad (6.43)$$

with $F[\rho]$ being the universal functional (3.17), and $F^S[\rho]$ defined in equation (3.34). The functional $S[\Phi]$ can be any functional which satisfies the three conditions outlined in § 3.6.3. Minimizing the energy functional (6.42) with respect to the GKS orbitals under the constraint of fixed density yields the GKS equations,

$$\left[\hat{O}^S[\{\phi_i\}] + v_R(\mathbf{r}) + v_{\text{en}}(\mathbf{r}) \right] \phi_j(\mathbf{r}) = \epsilon_j \phi_j(\mathbf{r}), \quad (6.44)$$

with

$$v_R(\mathbf{r}) = \frac{\delta R^S[\rho]}{\delta \rho(\mathbf{r})}. \quad (6.45)$$

In the above, we note that the operator $\hat{O}^S[\{\phi_i\}]$ is determined by taking the functional derivative of $S[\Phi]$ with respect to the *orbitals*, whereas the residual potential $v_R(\mathbf{r})$ is given by the functional derivative of $R^S[\rho]$ with respect to the *density*.

In the normal KS scheme, the energy functional $S[\Phi]$ is given by the kinetic energy functional, $S[\Phi] = \langle \Phi | \hat{T} | \Phi \rangle$. This means the residual functional $R^S[\rho]$ is equal to

$$R^S[\rho] = U_{\text{H}}[\rho] + E_{\text{xc}}[\rho], \quad (6.46)$$

which leads to the normal KS equations. However, the following choice for $S[\Phi]$ also satisfies the necessary conditions in § 3.6.3,

$$S[\Phi] = \langle \Phi | \hat{T} | \Phi \rangle + U_{\text{H}}[\rho] + E_{\text{xc}}[\{\phi_i[\rho]\}], \quad (6.47)$$

where we have specified that the xc-functional depends *implicitly* on the density through its *explicit* dependence on the GKS orbitals. With this definition for $S[\Phi]$, there is no residual functional, $R^S[\rho] = 0$.

Although this may seem a somewhat arbitrary transfer of terms between $S[\Phi]$ and $R^S[\rho]$, it changes the GKS equations. Consider, for example, the case in which the

exchange functional is given by the exact exchange functional, and the correlation functional is taken to be zero, $E_c[\rho] = 0$. With $S[\Phi]$ defined as the kinetic energy functional as in the normal KS scheme, the residual potential $v_R(\mathbf{r})$ is given by

$$v_R[\rho](\mathbf{r}) = \frac{\delta}{\delta\rho(\mathbf{r})} \left\{ U_H[\rho] + E_x[\{\phi_i[\rho]\}] \right\} = v_H(\mathbf{r}) + \frac{\delta E_x[\{\phi_i[\rho]\}]}{\delta\rho(\mathbf{r})} \quad (6.48)$$

with the functional derivative of the exact exchange energy with respect to the density determined by solving an OEP equation. However, if the functional $S[\Phi]$ is defined instead by equation (6.47), then the optimization over the Fock-exchange energy is performed directly over the orbitals rather than the density, which means the GKS equations become identical to the HF equations,

$$\left\{ -\frac{\nabla^2}{2} + v_{\text{en}}(\mathbf{r}) + v_H(\mathbf{r}) \right\} \phi_j(\mathbf{r}) + \int d\mathbf{r}' v_x^{\text{NL}}(\mathbf{r}, \mathbf{r}') \phi_j(\mathbf{r}') = \epsilon_j \phi_j(\mathbf{r}). \quad (6.49)$$

Now let us consider the case where the xc-functional depends implicitly on the density through its implicit dependence on the spin-densities. In this case, the functional derivative of $E_{\text{xc}}[\rho_{\Phi}^{\uparrow}, \rho_{\Phi}^{\downarrow}]$ with respect to the orbitals is equivalent to the functional derivative with respect to the spin-densities. Provided there is no restriction that the spin-up and spin-down spatial orbitals are the same, the GKS equations are thus identical to the spin-KS equations,

$$\left\{ -\frac{\nabla^2}{2} + v_{\text{en}}(\mathbf{r}) + v_H(\mathbf{r}) + v_{\text{xc}}^{\sigma}(\mathbf{r}) \right\} \phi_j^{\sigma}(\mathbf{r}) = \epsilon_j^{\sigma} \phi_j^{\sigma}(\mathbf{r}). \quad (6.50)$$

Although the above equations are identical to spin-DFT equations in the absence of a magnetic field, the spin-symmetry dilemma is no longer a dilemma. This is because GKS theory is an exact reformulation of DFT and not spin-DFT, and thus it can be expected to yield accurate ground-state energies and densities, but it should not be expected to yield the correct spin-density.

In summary, there are various definitions of the energy functional $S[\Phi]$ in GKS theory which are valid reformulations of DFT. Choosing it to be the kinetic energy functional leads to the standard KS theory, which means all the orbitals experience a common effective potential $v_s(\mathbf{r})$. However, if definition of $S[\Phi]$ is changed to

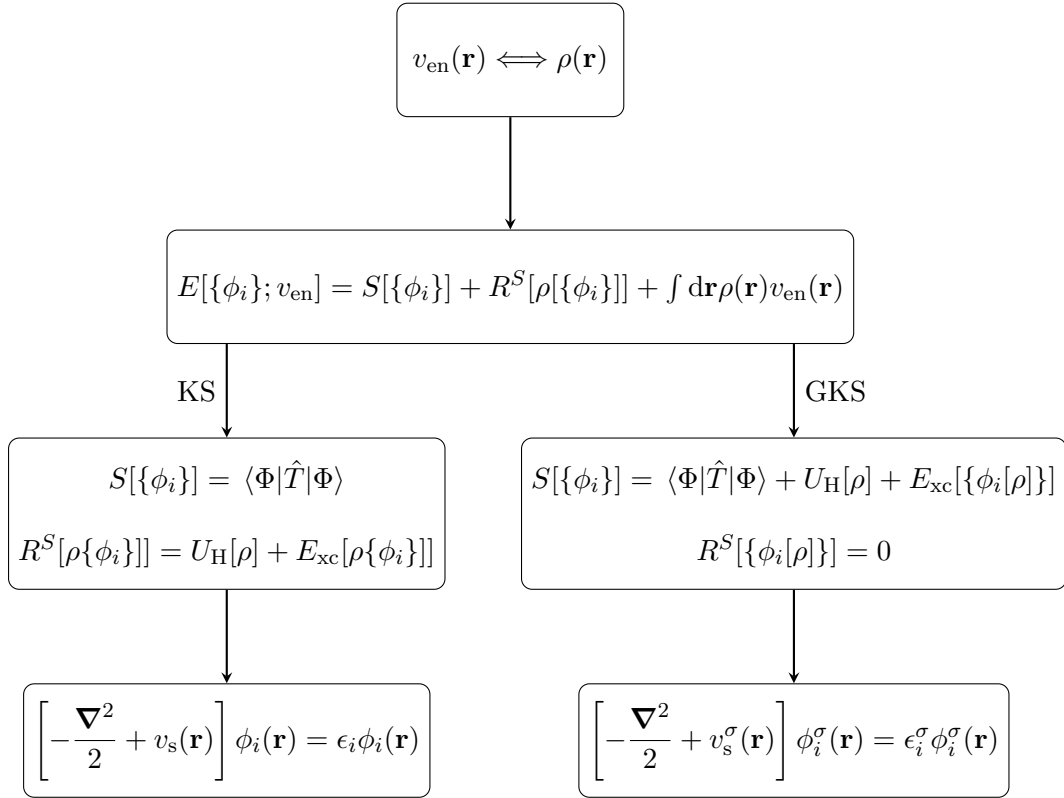


Figure 6.8: The KS vs GKS equations: For DFAs that depend explicitly on the spin-densities, minimizing wrt to the density leads to equations in which all orbitals share a common potential (KS); meanwhile minimizing wrt the orbitals leads to different equations for the spin-up and spin-down orbitals (GKS).

equation (6.47), this restriction is lifted, and the orbitals can experience different, or non-local, potentials. In the case that the xc-functional is a functional of the spin-densities, the former definition of $S[\Phi]$ leads to the restricted KS formalism which must be solved via an OEP equation for open-shell systems. In the latter definition of $S[\Phi]$, there is no requirement to compute the functional derivative with respect to the whole density which results in spin-unrestricted KS equations. The two different approaches are illustrated in Fig. 6.8.

Conclusions and further work

Density-functional theory (DFT) is a hugely popular tool for the prediction and analysis of various processes that require a quantum-mechanical description of electrons in matter. Despite the many successes of DFT — as evidenced by publication metrics [10, 11] and several impactful predictions [13–16] — common approximations in DFT suffer from certain qualitative failings. These include, for example, failure to accurately predict electron affinities, reaction barriers and diatomic binding energies [225, 278]; systematic under-estimation of the fundamental gap [117, 118]; struggles with strongly-correlated materials such as transition-metal oxides [137]; and even questions about the validity of the formalism for open-shell systems [262].

In this thesis, we have explored several routes towards a more systematic approach to functional development in DFT. Much of our work has incorporated insights and results from wave-function theories (WFT) — typically more accurate, but also more expensive, than DFT methods — to develop accurate KS potentials which could serve as references in the development of new xc-functionals. This theme formed the basis of chapters 4 and 5 of this thesis.

In Chapter 4, we reviewed an alternative derivation of the KS potential from a wave-function based expression [188]. Using this theory, we were able to derive perturbative expansions of the KS potential from perturbative expansions of the

wave-function. The main result from this chapter was the analytical derivation of a new KS potential with both exchange and correlation character to first order [220]. We expect this potential to yield more accurate predictions for quantities such as electron affinities and reaction barriers than typical xc-approximations.

In chapter 5, we developed a method to invert a given density to obtain the local KS potential which yields that density. Like the previous chapter, this offers an avenue to obtain accurate reference KS potentials, but in this case numerically through the inversion of WFT densities. In our method, the screening density was seen to play an important role, as it determines the asymptotic behaviour of the potential and is fixed during the optimization procedure. We verified the accuracy of our approach through the inversion of LDA densities, and we also saw that it could be applied successfully to HF and coupled cluster densities.

Finally, in chapter 6, we introduced a method to treat open-shell systems within restricted KS theory. In order for a correct treatment of exchange — between only whole electrons of the same spin — it is necessary to treat the usual spin-polarized density functional approximations as implicit functionals of the density. This leads to an OEP equation for the xc-potential; historically, solving the OEP equation in finite basis set codes has presented various mathematical and computational difficulties. Our method of solving the OEP equation, which is based on the approach in Ref. [179], avoids many of these difficulties and we obtain smooth potentials for both LDA and the EXX potential. We also revisited a well-known paradox in this chapter — the spin-symmetry dilemma [262] — and saw how this paradox is avoided by considering the xc-functional to be an implicit functional of the total density via its explicit dependence on the spin-densities, using either the OEP method or GKS formalism to determine the ground-state density and energy.

A clear direction for future work is the implementation of the new xc-potential derived in chapter 4. This implementation will involve the solution of an OEP equation, and it will therefore benefit from our progress in this area. Another possible extension being actively considered [279] is to use other forms of wave-function

expansions — in particular coupled cluster expansions — to derive analytical expressions for the KS potential based on those expansions. Both of these examples would be complemented by the density-inversion method in Chapter 6, as one could compare a KS potential from an inverted density with the corresponding potential derived analytically.

The ability to reliably solve the OEP equation opens up various research avenues. In this thesis, we have discussed at length the role of the screening density and its relationship with self-interactions. In earlier work [108, 109, 280], the usual KS energy expression was minimized under the following constraints on the screening density,

$$Q_{\text{scr}} = N - 1 \tag{7.1}$$

$$\rho_{\text{scr}} \geq 0. \tag{7.2}$$

The former condition, as discussed in § 5.3.2, mitigates against the effects of self-interactions (SIs) in the KS potential. The latter condition was introduced for two reasons: (i) to avoid shifting negative screening density to infinity as the size of the orbital and auxiliary basis sets increase and (ii) as a regularization technique to avoid pathological behaviour of the OEP solution, which in this prior work was solved without the complement terms. In Ref. [277], we explored relaxing the positivity constraint (a computational burden) using the improved approach to solving the OEP equation in Chapter 6. We observed for many examples in this paper that the positivity constraint can be safely relaxed, even for quite large auxiliary basis sets. As seen in Table 5.6, and the examples in Ref. [277], constraining the screening charge to equal $N - 1$ significantly improves the prediction of ionization potentials from the HOMO KS energy level.

The ‘constrained’ approach to DFAs described above attenuates the effects of SIs on the xc-potential by enforcing the correct asymptotic decay, but it is not a full SI correction as it has no effect on the energy functional. We plan to explore a more comprehensive SI correction, perhaps using as a starting template the method

in Ref. [149] which solves the Perdew-Zunger SI correction scheme using the OEP method. Looking further into the future, our approach of solving the OEP equation may be particularly useful in time-dependent applications of the OEP method; as discussed in Ref. [107], although CEDA and KLI are often good approximations to the full OEP solution (as seen also in Chapter 6), they are quite poor at predicting response properties which are ubiquitous in time-dependent DFT.

In Ref. [277], we also explored modelling the derivative discontinuity using standard DFAs with constraints on the screening density. In the following, we briefly summarise the results of our preliminary investigation.

7.1 Modelling the derivative discontinuity

We recall from § 3.7.2 the following definition of the derivative discontinuity (DD) in KS theory,

$$\Delta_{\text{xc}} = \lim_{\omega \rightarrow 0^+} \Delta_{\text{xc}}^{\omega}(\mathbf{r}) = \lim_{\omega \rightarrow 0^+} \left\{ v_{\text{xc}}^{N+\omega}(\mathbf{r}) - v_{\text{xc}}^{N-\omega}(\mathbf{r}) \right\}, \quad (7.3)$$

where $v_{\text{xc}}^{N\pm\omega}(\mathbf{r})$ is the xc-potential of an ensemble with $N \pm \omega$ electrons. The densities of the ensemble with $N \pm \omega$ electrons are defined as follows,

$$\rho^{N\pm\omega}(\mathbf{r}) = (1 - \omega)\rho^N(\mathbf{r}) + \omega\rho^{N\pm 1}(\mathbf{r}) \quad (7.4)$$

$$= (1 - \omega) \sum_{i=1}^N |\phi_i[\rho^N](\mathbf{r})|^2 + \omega \sum_{i=1}^{N\pm 1} |\phi_i[\rho^{N\pm 1}](\mathbf{r})|^2. \quad (7.5)$$

In the above, $\rho^M(\mathbf{r})$ denotes the density of the M -electron system.

We consider the behaviour of the ensemble xc-potentials in the asymptotic region. As proved in Ref. [247], the decay of the density in the asymptotic tail depends only on the highest-occupied KS orbital,

$$\lim_{|\mathbf{r}| \rightarrow \infty} \rho(\mathbf{r}) = e^{-2\sqrt{-2\epsilon_{\text{H}}}|\mathbf{r}|}. \quad (7.6)$$

For the ensemble with density $\rho^{N+\omega}(\mathbf{r})$, the highest occupied KS orbital coincides in the asymptotic region with the $N + 1^{\text{th}}$ orbital of the of the KS system with

$N + 1$ electrons, $\phi_{N+1}^{N+1}(\mathbf{r})$. We now draw a connection with the concept of screening density. We have earlier argued that the screening density is the electronic density ‘seen’ by one electron (or KS orbital) due to the other electrons. The KS orbital $\phi_{N+1}^{N+1}(\mathbf{r})$ experiences a repulsive field from a total charge of N -electrons, and thus its screening charge is $Q_{\text{scr}} = N$. Since the orbitals forming the ensemble experience a common KS potential, they must experience a common screening charge also; the screening charge for the $N + \omega$ ensemble is therefore given by $Q_{\text{scr}}^{N+\omega} = N$.

However, the dominant orbital in the ensemble with density $\rho^{N-\omega}(\mathbf{r})$ is the N th orbital of the KS system with N -electrons. This orbital experiences a field from a charge density of $N - 1$ electrons, and thus the screening charge for the $N - \omega$ electron system is given by $Q_{\text{scr}}^{N-\omega} = N - 1$, the same as the screening charge of the N -electron KS system. From the above reasoning, we conclude that there is a discontinuous jump in the screening charge as the density of the ensemble system crosses an integer number of electrons,

$$\Delta Q_{\text{scr}}^{N+\omega} = Q_{\text{scr}}^{N+\omega} - Q_{\text{scr}}^N = 1, \quad 0 < \omega \leq 1. \quad (7.7)$$

Using the above constraints on the screening charge and our method of solving the OEP equation, we could obtain the DD from equation (7.3) through an ensemble OEP calculation, in a similar manner to Ref. [123]. However, we propose to use the above property (7.7) of the screening charge to model the DD in a computationally inexpensive manner (a related approach was explored in Ref. [281]). We investigate the following approximation for the DD,

$$\Delta_{\text{xc}} \approx \Delta_{\text{xc}}^{\text{CDFA}} = v_{\text{xc}}^{N+}[\rho^N](\mathbf{r}) - v_{\text{xc}}^{N-}[\rho^N](\mathbf{r}), \quad (7.8)$$

where v_{xc}^{N+} is designed to mimic the xc-potential of the $N + \omega$ ensemble and thus has a screening charge $Q_{\text{scr}} = N$; and $v_{\text{xc}}^{N-}(\mathbf{r})$ is designed to mimic the xc-potential of the $N - \omega$ ensemble and thus has a screening charge $Q_{\text{scr}} = N - 1$. The xc-potentials are determined by two ground-state calculations for the N -electron system (rather than an ensemble OEP calculation), respectively constraining the screening charges

to be N and $N - 1$ (hence the acronym CDFA in the above equation standing for constrained DFA). This can be done for any chosen semi-local DFA using the procedure described in § 6.3.1 (which is equally valid for closed and open-shell systems).

Clearly, if this is to be considered a valid method for modelling the DD, then $\Delta_{\text{xc}}^{\text{CDFA}}$ should be flat and non-zero in the complete basis set limit. As the xc-potential is expanded in the form $v_{\text{xc}}(\mathbf{r}) = \int d\mathbf{r}' \rho_{\text{xc}}(\mathbf{r}')/|\mathbf{r} - \mathbf{r}'|$, the difference will always tend to zero in the asymptotic limit but should show the desired behaviour to a certain spatial extent.

We test our method for the Neon atom. In theory, we can obtain the true DD (7.3) by inverting the ensembles with densities $\rho^{N\pm\omega}(\mathbf{r})$ using the method in Chapter 5 to obtain the KS potential in each case. Unfortunately, this density-inversion method is currently inapplicable to systems with a HOMO/LUMO degeneracy, which is the case for the Neon cation (which forms part of the $N - \omega$ ensemble)*. Work is in progress to correct this deficiency. For the time-being, we instead consider the following approximation,

$$\Delta_{\text{xc}} \approx \lim_{\omega \rightarrow 0^+} \left\{ v_{\text{xc}}^{N+\omega}(\mathbf{r}) - v_{\text{xc}}^N(\mathbf{r}) \right\}; \quad (7.9)$$

where the screening charge for the $N + \omega$ ensemble is equal to N , and for the N -electron system is equal to $N - 1$ using the same arguments as before.

In Fig. 7.1, we show the approximate DD in the xc-potential (7.9) for various values of ω , with the ensemble density obtained from LDA calculations. We see convergence in the limit $\omega \rightarrow 0$; the difference $\Delta v_{\text{xc}}^\omega$ does not become completely flat due to numerical instabilities in the density inversion procedure which are exacerbated when the difference of two potentials is taken. However, we do not suggest this method as a means of computing the DD in a practical sense, but rather to compare with the CDFA method (7.8). We observe in this figure that $\Delta v_{\text{xc}}^{\text{CLDA}}$ is largely flat until $\sim 2.5a_0$, and close to the inverted ensemble approximation.

*A separate issue is that the Neon anion is not bound ($\epsilon_{\text{H}} > 0$); nevertheless, we get an indication of what to expect from the density-inversion calculation.

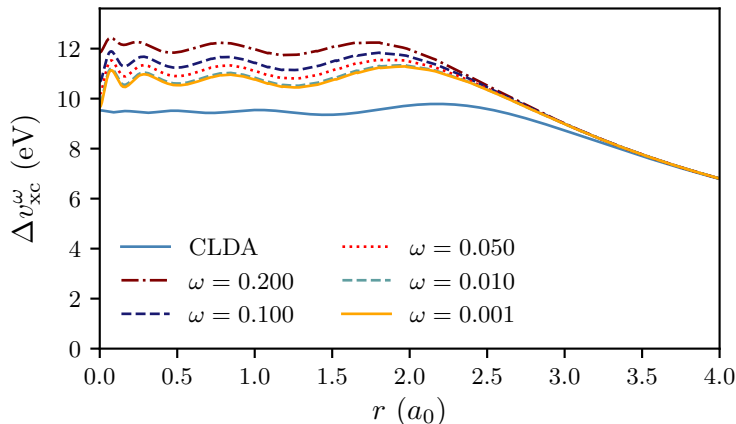


Figure 7.1: The approximate derivative (7.9) for various values of ω . The CLDA result (7.8) is shown for comparison. Orbital and auxiliary bases are both uncontracted cc-pVTZ.

Next, we investigate the convergence of $\Delta v_{xc}^{\text{CLDA}}$ with basis set size; we use the same (uncontracted) basis for the orbital and auxiliary bases for simplicity. In Fig. 7.2, we see evidence for the convergence of $\Delta v_{xc}^{\text{CLDA}}$ as the basis set size is increased; furthermore, the difference becomes flatter and extends further spatially with larger basis sets. The evidence for the difference $\Delta v_{xc}^{\text{CLDA}}$ being constant is also seen in the occupied KS eigenvalues, as shown in Table 7.1. The eigenvalue differences for the systems with screening charges N and $N - 1$ are in very close agreement for all the basis set sizes. These eigenvalue differences are a convenient measure of the DD, as it can be seen from Fig. 7.2 that they are in agreement with the difference $\Delta v_{xc}^{\text{CLDA}}$.

Finally, we have extrapolated the value of the DD to the complete basis set limit, as seen in the inset of Fig. 7.2. There appears to be a reasonably linear relationship between the inverse number of basis elements $(n_{\text{bas}})^{-1}$ and the value of $\Delta_{xc}^{\text{CLDA}}$, yielding an estimate of 6.14 eV for $\Delta_{xc}^{\text{CLDA}}$ in a complete basis set. This strongly suggests the gap is non-zero in the limit of a complete (orbital and auxiliary) basis set.

Clearly, there is work to be done if this method is to be employed in practical

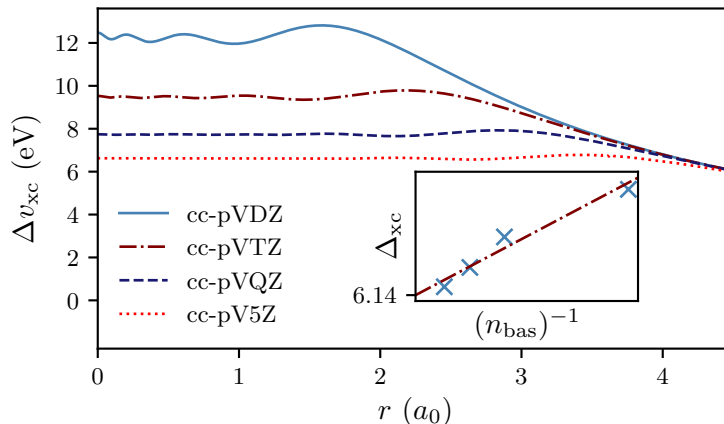


Figure 7.2: Main figure: convergence of $\Delta_{xc}^{\text{CLDA}}$ with basis set size (orbital and auxiliary basis both uncontracted cc-pVXZ). Inset: extrapolation of $\Delta_{xc}^{\text{CLDA}}$ with respect to number of basis elements N_{bas} .

calculations. Firstly, calculations for basis sets larger than cc-pVTZ are computationally very expensive even for the LDA functional; however, the value of $\Delta_{xc}^{\text{CLDA}}$ appears to change significantly with basis set size. We therefore need to investigate the possibility of obtaining accurate estimates in the complete basis set limit with smaller basis sets used for the extrapolation. The method is currently being more extensively tested [282] for various other atoms and molecules to verify it is widely applicable. Furthermore, modelling the DD is of principal interest in solid-state applications; the method would require various modifications in order to be applicable in periodic DFT codes. However, despite the above caveats, the method shows promise overall in estimating the DD in a computationally inexpensive manner.

$\Delta\epsilon_i$ (eV)	cc-pVDZ	cc-pVTZ	cc-pVQZ	cc-pV5Z
1s	12.24	9.48	7.74	6.61
2s	12.23	9.48	7.74	6.62
2p	12.21	9.48	7.73	6.62
$\Delta_{xc}^{\text{CLDA}}$	12.22	9.48	7.73	6.62

Table 7.1: Neon atom: the difference of the eigenvalues $\Delta_i = \epsilon_i^{N^+} - \epsilon_i^N$, of the CLDA xc-potentials v_{xc}^N and $v_{xc}^{N^+}$, for the orbitals $\phi_i = \phi_{1s}, \phi_{2s}, \phi_{2p}$. The average difference $\Delta\epsilon_i$ per basis set gives $\Delta_{xc}^{\text{CLDA}}$.

Quadratic line search method

In the density-to-potential inversion method of chapter 5, a quadratic line search is employed to find the optimal step size in the steepest-descent minimization of the objective functional $U[v]$ (5.6). We describe this method below.

If we vary v in the direction $v + \epsilon\delta v$, then provided $0 < \epsilon \ll 1$, $U[v + \epsilon\delta v]$ can be expanded parabolically about ϵ ,

$$U[v + \epsilon\delta v] = \epsilon^2 a_2 + \epsilon a_1 + a_0. \quad (\text{A.1})$$

The value of ϵ is then chosen to be that which minimizes the above expression, ie

$$U_1 < U_0 \epsilon_0 = \min_{\epsilon} \{\epsilon^2 a_2 + \epsilon a_1 + a_0\} = -\frac{a_1}{2a_2}. \quad (\text{A.2})$$

To determine ϵ_0 , we therefore need to compute a_1 and a_2 to construct the quadratic curve for $U[v + \epsilon\delta v]$. We do this by computing three points for $U[v + \epsilon\delta v]$ given three different values of ϵ ,

$$\epsilon = 0 \Rightarrow U_0 = a_0 \quad (\text{A.3})$$

$$\epsilon = \lambda \Rightarrow U_1 = \lambda^2 a_2 + \lambda a_1 + a_0 \quad (\text{A.4})$$

$$\epsilon = 2\lambda \Rightarrow U_2 = 4\lambda^2 a_2 + 2\lambda a_1 + a_0. \quad (\text{A.5})$$

We note that we need only compute two values for U since U_0 is already given by the value of U from the previous iteration in the optimization procedure. From the

above, the values of a_1 and a_2 are thus given by

$$a_2 = \frac{U_2 - 2U_1 + U_0}{2\lambda^2} \quad (\text{A.6})$$

$$a_1 = -\frac{U_2 - 4U_1 + 3U_0}{2\lambda}. \quad (\text{A.7})$$

The value of λ must be chosen such that U_1 is smaller than both U_0 and U_2 , ie

$$U_1 < U_0 \text{ and } U_1 < U_2. \quad (\text{A.8})$$

If the value of λ is too large, such that $U_1 < U_0$, then it must be decreased and the procedure repeated; likewise, if it is too small such that $U_1 > U_2$, then it must be increased. In practise, however, we have found that this is rarely necessary provided that λ is chosen to be the same value from the previous iteration.

Alternative construction of b_k in OEP equation

In the following, we discuss an alternative method which we have explored to construct the vector b_k from the right-hand side $b(\mathbf{r})$ of the OEP equation for semi-local DFAs (6.16). With the spin-dependent xc-potentials obtained from LIBXC, we directly substitute these into $\bar{b}(\mathbf{r})$ (6.16). We then follow the analysis in § 3.9.3, in which the response function is decomposed into its primary component $\chi_0(\mathbf{r}, \mathbf{r}')$ and complement $\bar{\chi}(\mathbf{r}, \mathbf{r}')$, for the right-hand side $b(\mathbf{r})$. This leads to the following expressions for $b_0(\mathbf{r})$ and $\bar{b}(\mathbf{r})$,

$$b_0(\mathbf{r}) = 2 \sum_{\sigma} \sum_{i=1}^{N_{\sigma}} \sum_{a=N_{\sigma}+1}^{n_{\text{bas}}} \frac{\langle \phi_i | v_{\text{xc}}^{\sigma} | \phi_a \rangle \phi_i(\mathbf{r}) \phi_a(\mathbf{r})}{\epsilon_i - \epsilon_a}, \quad (\text{B.1})$$

$$\begin{aligned} \bar{b}_v(\mathbf{r}) = -\frac{2}{\Delta} \sum_{\sigma} \sum_{i=1}^{N_{\sigma}} \left\{ \phi_i(\mathbf{r}) \int d\mathbf{r}' \delta(\mathbf{r} - \mathbf{r}') v_{\text{xc}}^{\sigma}(\mathbf{r}) \phi_i(\mathbf{r}') \right. \\ \left. - \sum_j^{\text{occ}} \langle \phi_i | v_{\text{xc}}^{\sigma} | \phi_j \rangle \phi_i(\mathbf{r}) \phi_j(\mathbf{r}) \right\}. \end{aligned} \quad (\text{B.2})$$

The vector b_k in the OEP matrix equation (3.95) is therefore given by

$$b_k = \langle \tilde{\theta}_k | b_0 \rangle + \lambda \langle \tilde{\theta}_k | \bar{b} \rangle = b_k^0 + \alpha \bar{b}_k, \quad (\text{B.3})$$

Energy (H)	OEP		CEDA	
	b_k^2	b_k^1	b_k^2	b_k^1
Li	-7.398145	-7.398140	-7.398133	-7.398133
LiH ⁺	-7.685603	-7.685599	-7.685600	-7.685599
Si*	-288.4503	-288.4503	-288.4503	-288.4503
Si [†]	-288.4905	-288.4904	-288.4904	-288.4905
O ₂ *	-149.5821	-149.5821	-149.5821	-149.5821
O ₂ [†]	-149.6382	-149.6381	-149.6382	-149.6382
OH	-75.37088	-75.37078	-75.37078	-75.37074
NH ₄	-56.80394	-56.80394	-56.80390	-56.80390
Na	-161.6571	-161.6569	-161.6571	-161.6571

*Singlet state

[†]Triplet state

Table B.1: A comparison of ground-state total energies from the implicit LDA (iLDA) method, with the xc-potential determined from both the full OEP equation (with $\alpha = 10^{-2}$) and CEDA, using the two different constructions for b_k . The energies are essentially identical for all the different approaches. All states doublets unless otherwise stated.

with

$$b_k^0 = 2 \sum_{\sigma} \sum_{i=1}^{N_{\sigma}} \sum_{a=N_{\sigma}+1}^{n_{\text{bas}}} \frac{\langle \phi_i | v_{\text{xc}}^{\sigma} | \phi_a \rangle \langle \phi_a | \tilde{\theta}_k | \phi_i \rangle}{\epsilon_i - \epsilon_a}, \quad (\text{B.4})$$

$$\bar{b}_k = 2 \sum_{\sigma} \left\{ \sum_{i=1}^{N_{\sigma}} \sum_{j=1}^{N_{\sigma}} \langle \phi_i | v_{\text{xc}}^{\sigma} | \phi_j \rangle \langle \phi_j | \tilde{\theta}_k | \phi_i \rangle - \int d\mathbf{r} \rho^{\sigma}(\mathbf{r}) v_{\text{xc}}^{\sigma}(\mathbf{r}) \tilde{\theta}_k(\mathbf{r}) \right\}. \quad (\text{B.5})$$

In theory, the above construction of b_k is equivalent to that described in § 6.3.1; however, this might not be the case in practise due to finite basis set effects. We shall compare results for the two different constructions, henceforth referring to the approach in § 6.3.1 as the first construction, and the approach in this section as the second construction. In Table B.1, we compare total energies across the two methods for a number of (mostly) open-shell systems, including both CEDA results and results for the full OEP equation (with $\alpha = 10^{-2}$). These results demonstrate almost no difference between either construction, nor between CEDA and the full OEP equation. Based on this, the choice of whether to use one construction over the other seems somewhat arbitrary.

In Table B.2, we compare values of the HOMO KS eigenvalue across the two meth-

ods, which may be more sensitive to any differences. Indeed, we see quantifiable differences between the results in this case; these differences mean the orbitals are slightly different but this is barely reflected in the total energy, suggesting the L(S)DA functional is resilient to changes in the orbitals. In both constructions, the CEDA eigenvalues are usually close to the full OEP eigenvalues, especially for the second construction of b_k ; this suggests CEDA is a rather accurate approximation in this case. Finally, we have included the LSDA (spin-DFT) results for comparison; we observe that the eigenvalues from the first construction are noticeably closer to the LSDA eigenvalues than those of the second construction. Since the LSDA results are not spin-contaminated for these examples, we expect the iLDA results to be close to L(S)DA: this suggests the first construction may be more accurate.

However, one possible advantage of the second construction of b_k may be in the application of the OEP method to GGA functionals. In the expressions for b_k^0 and the complement \bar{b}_k , one can substitute the form of $v_{xc}^\sigma(\mathbf{r})$ from equation (6.20), and then use the product rule to transform the gradient to act on terms other than $v_{xc}^\sigma(\mathbf{r})$ (which contains the gradient of Gaussian basis functions). This can be performed efficiently for b_k^0 (B.1) and for the first term in the complement \bar{b}_k (B.2). However, it presents difficulties for the second term in the complement, as calculating $\nabla\{\rho^\sigma(\mathbf{r})\tilde{\theta}_k(\mathbf{r})\}$ is computationally very expensive. Therefore, we have not found a better way to compute the complement \bar{b}_k than using the first construction as described in § 6.3.1; work is in progress to develop a method which avoids the calculation of $\nabla^2\rho^\sigma(\mathbf{r})$.

Furthermore, we note that the OEP equation always requires the computation of the matrix A_{kl} . In the first construction of b_k described in § 6.3.1, the spin-dependent matrices A_{kl}^σ which are used to construct b_k can also be added together to compute A_{kl} , making that construction computationally cheaper than the one described in this appendix. We therefore use by default the first construction of b_k from § 6.3.1, for both efficiency and (potential) accuracy gains.

$-\epsilon_H$ (eV)	OEP		CEDA		LSDA
	b_k^2	b_k^1	b_k^2	b_k^1	
Li	3.45	3.56	3.36	3.57	3.58
LiH ⁺	13.12	13.87	12.48	14.19	14.59
Si*	4.47	4.72	4.63	4.64	4.96
O ₂ *	6.43	6.54	5.99	6.41	7.27
OH	7.31	8.07	7.71	8.13	8.39
NH ₄	1.61	1.73	1.58	1.75	2.26
Na	3.45	3.51	4.15	3.59	3.49
$\langle \Delta\epsilon_H \rangle$	11%	6.9%	15%	7.1%	

*Triplet state

Table B.2: A comparison of HOMO KS eigenvalues ϵ_H from the iLDA method, with the xc-potential determined from both the full OEP equation (with $\alpha = 10^{-2}$) and CEDA, using the two different constructions for b_k . For reference, the final column shows the LSDA (UKS) values, with $\langle \Delta\epsilon_H \rangle$ being the average % difference between the LSDA and iLDA values. All states doublets unless otherwise stated.

Bibliography

- (1) G. E. Moore, *Proc. IEEE*, 1998, **86**, 82–85, <https://ieeexplore.ieee.org/document/658762>.
- (2) D. Adam, *Nature*, 2020, **580**, 316, <https://www.nature.com/articles/d41586-020-01003-6>.
- (3) T. S. Lontzek, Y. Cai, K. L. Judd and T. M. Lenton, *Nat. Clim. Change*, 2015, **5**, 441–444, <https://doi.org/10.1038/nclimate2570>.
- (4) R. S. Pindyck, *Rev. Environ. Econ. Policy*, 2017, **11**, 100–114, <https://doi.org/10.1093/reep/rew012>.
- (5) E. Oldfield, *Annu. Rev. Phys. Chem.*, 2002, **53**, 349–378, <https://doi.org/10.1146/annurev.physchem.53.082201.124235>.
- (6) M. D. Knudson, M. P. Desjarlais, R. W. Lemke, T. R. Mattsson, M. French, N. Nettelmann and R. Redmer, *Phys. Rev. Lett.*, 2012, **108**, 091102, <https://link.aps.org/doi/10.1103/PhysRevLett.108.091102>.
- (7) G. Csányi, *Machine learning the quantum mechanics of materials and molecules*, <https://www.youtube.com/watch?v=ZjBff6-5amo>, 2020.
- (8) P. Hohenberg and W. Kohn, *Phys. Rev.*, 1964, **136**, B864–B871, <https://link.aps.org/doi/10.1103/PhysRev.136.B864>.
- (9) W. Kohn and L. J. Sham, *Phys. Rev.*, 1965, **140**, A1133–A1138, <https://link.aps.org/doi/10.1103/PhysRev.140.A1133>.
- (10) R. Van Noorden, B. Maher and R. Nuzzo, *Nature News*, 2014, **514**, 550, <https://www.nature.com/news/the-top-100-papers-1.16224>.
- (11) A. Pribram-Jones, D. A. Gross and K. Burke, *Annu. Rev. Phys. Chem.*, 2015, **66**, 283–304, <https://doi.org/10.1146/annurev-physchem-040214-121420>.

-
- (12) K. Lejaeghere, G. Bihlmayer, T. Björkman, P. Blaha, S. Blügel, V. Blum, D. Caliste, I. E. Castelli, S. J. Clark, A. Dal Corso, S. de Gironcoli, T. Deutsch, J. K. Dewhurst, I. Di Marco, C. Draxl, M. Dulak, O. Eriksson, J. A. Flores-Livas, K. F. Garrity, L. Genovese, P. Giannozzi, M. Giantomassi, S. Goedecker, X. Gonze, O. Granäs, E. K. U. Gross, A. Gulans, F. Gygi, D. R. Hamann, P. J. Hasnip, N. A. W. Holzwarth, D. Iuşan, D. B. Jochym, F. Jollet, D. Jones, G. Kresse, K. Koepnik, E. Küçükbenli, Y. O. Kvashnin, I. L. M. Locht, S. Lubeck, M. Marsman, N. Marzari, U. Nitzsche, L. Nordström, T. Ozaki, L. Paulatto, C. J. Pickard, W. Poelmans, M. I. J. Probert, K. Refson, M. Richter, G.-M. Rignanese, S. Saha, M. Scheffler, M. Schlipf, K. Schwarz, S. Sharma, F. Tavazza, P. Thunström, A. Tkatchenko, M. Torrent, D. Vanderbilt, M. J. van Setten, V. Van Speybroeck, J. M. Wills, J. R. Yates, G.-X. Zhang and S. Cottenier, *Science*, 2016, **351**, DOI: 10.1126/science.aad3000, <https://science.sciencemag.org/content/351/6280/aad3000>.
- (13) C. J. Pickard and R. J. Needs, *Nat. Phys.*, 2007, **3**, 473–476, <https://doi.org/10.1038/nphys625>.
- (14) Y. Li, J. Hao, H. Liu, Y. Li and Y. Ma, *J. Chem. Phys.*, 2014, **140**, 174712, <https://doi.org/10.1063/1.4874158>.
- (15) Á. Valdés, J. Brilllet, M. Grätzel, H. Gudmundsdóttir, H. A. Hansen, H. Jónsson, P. Klüpfel, G.-J. Kroes, F. Le Formal, I. C. Man, R. S. Martins, J. K. Nørskov, J. Rossmeisl, K. Sivula, A. Vojvodic and M. Zäch, *Phys. Chem. Chem. Phys.*, 2012, **14**, 49–70, <http://dx.doi.org/10.1039/C1CP23212F>.
- (16) Y. Mo, S. P. Ong and G. Ceder, *Phys. Rev. B*, 2011, **84**, 205446, <https://link.aps.org/doi/10.1103/PhysRevB.84.205446>.
- (17) J. A. Pople, *Rev. Mod. Phys.*, 1999, **71**, 1267–1274, <https://link.aps.org/doi/10.1103/RevModPhys.71.1267>.
- (18) P. J. Stephens, F. Devlin, C. Chabalowski and M. J. Frisch, *J. Phys. Chem.*, 1994, **98**, 11623–11627, <https://pubs.acs.org/doi/10.1021/j100096a001>.
- (19) J. P. Perdew, K. Burke and M. Ernzerhof, *Phys. Rev. Lett.*, 1996, **77**, 3865–3868, <https://link.aps.org/doi/10.1103/PhysRevLett.77.3865>.
- (20) M. Born and R. Oppenheimer, *Annalen der Physik*, 1927, **389**, 457–484, <https://onlinelibrary.wiley.com/doi/abs/10.1002/andp.19273892002>.
- (21) N. I. Gidopoulos and E. K. U. Gross, *Philos. Trans. R. Soc. A*, 2014, **372**, 20130059, <https://royalsocietypublishing.org/doi/abs/10.1098/rsta.2013.0059>.
- (22) W. Kohn, *Rev. Mod. Phys.*, 1999, **71**, 1253–1266, <https://link.aps.org/doi/10.1103/RevModPhys.71.1253>.
- (23) P. Echenique and J. L. Alonso, *Mol. Phys.*, 2007, **105**, 3057–3098, <https://doi.org/10.1080/00268970701757875>.
- (24) T. Koopmans, *Physica*, 1934, **1**, 104–113, <http://www.sciencedirect.com/science/article/pii/S0031891434900112>.
-

-
- (25) C. C. J. Roothaan, *Rev. Mod. Phys.*, 1951, **23**, 69–89, <https://link.aps.org/doi/10.1103/RevModPhys.23.69>.
- (26) G. G. Hall and J. E. Lennard-Jones, *Proceedings of the Royal Society of London. Series A. Mathematical and Physical Sciences*, 1951, **205**, 541–552, <https://royalsocietypublishing.org/doi/abs/10.1098/rspa.1951.0048>.
- (27) C. C. J. Roothaan, *Rev. Mod. Phys.*, 1960, **32**, 179–185, <https://link.aps.org/doi/10.1103/RevModPhys.32.179>.
- (28) J. S. Andrews, D. Jayatilaka, R. G. Bone, N. C. Handy and R. D. Amos, *Chem. Phys. Lett.*, 1991, **183**, 423–431, <http://www.sciencedirect.com/science/article/pii/000926149190405X>.
- (29) H. B. Schlegel, *The Journal of Chemical Physics*, 1986, **84**, 4530–4534, <https://doi.org/10.1063/1.450026>.
- (30) C. Sosa and H. Bernhard Schlegel, *International Journal of Quantum Chemistry*, 1986, **29**, 1001–1015, <https://onlinelibrary.wiley.com/doi/abs/10.1002/qua.560290435>.
- (31) J. J. W. McDouall and H. B. Schlegel, *The Journal of Chemical Physics*, 1989, **90**, 2363–2369, <https://doi.org/10.1063/1.455978>.
- (32) R. J. Bartlett and J. F. Stanton, in *Reviews in Computational Chemistry*, John Wiley & Sons, Ltd, 2007, pp. 65–169, <https://onlinelibrary.wiley.com/doi/abs/10.1002/9780470125823.ch2>.
- (33) J. W. Hollett and P. M. W. Gill, *J. Chem. Phys.*, 2011, **134**, 114111, <https://doi.org/10.1063/1.3570574>.
- (34) C. L. Benavides-Riveros, N. N. Lathiotakis and M. A. L. Marques, *Phys. Chem. Chem. Phys.*, 2017, **19**, 12655–12664, <http://dx.doi.org/10.1039/C7CP01137G>.
- (35) L. Reining, *WIREs Computational Molecular Science*, 2018, **8**, e1344, <https://onlinelibrary.wiley.com/doi/abs/10.1002/wcms.1344>.
- (36) C. D. Sherrill and H. F. Schaefer, in *Advances in Quantum Chemistry*, ed. P.-O. Löwdin, J. R. Sabin, M. C. Zerner and E. Brändas, Academic Press, 1999, vol. 34, pp. 143–269, <http://www.sciencedirect.com/science/article/pii/S0065327608605328>.
- (37) G. H. Booth, A. J. W. Thom and A. Alavi, *J. Chem. Phys.*, 2009, **131**, 054106, <https://aip.scitation.org/doi/abs/10.1063/1.3193710>.
- (38) G. H. Booth, A. Grüneis, G. Kresse and A. Alavi, *Nature*, 2013, **493**, 365–370, <https://doi.org/10.1038/nature11770>.
- (39) A. Szabo and N. S. Ostlund, *Modern Quantum Chemistry*, New York: Macmillan, 2012.
- (40) C. Möller and M. S. Plesset, *Phys. Rev.*, 1934, **46**, 618–622, <https://link.aps.org/doi/10.1103/PhysRev.46.618>.
- (41) J. A. Pople, J. S. Binkley and R. Seeger, *Int. J. Quantum Chem.*, 1976, **10**, 1–19, <https://onlinelibrary.wiley.com/doi/abs/10.1002/qua.560100802>.
-

-
- (42) R. J. Bartlett and D. M. Silver, *Int. J. Quantum Chem.*, 1975, **9**, 183–198, <https://onlinelibrary.wiley.com/doi/abs/10.1002/qua.560090825>.
- (43) F. Jensen, *Introduction to Computational Chemistry*, John Wiley & Sons, 2017.
- (44) J. Čížek, in *Advances in Chemical Physics*, John Wiley & Sons, Ltd, 2007, pp. 35–89, <https://onlinelibrary.wiley.com/doi/abs/10.1002/9780470143599.ch2>.
- (45) R. J. Bartlett, J. Watts, S. Kucharski and J. Noga, *Chem. Phys. Lett.*, 1990, **165**, 513–522, [https://doi.org/10.1016/0009-2614\(90\)87031-L](https://doi.org/10.1016/0009-2614(90)87031-L).
- (46) N. Schuch and F. Verstraete, *Nature Physics*, 2009, **5**, 732–735, <https://doi.org/10.1038/nphys1370>.
- (47) H. S. Yu, S. L. Li and D. G. Truhlar, *The Journal of Chemical Physics*, 2016, **145**, 130901, <https://doi.org/10.1063/1.4963168>.
- (48) R. G. Parr, R. A. Donnelly, M. Levy and W. E. Palke, *J. Chem. Phys.*, 1978, **68**, 3801–3807, <https://doi.org/10.1063/1.436185>.
- (49) N. D. Mermin, *Phys. Rev.*, 1965, **137**, A1441–A1443, <https://link.aps.org/doi/10.1103/PhysRev.137.A1441>.
- (50) M. Levy, *Proceedings of the National Academy of Sciences*, 1979, **76**, 6062–6065, <https://www.pnas.org/content/76/12/6062>.
- (51) M. Levy, *Phys. Rev. A*, 1982, **26**, 1200–1208, <https://link.aps.org/doi/10.1103/PhysRevA.26.1200>.
- (52) E. H. Lieb, *Int. J. of Quant. Chem.*, 1983, **24**, 243–277, <http://dx.doi.org/10.1002/qua.560240302>.
- (53) L. H. Thomas, *Mathematical Proceedings of the Cambridge Philosophical Society*, 1927, **23**, 542–548, <https://doi.org/10.1017/S0305004100011683>.
- (54) E. Fermi, *Rend. Accad. Naz. Lincei*, 1927, **6**, 32.
- (55) V. L. Lignères and E. A. Carter, in *Handbook of Materials Modeling: Methods*, Springer Netherlands, Dordrecht, 2005, pp. 137–148, https://doi.org/10.1007/978-1-4020-3286-8_9.
- (56) V. V. Karasiev and S. B. Trickey, in *Concepts of Mathematical Physics in Chemistry: A Tribute to Frank E. Harris - Part A*, ed. J. R. Sabin and R. Cabrera-Trujillo, Academic Press, 2015, vol. 71, pp. 221–245, <http://www.sciencedirect.com/science/article/pii/S0065327615000052>.
- (57) B. Zhou, V. L. Lignerés and E. A. Carter, *J. Chem. Phys.*, 2005, **122**, 044103, <https://doi.org/10.1063/1.1834563>.
- (58) J. C. Snyder, M. Rupp, K. Hansen, K.-R. Müller and K. Burke, *Phys. Rev. Lett.*, 2012, **108**, 253002, <https://link.aps.org/doi/10.1103/PhysRevLett.108.253002>.
- (59) J. C. Snyder, M. Rupp, K. Hansen, L. Blooston, K.-R. Müller and K. Burke, *J. Chem. Phys.*, 2013, **139**, 224104, <https://doi.org/10.1063/1.4834075>.
-

-
- (60) L. Li, J. C. Snyder, I. M. Pelaschier, J. Huang, U.-N. Niranjan, P. Duncan, M. Rupp, K.-R. Müller and K. Burke, *Int. J. Quantum Chem.*, 2016, **116**, 819–833, <https://onlinelibrary.wiley.com/doi/abs/10.1002/qua.25040>.
- (61) F. Brockherde, L. Vogt, L. Li, M. E. Tuckerman, K. Burke and K.-R. Müller, *Nat. Commun.*, 2017, **8**, 872, <https://doi.org/10.1038/s41467-017-00839-3>.
- (62) U. von Barth and L. Hedin, *J. Phys. C*, 1972, **5**, 1629, <https://iopscience.iop.org/article/10.1088/0022-3719/5/13/012>.
- (63) K. Capelle and G. Vignale, *Phys. Rev. Lett.*, 2001, **86**, 5546–5549, <https://link.aps.org/doi/10.1103/PhysRevLett.86.5546>.
- (64) H. Eschrig and W. Pickett, *Solid State Commun.*, 2001, **118**, 123–127, <http://www.sciencedirect.com/science/article/pii/S0038109801000539>.
- (65) C. A. Ullrich, *Phys. Rev. B*, 2005, **72**, 073102, <https://link.aps.org/doi/10.1103/PhysRevB.72.073102>.
- (66) N. I. Gidopoulos, *Phys. Rev. B*, 2007, **75**, 134408, <https://link.aps.org/doi/10.1103/PhysRevB.75.134408>.
- (67) C. R. Jacob and M. Reiher, *Int. J. Quantum Chem.*, 2012, **112**, 3661–3684, <https://onlinelibrary.wiley.com/doi/pdf/10.1002/qua.24309>.
- (68) S. H. Vosko, L. Wilk and M. Nusair, *Can. J. Phys.*, 1980, **58**, 1200–1211, <https://doi.org/10.1139/p80-159>.
- (69) J. P. Perdew and A. Zunger, *Phys. Rev. B*, 1981, **23**, 5048–5079, <https://link.aps.org/doi/10.1103/PhysRevB.23.5048>.
- (70) J. P. Perdew and Y. Wang, *Phys. Rev. B*, 1992, **45**, 13244–13249, <https://link.aps.org/doi/10.1103/PhysRevB.45.13244>.
- (71) J. P. Perdew and S. Kurth, in *A primer in density functional theory*, Springer, 2003, pp. 1–55.
- (72) A. D. Becke, *J. Chem. Phys.*, 1986, **84**, 4524–4529, <https://doi.org/10.1063/1.450025>.
- (73) A. D. Becke, *Phys. Rev. A*, 1988, **38**, 3098–3100, <https://link.aps.org/doi/10.1103/PhysRevA.38.3098>.
- (74) C. Lee, W. Yang and R. G. Parr, *Phys. Rev. B*, 1988, **37**, 785–789, <https://link.aps.org/doi/10.1103/PhysRevB.37.785>.
- (75) A. D. Becke, *J. Chem. Phys.*, 1992, **96**, 2155–2160, <https://doi.org/10.1063/1.462066>.
- (76) A. D. Becke, *J. Chem. Phys.*, 1993, **98**, 1372–1377, <https://doi.org/10.1063/1.464304>.
- (77) J. Harris and R. O. Jones, *J. Phys. F*, 1974, **4**, 1170, <http://stacks.iop.org/0305-4608/4/i=8/a=013>.
- (78) D. Langreth and J. Perdew, *J. Solid State Commun.*, 1975, **17**, 1425–1429, <http://www.sciencedirect.com/science/article/pii/0038109875906183>.
-

-
- (79) O. Gunnarsson and B. I. Lundqvist, *Phys. Rev. B*, 1976, **13**, 4274–4298, <https://link.aps.org/doi/10.1103/PhysRevB.13.4274>.
- (80) A. Seidl, A. Görling, P. Vogl, J. A. Majewski and M. Levy, *Phys. Rev. B*, 1996, **53**, 3764–3774, <https://link.aps.org/doi/10.1103/PhysRevB.53.3764>.
- (81) A. D. Becke, *J. Chem. Phys.*, 1993, **98**, 5648–5652, <https://doi.org/10.1063/1.464913>.
- (82) C. Adamo and V. Barone, *J. Chem. Phys.*, 1999, **110**, 6158–6170, <https://doi.org/10.1063/1.478522>.
- (83) A. D. Becke, *J. Chem. Phys.*, 1997, **107**, 8554–8560, <https://doi.org/10.1063/1.475007>.
- (84) F. A. Hamprecht, A. J. Cohen, D. J. Tozer and N. C. Handy, *J. Chem. Phys.*, 1998, **109**, 6264–6271, <https://doi.org/10.1063/1.477267>.
- (85) J. P. Perdew, A. Ruzsinszky, G. I. Csonka, O. A. Vydrov, G. E. Scuseria, L. A. Constantin, X. Zhou and K. Burke, *Phys. Rev. Lett.*, 2008, **100**, 136406, <https://link.aps.org/doi/10.1103/PhysRevLett.100.136406>.
- (86) J. P. Perdew, V. N. Staroverov, J. Tao and G. E. Scuseria, *Phys. Rev. A*, 2008, **78**, 052513, <https://link.aps.org/doi/10.1103/PhysRevA.78.052513>.
- (87) A. Savin, in *Recent Developments and Applications of Modern Density Functional Theory*, ed. J. Seminario, Elsevier, Amsterdam, 1996, ch. 9, pp. 327–357.
- (88) P. M. W. Gill, R. D. Adamson and J. A. Pople, *Mol. Phys.*, 1996, **88**, 1005–1009, <https://doi.org/10.1080/00268979609484488>.
- (89) T. Leininger, H. Stoll, H.-J. Werner and A. Savin, *Chem. Phys. Lett.*, 1997, **275**, 151–160, <http://www.sciencedirect.com/science/article/pii/S0009261497007586>.
- (90) T. Yanai, D. P. Tew and N. C. Handy, *Chem. Phys. Lett.*, 2004, **393**, 51–57, <http://www.sciencedirect.com/science/article/pii/S0009261404008620>.
- (91) O. A. Vydrov and G. E. Scuseria, *J. Chem. Phys.*, 2006, **125**, 234109, <https://doi.org/10.1063/1.2409292>.
- (92) J. Heyd, G. E. Scuseria and M. Ernzerhof, *J. Chem. Phys.*, 2003, **118**, 8207–8215, <https://doi.org/10.1063/1.1564060>.
- (93) K. Burke, M. Ernzerhof and J. P. Perdew, *Chem. Phys. Lett.*, 1997, **265**, 115–120, <http://www.sciencedirect.com/science/article/pii/S0009261496013735>.
- (94) J. P. Perdew, W. Yang, K. Burke, Z. Yang, E. K. U. Gross, M. Scheffler, G. E. Scuseria, T. M. Henderson, I. Y. Zhang, A. Ruzsinszky, H. Peng, J. Sun, E. Trushin and A. Görling, *Proceedings of the National Academy of Sciences*, 2017, **114**, 2801–2806, <https://www.pnas.org/content/114/11/2801>.
-

-
- (95) A. D. Becke, *J. Chem. Phys.*, 1998, **109**, 2092–2098, <https://doi.org/10.1063/1.476722>.
- (96) J. Tao, J. P. Perdew, V. N. Staroverov and G. E. Scuseria, *Phys. Rev. Lett.*, 2003, **91**, 146401, <https://link.aps.org/doi/10.1103/PhysRevLett.91.146401>.
- (97) J. Sun, A. Ruzsinszky and J. P. Perdew, *Phys. Rev. Lett.*, 2015, **115**, 036402, <https://link.aps.org/doi/10.1103/PhysRevLett.115.036402>.
- (98) A. V. Arbuznikov and M. Kaupp, *Chem. Phys. Lett.*, 2003, **381**, 495–504, <http://www.sciencedirect.com/science/article/pii/S0009261403017548>.
- (99) R. Neumann, R. H. Nobes and N. C. Handy, *Mol. Phys.*, 1996, **87**, 1–36, <https://doi.org/10.1080/00268979600100011>.
- (100) R. J. Bartlett, *J. Chem. Phys.*, 2019, **151**, 160901, <https://doi.org/10.1063/1.5116338>.
- (101) J. Perdew and K. Schmidt, in *Density Functional Theory and its Applications to Materials*, American Institute of Physics, Melville, New York, 2001, vol. 577, pp. 1–20.
- (102) A. J. Cohen, P. Mori-Sánchez and W. Yang, *Chem. Rev.*, 2012, **112**, 289–320, <https://doi.org/10.1021/cr200107z>.
- (103) K. Burke, *J. Chem. Phys.*, 2012, **136**, 150901, <https://doi.org/10.1063/1.4704546>.
- (104) Y. Zhang and W. Yang, *J. Chem. Phys.*, 1998, **109**, 2604–2608, <https://doi.org/10.1063/1.476859>.
- (105) P. Mori-Sánchez, A. J. Cohen and W. Yang, *J. Chem. Phys.*, 2006, **125**, 201102, <https://doi.org/10.1063/1.2403848>.
- (106) A. Ruzsinszky, J. P. Perdew, G. I. Csonka, O. A. Vydrov and G. E. Scuseria, *J. Chem. Phys.*, 2007, **126**, 104102, <https://doi.org/10.1063/1.2566637>.
- (107) S. Kümmel and L. Kronik, *Rev. Mod. Phys.*, 2008, **80**, 3–60, <https://link.aps.org/doi/10.1103/RevModPhys.80.3>.
- (108) N. I. Gidopoulos and N. N. Lathiotakis, *J. Chem. Phys.*, 2012, **136**, 224109, <https://doi.org/10.1063/1.4728156>.
- (109) T. Pitts, N. I. Gidopoulos and N. N. Lathiotakis, *Eur. Phys. J. B*, 2018, **91**, 130, <https://doi.org/10.1140/epjb/e2018-90123-8>.
- (110) A. Görling, *Phys. Rev. Lett.*, 1999, **83**, 5459–5462, <https://link.aps.org/doi/10.1103/PhysRevLett.83.5459>.
- (111) S. Liu, P. W. Ayers and R. G. Parr, *J. Chem. Phys.*, 1999, **111**, 6197–6203, <https://doi.org/10.1063/1.479924>.
- (112) M. R. Pederson, R. A. Heaton and C. C. Lin, *J. Chem. Phys.*, 1985, **82**, 2688–2699, <https://doi.org/10.1063/1.448266>.
- (113) O. A. Vydrov and G. E. Scuseria, *J. Chem. Phys.*, 2004, **121**, 8187–8193, <https://aip.scitation.org/doi/abs/10.1063/1.1794633>.
-

-
- (114) D. Cremer, *Mol. Phys.*, 2001, **99**, 1899–1940, <https://doi.org/10.1080/00268970110083564>.
- (115) A. D. Becke, *J. Chem. Phys.*, 2005, **122**, 064101, <https://doi.org/10.1063/1.1844493>.
- (116) A. J. Cohen, P. Mori-Sánchez and W. Yang, *J. Chem. Phys.*, 2007, **126**, 191109, <https://doi.org/10.1063/1.2741248>.
- (117) L. Schimka, J. Harl and G. Kresse, *J. Chem. Phys.*, 2011, **134**, 024116, <https://doi.org/10.1063/1.3524336>.
- (118) F. Tran and P. Blaha, *Phys. Rev. Lett.*, 2009, **102**, 226401, <https://link.aps.org/doi/10.1103/PhysRevLett.102.226401>.
- (119) J. P. Perdew, R. G. Parr, M. Levy and J. L. Balduz, *Phys. Rev. Lett.*, 1982, **49**, 1691–1694, <https://link.aps.org/doi/10.1103/PhysRevLett.49.1691>.
- (120) C. A. Ullrich, *Time-Dependent Density-Functional Theory: Concepts and Applications*, Oxford University Press, Great Clarendon Street, Oxford, 2012, ch. 2, p. 27.
- (121) A. J. Cohen, P. Mori-Sánchez and W. Yang, *Science*, 2008, **321**, 792–794, <https://science.sciencemag.org/content/321/5890/792>.
- (122) P. Mori-Sánchez, A. J. Cohen and W. Yang, *Phys. Rev. Lett.*, 2008, **100**, 146401, <https://link.aps.org/doi/10.1103/PhysRevLett.100.146401>.
- (123) E. Kraisler and L. Kronik, *Phys. Rev. Lett.*, 2013, **110**, 126403, <https://link.aps.org/doi/10.1103/PhysRevLett.110.126403>.
- (124) E. Kraisler and L. Kronik, *J. Chem. Phys.*, 2014, **140**, 18A540, <https://doi.org/10.1063/1.4871462>.
- (125) M. J. P. Hodgson, E. Kraisler, A. Schild and E. K. U. Gross, *J. Phys. Chem. Lett.*, 2017, **8**, 5974–5980, <https://doi.org/10.1021/acs.jpcclett.7b02615>.
- (126) M. J. P. Hodgson, J. D. Ramsden and R. W. Godby, *Phys. Rev. B*, 2016, **93**, 155146, <https://link.aps.org/doi/10.1103/PhysRevB.93.155146>.
- (127) D. Hofmann and S. Kümmel, *Phys. Rev. B*, 2012, **86**, 201109, <https://link.aps.org/doi/10.1103/PhysRevB.86.201109>.
- (128) R. Armiento and S. Kümmel, *Phys. Rev. Lett.*, 2013, **111**, 036402, <https://link.aps.org/doi/10.1103/PhysRevLett.111.036402>.
- (129) J. W. Hollett, H. Hosseini and C. Menzies, *J. Chem. Phys.*, 2016, **145**, 084106, <https://doi.org/10.1063/1.4961243>.
- (130) R. O. Jones and O. Gunnarsson, *Rev. Mod. Phys.*, 1989, **61**, 689–746, <https://link.aps.org/doi/10.1103/RevModPhys.61.689>.
- (131) Y. Andersson, E. Hult, H. Rydberg, P. Apell, B. I. Lundqvist and D. C. Langreth, in *Electronic Density Functional Theory: Recent Progress and New Directions*, ed. J. F. Dobson, G. Vignale and M. P. Das, Springer US, Boston, MA, 1998, pp. 243–260, https://doi.org/10.1007/978-1-4899-0316-7_17.
-

-
- (132) M. Dion, H. Rydberg, E. Schröder, D. C. Langreth and B. I. Lundqvist, *Phys. Rev. Lett.*, 2004, **92**, 246401, <https://link.aps.org/doi/10.1103/PhysRevLett.92.246401>.
- (133) S. Grimme, *J. Comput. Chem.*, 2004, **25**, 1463–1473, <https://onlinelibrary.wiley.com/doi/abs/10.1002/jcc.20078>.
- (134) S. Grimme, *J. Comput. Chem.*, 2006, **27**, 1787–1799, <https://onlinelibrary.wiley.com/doi/abs/10.1002/jcc.20495>.
- (135) A. Tkatchenko and M. Scheffler, *Phys. Rev. Lett.*, 2009, **102**, 073005, <https://link.aps.org/doi/10.1103/PhysRevLett.102.073005>.
- (136) E. J. Baerends, *Phys. Rev. Lett.*, 2001, **87**, 133004, <https://link.aps.org/doi/10.1103/PhysRevLett.87.133004>.
- (137) K. Terakura, T. Oguchi, A. R. Williams and J. Kübler, *Phys. Rev. B*, 1984, **30**, 4734–4747, <https://link.aps.org/doi/10.1103/PhysRevB.30.4734>.
- (138) A. J. Cohen, P. Mori-Sánchez and W. Yang, *J. Chem. Phys.*, 2008, **129**, 121104, <https://doi.org/10.1063/1.2987202>.
- (139) P. Mori-Sánchez, A. J. Cohen and W. Yang, *Phys. Rev. Lett.*, 2009, **102**, 066403, <https://link.aps.org/doi/10.1103/PhysRevLett.102.066403>.
- (140) V. I. Anisimov, J. Zaanen and O. K. Andersen, *Phys. Rev. B*, 1991, **44**, 943–954, <https://link.aps.org/doi/10.1103/PhysRevB.44.943>.
- (141) R. T. Sharp and G. K. Horton, *Phys. Rev.*, 1953, **90**, 317–317, <https://link.aps.org/doi/10.1103/PhysRev.90.317>.
- (142) J. D. Talman and W. F. Shadwick, *Phys. Rev. A*, 1976, **14**, 36–40, <https://link.aps.org/doi/10.1103/PhysRevA.14.36>.
- (143) E. Engel, in *A Primer in Density Functional Theory*, Springer, 2003, pp. 56–122.
- (144) J. B. Krieger, Y. Li and G. J. Iafrate, *Phys. Rev. A*, 1992, **45**, 101–126, <https://link.aps.org/doi/10.1103/PhysRevA.45.101>.
- (145) J. B. Krieger, Y. Li and G. J. Iafrate, *Phys. Rev. A*, 1992, **46**, 5453–5458, <https://link.aps.org/doi/10.1103/PhysRevA.46.5453>.
- (146) O. V. Gritsenko and E. J. Baerends, *Phys. Rev. A*, 2001, **64**, 042506, <https://link.aps.org/doi/10.1103/PhysRevA.64.042506>.
- (147) F. D. Sala and A. Görling, *J. Chem. Phys.*, 2001, **115**, 5718–5732, <https://doi.org/10.1063/1.1398093>.
- (148) A. Unsöld, *Zeitschrift für Physik*, 1927, **43**, 563–574.
- (149) T. Körzdörfer, S. Kümmel and M. Mundt, *J. Chem. Phys.*, 2008, **129**, 014110, <https://doi.org/10.1063/1.2944272>.
- (150) M. W. Schmidt, K. K. Baldridge, J. A. Boatz, S. T. Elbert, M. S. Gordon, J. H. Jensen, S. Koseki, N. Matsunaga, K. A. Nguyen, S. Su, T. L. Windus, M. Dupuis and J. A. Montgomery Jr, *J. Comput. Chem.*, 1993, **14**, 1347–1363, <https://onlinelibrary.wiley.com/doi/abs/10.1002/jcc.540141112>.
-

-
- (151) M. S. Gordon and M. W. Schmidt, in *Theory and Applications of Computational Chemistry*, ed. C. E. Dykstra, G. Frenking, K. S. Kim and G. E. Scuseria, Elsevier, Amsterdam, 2005, pp. 1167–1189, <http://www.sciencedirect.com/science/article/pii/B9780444517197500846>.
- (152) R. M. Parrish, L. A. Burns, D. G. A. Smith, A. C. Simmonett, A. E. DePrince, E. G. Hohenstein, U. Bozkaya, A. Y. Sokolov, R. Di Remigio, R. M. Richard, J. F. Gonthier, A. M. James, H. R. McAlexander, A. Kumar, M. Saitow, X. Wang, B. P. Pritchard, P. Verma, H. F. Schaefer, K. Patkowski, R. A. King, E. F. Valeev, F. A. Evangelista, J. M. Turney, T. D. Crawford and C. D. Sherrill, *J. Chem. Theory Comput.*, 2017, **13**, 3185–3197, <https://doi.org/10.1021/acs.jctc.7b00174>.
- (153) U. Bozkaya and C. D. Sherrill, *J. Chem. Phys.*, 2017, **147**, 044104, <https://aip.scitation.org/doi/abs/10.1063/1.4994918>.
- (154) J. A. Pople, *Int. J. Quantum Chem.*, 1971, **5**, 175–182, <https://onlinelibrary.wiley.com/doi/abs/10.1002/qua.560050823>.
- (155) J. Lee, L. W. Bertels, D. W. Small and M. Head-Gordon, *Phys. Rev. Lett.*, 2019, **123**, 113001, <https://link.aps.org/doi/10.1103/PhysRevLett.123.113001>.
- (156) E. Baerends, D. Ellis and P. Ros, *Chem. Phys.*, 1973, **2**, 41–51, <http://www.sciencedirect.com/science/article/pii/030101047380059X>.
- (157) B. I. Dunlap, J. W. D. Connolly and J. R. Sabin, *J. Chem. Phys.*, 1979, **71**, 3396–3402, <https://doi.org/10.1063/1.438728>.
- (158) K. Eichkorn, O. Treutler, H. Öhm, M. Häser and R. Ahlrichs, *Chem. Phys. Lett.*, 1995, **242**, 652–660, <http://www.sciencedirect.com/science/article/pii/000926149500838U>.
- (159) A. D. Becke, *J. Chem. Phys.*, 1988, **88**, 2547–2553, <https://doi.org/10.1063/1.454033>.
- (160) C. W. Murray, N. C. Handy and G. J. Laming, *Mol. Phys.*, 1993, **78**, 997–1014, <https://doi.org/10.1080/00268979300100651>.
- (161) S. Lehtola, C. Steigemann, M. J. Oliveira and M. A. Marques, *SoftwareX*, 2018, **7**, 1–5, <http://www.sciencedirect.com/science/article/pii/S2352711017300602>.
- (162) W. J. Hehre, R. Ditchfield and J. A. Pople, *J. Chem. Phys.*, 1972, **56**, 2257–2261, <https://doi.org/10.1063/1.1677527>.
- (163) T. H. Dunning, *J. Chem. Phys.*, 1989, **90**, 1007–1023, <https://doi.org/10.1063/1.456153>.
- (164) D. E. Woon and T. H. Dunning, *J. Chem. Phys.*, 1993, **98**, 1358–1371, <https://doi.org/10.1063/1.464303>.
- (165) F. Jensen, *J. Chem. Phys.*, 2001, **115**, 9113–9125, <https://doi.org/10.1063/1.1413524>.
- (166) B. P. Pritchard, D. Altarawy, B. Didier, T. D. Gibson and T. L. Windus, *J. Chem. Inf. Model.*, 2019, **59**, 4814–4820, <https://doi.org/10.1021/acs.jcim.9b00725>.
-

-
- (167) D. Feller, *J. Comput. Chem.*, 1996, **17**, 1571–1586, [https://doi.org/10.1002/\(SICI\)1096-987X\(199610\)17:13%3C1571::AID-JCC9%3E3.0.CO;2-P](https://doi.org/10.1002/(SICI)1096-987X(199610)17:13%3C1571::AID-JCC9%3E3.0.CO;2-P).
- (168) K. L. Schuchardt, B. T. Didier, T. Elsethagen, L. Sun, V. Gurumoorthi, J. Chase, J. Li and T. L. Windus, *J. Chem. Inf. Model.*, 2007, **47**, 1045–1052, <https://pubs.acs.org/doi/10.1021/ci600510j>.
- (169) P. Pulay, *Chem. Phys. Lett.*, 1980, **73**, 393–398, <http://www.sciencedirect.com/science/article/pii/0009261480803964>.
- (170) V. R. Saunders and I. H. Hillier, *Int. J. Quantum Chem.*, 1973, **7**, 699–705, <https://onlinelibrary.wiley.com/doi/abs/10.1002/qua.560070407>.
- (171) T. H. Fischer and J. Almlof, *J. Phys. Chem.*, 1992, **96**, 9768–9774, <https://doi.org/10.1021/j100203a036>.
- (172) A. T. B. Gilbert, N. A. Besley and P. M. W. Gill, *J. Phys. Chem. A*, 2008, **112**, 13164–13171, <https://doi.org/10.1021/jp801738f>.
- (173) A. Heßelmann, A. W. Götz, F. Della Sala and A. Görling, *J. Chem. Phys.*, 2007, **127**, 054102, <https://doi.org/10.1063/1.2751159>.
- (174) S. Hirata, S. Ivanov, I. Grabowski, R. J. Bartlett, K. Burke and J. D. Talman, *J. Chem. Phys.*, 2001, **115**, 1635–1649, <https://doi.org/10.1063/1.1381013>.
- (175) J. Krieger, Y. Li and G. Iafrate, *Phys. Lett. A*, 1990, **148**, 470–474, <http://www.sciencedirect.com/science/article/pii/037596019090501E>.
- (176) M. Levy and A. Görling, *Phys. Rev. A*, 1996, **53**, 3140–3142, <https://link.aps.org/doi/10.1103/PhysRevA.53.3140>.
- (177) T. Grabo, T. Kreibich, S. Kurth and E. Gross, in *Strong Coulomb Correlations in Electronic Structure Calculations*, ed. V. Anisimov, Gordon and Breach Science Publishers, Amsterdam, 2000, ch. 4, pp. 217–235.
- (178) V. N. Staroverov, G. E. Scuseria and E. R. Davidson, *J. Chem. Phys.*, 2006, **124**, 141103, <https://doi.org/10.1063/1.2194546>.
- (179) N. I. Gidopoulos and N. N. Lathiotakis, *Phys. Rev. A*, 2012, **85**, 052508, <https://link.aps.org/doi/10.1103/PhysRevA.85.052508>.
- (180) A. Görling, A. Heßelmann, M. Jones and M. Levy, *J. Chem. Phys.*, 2008, **128**, 104104, <https://doi.org/10.1063/1.2826366>.
- (181) Q. Wu and W. Yang, *J. Theor. Comput. Chem.*, 2003, **02**, 627–638, <https://doi.org/10.1142/S0219633603000690>.
- (182) T. Heaton-Burgess, F. A. Bulat and W. Yang, *Phys. Rev. Lett.*, 2007, **98**, 256401, <https://link.aps.org/doi/10.1103/PhysRevLett.98.256401>.
- (183) C. Kollmar and M. Filatov, *J. Chem. Phys.*, 2008, **128**, 064101, <https://doi.org/10.1063/1.2834214>.
- (184) V. N. Staroverov, G. E. Scuseria and E. R. Davidson, *J. Chem. Phys.*, 2006, **125**, 081104, <https://doi.org/10.1063/1.2345650>.
- (185) A. F. Izmaylov, V. N. Staroverov, G. E. Scuseria, E. R. Davidson, G. Stoltz and E. Cancès, *J. Chem. Phys.*, 2007, **126**, 084107.
-

-
- (186) A. Görling and M. Levy, *Phys. Rev. B*, 1993, **47**, 13105–13113, <https://link.aps.org/doi/10.1103/PhysRevB.47.13105>.
- (187) A. Görling and M. Levy, *Phys. Rev. A*, 1994, **50**, 196–204, <https://link.aps.org/doi/10.1103/PhysRevA.50.196>.
- (188) N. I. Gidopoulos, *Phys. Rev. A*, 2011, **83**, 040502, <https://link.aps.org/doi/10.1103/PhysRevA.83.040502>.
- (189) I. G. Ryabinkin, A. A. Kananenka and V. N. Staroverov, *Phys. Rev. Lett.*, 2013, **111**, 013001, <https://link.aps.org/doi/10.1103/PhysRevLett.111.013001>.
- (190) T. Hollins, S. Clark, K. Refson and N. Gidopoulos, *J. Phys. Condens. Matter*, 2016, **29**, 04LT01, <http://stacks.iop.org/0953-8984/29/i=4/a=04LT01>.
- (191) E. Engel, A. Höck and R. M. Dreizler, *Phys. Rev. A*, 2000, **61**, 032502, <https://link.aps.org/doi/10.1103/PhysRevA.61.032502>.
- (192) P. Mori-Sánchez, Q. Wu and W. Yang, *J. Chem. Phys.*, 2005, **123**, 062204, <https://doi.org/10.1063/1.1904584>.
- (193) I. Grabowski, S. Hirata, S. Ivanov and R. J. Bartlett, *J. Chem. Phys.*, 2002, **116**, 4415–4425, <https://doi.org/10.1063/1.1445117>.
- (194) R. J. Bartlett, V. F. Lotrich and I. V. Schweigert, *J. Chem. Phys.*, 2005, **123**, 062205, <https://doi.org/10.1063/1.1904585>.
- (195) I. V. Schweigert, V. F. Lotrich and R. J. Bartlett, *J. Chem. Phys.*, 2006, **125**, 104108, <https://doi.org/10.1063/1.2212936>.
- (196) I. Grabowski, V. Lotrich and R. J. Bartlett, *J. Chem. Phys.*, 2007, **127**, 154111, <https://doi.org/10.1063/1.2790013>.
- (197) R. J. Bartlett, *Mol. Phys.*, 2010, **108**, 3299–3311, <https://doi.org/10.1080/00268976.2010.532818>.
- (198) R. Kubo, *Rep. Prog. Phys.*, 1966, **29**, 255–284, <https://doi.org/10.1088/0034-4885/29/1/306>.
- (199) S. Kurth and J. P. Perdew, *Phys. Rev. B*, 1999, **59**, 10461–10468, <https://link.aps.org/doi/10.1103/PhysRevB.59.10461>.
- (200) P. Verma and R. J. Bartlett, *J. Chem. Phys.*, 2012, **136**, 044105, <https://doi.org/10.1063/1.3678180>.
- (201) M. Hellgren, D. R. Rohr and E. K. U. Gross, *J. Chem. Phys.*, 2012, **136**, 034106, <https://doi.org/10.1063/1.3676174>.
- (202) P. Bleiziffer, A. Heßelmann and A. Görling, *J. Chem. Phys.*, 2012, **136**, 134102, <https://doi.org/10.1063/1.3697845>.
- (203) P. Bleiziffer, M. Krug and A. Görling, *J. Chem. Phys.*, 2015, **142**, 244108, <https://doi.org/10.1063/1.4922517>.
- (204) H.-V. Nguyen and S. de Gironcoli, *Phys. Rev. B*, 2009, **79**, 205114, <https://link.aps.org/doi/10.1103/PhysRevB.79.205114>.
-

-
- (205) G. P. Chen, V. K. Voora, M. M. Agee, S. G. Balasubramani and F. Furche, *Annu. Rev. Phys. Chem.*, 2017, **68**, 421–445, <https://doi.org/10.1146/annurev-physchem-040215-112308>.
- (206) X. Ren, P. Rinke, C. Joas and M. Scheffler, *J. Mater. Sci.*, 2012, **47**, 7447–7471, <https://doi.org/10.1007/s10853-012-6570-4>.
- (207) L. J. Sham and M. Schlüter, *Phys. Rev. Lett.*, 1983, **51**, 1888–1891, <https://link.aps.org/doi/10.1103/PhysRevLett.51.1888>.
- (208) R. W. Godby, M. Schlüter and L. J. Sham, *Phys. Rev. B*, 1988, **37**, 10159–10175, <https://link.aps.org/doi/10.1103/PhysRevB.37.10159>.
- (209) M. E. Casida, *Phys. Rev. A*, 1995, **51**, 2005–2013, <https://link.aps.org/doi/10.1103/PhysRevA.51.2005>.
- (210) E. R. Davidson, *Reduced Density Matrices in Quantum Chemistry*, Academic Press, New York, 1976, vol. 6, ch. 3, pp. 22–26.
- (211) T. J. P. Irons, J. W. Furness, M. S. Ryley, J. Zemen, T. Helgaker and A. M. Teale, *J. Chem. Phys.*, 2017, **147**, 134107, <https://doi.org/10.1063/1.4985883>.
- (212) M. Seidl, J. P. Perdew and S. Kurth, *Phys. Rev. Lett.*, 2000, **84**, 5070–5073, <https://link.aps.org/doi/10.1103/PhysRevLett.84.5070>.
- (213) A. Facco Bonetti, E. Engel, R. N. Schmid and R. M. Dreizler, *Phys. Rev. Lett.*, 2001, **86**, 2241–2244, <https://link.aps.org/doi/10.1103/PhysRevLett.86.2241>.
- (214) D. Rohr, O. Gritsenko and E. J. Baerends, *Chem. Phys. Lett.*, 2006, **432**, 336–342, <http://www.sciencedirect.com/science/article/pii/S0009261406015132>.
- (215) D. Bokhan and R. J. Bartlett, *Chem. Phys. Lett.*, 2006, **427**, 466–471, <http://www.sciencedirect.com/science/article/pii/S000926140601030X>.
- (216) P. W. Payne, *J. Chem. Phys.*, 1979, **71**, 490–496, <https://doi.org/10.1063/1.438124>.
- (217) S. V. Kohut, I. G. Ryabinkin and V. N. Staroverov, *J. Chem. Phys.*, 2014, **140**, 18A535, <https://doi.org/10.1063/1.4871500>.
- (218) S. J. Clark, T. W. Hollins, K. Refson and N. I. Gidopoulos, *J. Phys. Condens. Matter*, 2017, **29**, 374002, <https://doi.org/10.1088/1361-648x/aa7ba6>.
- (219) T. J. Callow, N. N. Lathiotakis and N. I. Gidopoulos, *J. Chem. Phys.*, 2020, **152**, 164114, <https://doi.org/10.1063/5.0005781>.
- (220) T. J. Callow and N. I. Gidopoulos, *Eur. Phys. J. B*, 2018, **91**, 209, <https://doi.org/10.1140/epjb/e2018-90189-2>.
- (221) Y. Wang and R. G. Parr, *Phys. Rev. A*, 1993, **47**, R1591–R1593, <https://link.aps.org/doi/10.1103/PhysRevA.47.R1591>.
- (222) Q. Zhao, R. C. Morrison and R. G. Parr, *Phys. Rev. A*, 1994, **50**, 2138–2142, <https://link.aps.org/doi/10.1103/PhysRevA.50.2138>.
-

-
- (223) N. T. Maitra, *J. Phys. Condens. Matter*, 2017, **29**, 423001, <https://doi.org/10.1088/1361-648x/aa836e>.
- (224) A. Thierbach, D. Schmidtel and A. Görling, *J. Chem. Phys.*, 2019, **151**, 144117, <https://doi.org/10.1063/1.5120587>.
- (225) M.-C. Kim, H. Park, S. Son, E. Sim and K. Burke, *J. Phys. Chem. Lett.*, 2015, **6**, 3802–3807, <https://doi.org/10.1021/acs.jpcllett.5b01724>.
- (226) C. Li, X. Zheng, A. J. Cohen, P. Mori-Sánchez and W. Yang, *Phys. Rev. Lett.*, 2015, **114**, 053001, <https://link.aps.org/doi/10.1103/PhysRevLett.114.053001>.
- (227) M. Banafsheh and T. Adam Wesolowski, *Int. J. Quantum Chem.*, 2018, **118**, e25410, <https://onlinelibrary.wiley.com/doi/abs/10.1002/qua.25410>.
- (228) J. Nafziger and A. Wasserman, *J. Phys. Chem. A*, 2014, **118**, 7623–7639, <https://doi.org/10.1021/jp504058s>.
- (229) R. Nagai, R. Akashi, S. Sasaki and S. Tsuneyuki, *The Journal of Chemical Physics*, 2018, **148**, 241737, <https://doi.org/10.1063/1.5029279>.
- (230) J. Schmidt, C. L. Benavides-Riveros and M. A. L. Marques, *The Journal of Physical Chemistry Letters*, 2019, **10**, 6425–6431, <https://doi.org/10.1021/acs.jpcllett.9b02422>.
- (231) S. Nam, S. Song, E. Sim and K. Burke, *arXiv preprint arXiv:2004.11595*, 2020, <https://arxiv.org/abs/2004.11595>.
- (232) C. O. Almbladh and A. C. Pedroza, *Phys. Rev. A*, 1984, **29**, 2322–2330, <https://link.aps.org/doi/10.1103/PhysRevA.29.2322>.
- (233) F. Aryasetiawan and M. J. Stott, *Phys. Rev. B*, 1988, **38**, 2974–2987, <https://link.aps.org/doi/10.1103/PhysRevB.38.2974>.
- (234) A. Nagy, *J. Phys. B.*, 1993, **26**, 43–48, <https://doi.org/10.1088/0953-4075/26/1/004>.
- (235) A. Nagy, *Philos. Mag. B*, 1994, **69**, 779–785, <https://doi.org/10.1080/01418639408240147>.
- (236) A. Nagy and N. H. March, *Phys. Rev. A*, 1989, **39**, 5512–5514, <https://link.aps.org/doi/10.1103/PhysRevA.39.5512>.
- (237) Á. Nagy and N. H. March, *Phys. Rev. A*, 1989, **40**, 554–557, <https://link.aps.org/doi/10.1103/PhysRevA.40.554>.
- (238) Q. Wu and W. Yang, *J. Chem. Phys.*, 2003, **118**, 2498–2509, <https://aip.scitation.org/doi/abs/10.1063/1.1535422>.
- (239) S. H. Werden and E. E. Davidson, in *Local Density Approximations in Quantum Chemistry and Solid State Physics*, ed. J. P. Dahl and J. Avery, Plenum, New York, 1st edn., 1984, ch. 3, pp. 33–42.
- (240) A. Görling, *Phys. Rev. A*, 1992, **46**, 3753–3757, <https://link.aps.org/doi/10.1103/PhysRevA.46.3753>.
- (241) R. van Leeuwen and E. J. Baerends, *Phys. Rev. A*, 1994, **49**, 2421–2431, <https://link.aps.org/doi/10.1103/PhysRevA.49.2421>.
-

-
- (242) K. Peirs, D. Van Neck and M. Waroquier, *Phys. Rev. A*, 2003, **67**, 012505, <https://link.aps.org/doi/10.1103/PhysRevA.67.012505>.
- (243) E. S. Kadantsev and M. J. Stott, *Phys. Rev. A*, 2004, **69**, 012502, <https://link.aps.org/doi/10.1103/PhysRevA.69.012502>.
- (244) L. O. Wagner, T. E. Baker, E. M. Stoudenmire, K. Burke and S. R. White, *Phys. Rev. B*, 2014, **90**, 045109, <https://link.aps.org/doi/10.1103/PhysRevB.90.045109>.
- (245) K. Finzel, P. W. Ayers and P. Bultinck, *Theor. Chem. Acc.*, 2018, **137**, 30, <https://doi.org/10.1007/s00214-018-2209-0>.
- (246) A. Kumar, R. Singh and M. K. Harbola, *J. Phys. B.*, 2019, **52**, 075007, <https://doi.org/10.1088/1361-6455/ab04e8>.
- (247) M. Levy, J. P. Perdew and V. Sahni, *Phys. Rev. A*, 1984, **30**, 2745–2748, <https://link.aps.org/doi/10.1103/PhysRevA.30.2745>.
- (248) D. S. Jensen and A. Wasserman, *Int. J. Quantum Chem.*, 2018, **118**, e25425, <https://onlinelibrary.wiley.com/doi/abs/10.1002/qua.25425>.
- (249) B. Kanungo, P. M. Zimmerman and V. Gavini, *Nat. Commun.*, **10**, 4497, <https://doi.org/10.1038/s41467-019-12467-0>.
- (250) M. J. P. Hodgson, J. D. Ramsden, J. B. J. Chapman, P. Lillystone and R. W. Godby, *Phys. Rev. B*, 2013, **88**, 241102, <https://link.aps.org/doi/10.1103/PhysRevB.88.241102>.
- (251) S. E. B. Nielsen, M. Ruggenthaler and R. van Leeuwen, *EPL*, 2013, **101**, 33001, <https://doi.org/10.1209/0295-5075/101/33001>.
- (252) C. Hättig, *Phys. Chem. Chem. Phys.*, 2005, **7**, 59–66, <http://dx.doi.org/10.1039/B415208E>.
- (253) W. Yang, P. W. Ayers and Q. Wu, *Phys. Rev. Lett.*, 2004, **92**, 146404, <https://link.aps.org/doi/10.1103/PhysRevLett.92.146404>.
- (254) W. Kohn, *Phys. Rev. Lett.*, 1983, **51**, 1596–1598, <https://link.aps.org/doi/10.1103/PhysRevLett.51.1596>.
- (255) A. Schindlmayr and R. W. Godby, *Phys. Rev. B*, 1995, **51**, 10427–10435, <https://link.aps.org/doi/10.1103/PhysRevB.51.10427>.
- (256) J. Chen and M. J. Stott, *Phys. Rev. A*, 1991, **44**, 2816–2822, <https://link.aps.org/doi/10.1103/PhysRevA.44.2816>.
- (257) J. Chen and M. J. Stott, *Phys. Rev. A*, 1993, **47**, 153–160, <https://link.aps.org/doi/10.1103/PhysRevA.47.153>.
- (258) M. Däne and A. Gonis, *Computation*, 2016, **4**, 24, <https://doi.org/10.3390/computation4030024>.
- (259) I. Mayer, I. Pápai, I. Bakó and Á. Nagy, *Journal of Chemical Theory and Computation*, 2017, **13**, 3961–3963, <https://doi.org/10.1021/acs.jctc.7b00562>.
- (260) S. G. Lias, in *NIST Chemistry WebBook, NIST Standard Reference Database Number 69*, ed. P. Linstrom and W. Mallard, National Institute of Standards and Technology, Gaithersburg MD, 20899.
-

-
- (261) C. D. Sherrill and H. F. Schaefer, in *Reviews in Computational Chemistry*, ed. K. B. Lipkowitz and D. B. Boyd, Wiley-VCH, 2000, vol. 14, ch. 2, pp. 33–136.
- (262) J. P. Perdew, A. Savin and K. Burke, *Phys. Rev. A*, 1995, **51**, 4531–4541, <https://link.aps.org/doi/10.1103/PhysRevA.51.4531>.
- (263) W. Koch and M. C. Holthausen, *A Chemist's Guide to Density Functional Theory*, Wiley-VCH, Weinheim, 2nd edn., 2001, ch. 5, p. 52.
- (264) R. G. Parr and W. Yang, *Density Functional Theory of Atoms and Molecules*, ed. O. U. Press, Oxford University Press, 1989, ch. 8, pp. 173–174.
- (265) T. Gould and J. F. Dobson, *J. Chem. Phys.*, 2013, **138**, 014103, <https://doi.org/10.1063/1.4773284>.
- (266) N. I. Gidopoulos, P. G. Papaconstantinou and E. K. U. Gross, *Phys. Rev. Lett.*, 2002, **88**, 033003, <https://link.aps.org/doi/10.1103/PhysRevLett.88.033003>.
- (267) J. Baker, A. Scheiner and J. Andzelm, *Chem. Phys. Lett.*, 1993, **216**, 380–388, <http://www.sciencedirect.com/science/article/pii/S000926149390113F>.
- (268) A. A. Ovchinnikov and J. K. Labanowski, *Phys. Rev. A*, 1996, **53**, 3946–3952, <https://link.aps.org/doi/10.1103/PhysRevA.53.3946>.
- (269) M. Reiher, *Faraday Discuss.*, 2007, **135**, 97–124, <http://dx.doi.org/10.1039/B605229K>.
- (270) M. Filatov and S. Shaik, *Chem. Phys. Lett.*, 1998, **288**, 689–697, <http://www.sciencedirect.com/science/article/pii/S0009261498003649>.
- (271) M. Filatov and S. Shaik, *J. Chem. Phys.*, 1999, **110**, 116–125, <https://doi.org/10.1063/1.477941>.
- (272) J. Gräfenstein, E. Kraka and D. Cremer, *Chem. Phys. Lett.*, 1998, **288**, 593–602, <http://www.sciencedirect.com/science/article/pii/S0009261498003352>.
- (273) A. Görling, *Phys. Rev. A*, 1993, **47**, 2783–2799, <https://link.aps.org/doi/10.1103/PhysRevA.47.2783>.
- (274) A. Görling, *Phys. Rev. Lett.*, 2000, **85**, 4229–4232, <https://link.aps.org/doi/10.1103/PhysRevLett.85.4229>.
- (275) G. L. Oliver and J. P. Perdew, *Phys. Rev. A*, 1979, **20**, 397–403, <https://link.aps.org/doi/10.1103/PhysRevA.20.397>.
- (276) F. Della Sala and A. Görling, *J. Chem. Phys.*, 2003, **118**, 10439–10454, <https://doi.org/10.1063/1.1560132>.
- (277) T. J. Callow, B. J. Pearce, T. Pitts, N. N. Lathiotakis, M. J. Hodgson and N. I. Gidopoulos, *Faraday Discuss.*, 2020, <http://dx.doi.org/10.1039/D0FD00069H>.
- (278) E. Sim, S. Song and K. Burke, *J. Phys. Chem. Lett.*, 2018, **9**, 6385–6392, <https://doi.org/10.1021/acs.jpcllett.8b02855>.
- (279) N. I. Gidopoulos and R. J. Bartlett, in preparation.
-

- (280) N. Gidopoulos and N. N. Lathiotakis, in *Advances In Atomic, Molecular, and Optical Physics*, ed. E. Arimondo, C. C. Lin and S. F. Yelin, Academic Press, 2015, vol. 64, ch. 6, pp. 129–142, <http://www.sciencedirect.com/science/article/pii/S1049250X15000063>.
- (281) X. Andrade and A. Aspuru-Guzik, *Phys. Rev. Lett.*, 2011, **107**, 183002, <https://link.aps.org/doi/10.1103/PhysRevLett.107.183002>.
- (282) B. J. Pearce, M. J. P. Hodgson and N. I. Gidopoulos, in preparation.

Colophon

This thesis is based on a template developed by Matthew Townson and Andrew Reeves. It was typeset with L^AT_EX 2_ε. It was created using the *memoir* package, maintained by Lars Madsen, with the *madsen* chapter style. The font used is Latin Modern, derived from fonts designed by Donald E. Kunith.